

THE UNIVERSITY OF CALGARY

Superradiance and Quantum Electrodynamics in the Presence of Surface
Plasmons

by

J r mie J Choquette

A DISSERTATION

SUBMITTED TO THE FACULTY OF GRADUATE STUDIES
IN PARTIAL FULFILLMENT OF THE REQUIREMENTS FOR THE
DEGREE OF Philosophy Doctorate

DEPARTMENT OF Physics and Astronomy

CALGARY, ALBERTA

January, 2012

  J r mie J Choquette 2012

THE UNIVERSITY OF CALGARY
FACULTY OF GRADUATE STUDIES

The undersigned certify that they have read, and recommend to the Faculty of Graduate Studies for acceptance, a dissertation entitled “Superradiance and Quantum Electrodynamics in the Presence of Surface Plasmons” submitted by Jérémie J Choquette in partial fulfillment of the requirements for the degree of Philosophy Doctorate.

Supervisor, Dr. Karl-Peter Marzlin
Department of Physics and Astronomy

Dr. Wolfgang Tittel
Department of Physics and Astronomy

Co-Supervisor, Dr. Robert I. Thompson
Department of Physics and Astronomy

Dr. Simon Trudel
Department of Chemistry

Dr. Barry C. Sanders
Department of Physics and Astronomy

Dr. Shohini Ghose
Department of Physics, Wilfred Laurier University

Date

Abstract

Surface plasmon polaritons are charge density waves of electrons in a metal, which are coupled to an electromagnetic field at a metal-dielectric interface. The electromagnetic field associated with surface plasmons is confined, resulting in increased field intensities near the interface. Optical emitters placed near a metal film interact strongly with the surface plasmon modes present, not only modifying the radiation rates, but also the radiation profile. These emitters may be used to store and process information, and understanding their behaviour in the presence of a lossy metal film is important in determining the advantages and limitations of using surface plasmons. In this thesis, we wish to understand how we can optically control atoms by exploring two physical phenomena: first, the influence of surface plasmons on collective effects in an ensemble of emitters. Secondly, the single photon excitation of an emitter near a metal film.

In the first case, we analyze the collective radiative behaviour of multiple classical emitters near a metal film that radiatively couple to the far-field through surface plasmon modes. We demonstrate that the contributions of dipolar image charges within the metal film significantly affect the cooperative emission of nearby sources, generating sub- and super-radiant emission that can be controlled with a suitably detuned external driving field.

In the second case, we determine the excitation probability of an atom near a metal film by a single photon pulse that is time reversed. Using a quantum electrodynamic description of absorbing dielectrics, we show that non-radiative decay will limit the excitation probability to about half of the maximum that could be achieved

in the absence of losses.

Acknowledgements

Foremost, I must thank my family who have brought me through the years leading to this point of my life: My parents Sara Ripley, and Mark Hayden, along with my brother and sister, Daniel and Jacqueline Choquette.

I would also like to thank my advisor Peter Marzlin for his guidance and support over the many years. His dedication was a large motivation to helping me finish this program, and our conversations ranging from music to physics have always been engaging. Even though Peter and his family hail from Germany, they embrace the Maritime spirit, and I always felt at home in their company.

I'm also grateful for the supervision and advice provided by Barry Sanders. Barry provided much in the way of constructive feedback and criticism that has proved valuable over the years. His words of encouragement, and humour in regards to all things including Red Dwarf, helped me maintain some levity and levelheadedness in the world.

I must also thank Rob Thompson, for not only molding me through my early days as a grad student, but also helping maintain my sensibilities and being an anchor at the University of Calgary. My days as a fellow Free Radical are days I sorely miss.

I would also like to thank Rene Stock, with whom I collaborated initially on this project, and shared his expertise on surface plasmons. If it was not for Rene, I would have never been down the path that brought me to this point.

I would also like to thank Wolfgang Tittel, if not for his simple statement "I see Quantum Information is half your title." This helped me focus my research in more desirable directions, and for that I am grateful.

I would also like to thank Tracy Korsgaard and Leslie Holmes for all their assistance over the years and for just being awesome. They were always a highlight on my trips to the office.

From my stay in Antigonish, there are those I must thank for giving me some manner of sanctuary from the doldrums of small town life. Brandon, with whom I had the pleasure of enjoying the life of Antigonish with, as my life in Antigonish would have been made much the duller without his wit and companionship. And there is Shah, whose enthusiasm for and knowledge of movies and music is hardly matched by any I know. Our discussions were always a highlight and made the one screen theatre much more entertaining. Then of course, there's my office mate, and mother away from home, Bonnie. Her blueberry muffins, and wonderful dogs, were always highlights to my day. I can only hope we get the chance to play Scrabble across the table someday.

My good friend Louis Poirier has always been there for me, as we shared many of the same frustrations. His breadth in interests often ran parallel to mine, and his company has always been a sure recipe for a good time.

Finally, but not least, there are my wonderful friends Kyle and Marie-Claire Gould, who I seemingly met under the unlikeliest terms, that have always been there to support me. Plus they're the only people to ever give me a surprise birthday party, which was, well... surprising. They are one of the fundamental reasons why I find Calgary to feel like home.

Publications

The results contained in this thesis are also described in the following articles

- *Superradiance, subradiance, and suppressed superradiance of dipoles near a metal interface*, J. J. Choquette, K.-P. Marzlin, and B. C. Sanders, Phys. Rev. A **82**, 023827 (2010)
- *Excitation of atoms by single-photon pulses in the presence of surface plasmons*, J. J. Choquette, and K.-P. Marzlin, Phys. Rev. A **85**, 063841 (2012)

Acronyms

This is a list of acronyms that can be found in this thesis:

ATR Attenuated Total Reflection

QED Quantum Electrodynamics

SPASER Surface Plasmon Amplification by Stimulated Emission of Radiation

SPP Surface Plasmon Polariton

SP Surface Plasmon

TE Transverse Electric

TM Transverse Magnetic

Table of Contents

Approval Page	ii
Abstract	iii
Acknowledgements	v
Publications	vii
Acronyms	viii
Table of Contents	ix
1 Introduction	1
1.1 Surface plasmons	1
1.1.1 Surface Plasmon Historical Milestones	1
1.1.2 Modern studies of surface plasmons: Nanoplasmonics	4
1.2 Optical phenomena extended to surface plasmons	6
1.2.1 Superradiant emission	7
1.2.2 Single-photon excitation of atoms	9
1.3 Outline for the Thesis	11
2 Electrodynamics of Surface Plasmon Polaritons	13
2.1 Electromagnetic fields and dielectrics	13
2.1.1 Green's function solution - bulk dielectric	16
2.1.2 Green's function solution - planar interfaces	17
2.2 Drude Model	20
2.3 Surface Plasmon resonance	23
2.3.1 Optical Excitation of Surface Plasmons	25
2.3.2 Surface plasmon coupling and electromagnetic field enhancement	28
2.4 Summary	32
3 Collective Radiation in the Presence of Surface Plasmons	33
3.1 Radiation of oscillating emitters near an interface	35
3.2 Driving oscillators between super- and sub-radiant emission	38
3.3 Collective decay of classical emitters	44
3.3.1 Decay rate	45
3.3.2 Far-field radiation	50
3.3.3 Suppressed superradiance	54

3.4	Summary	56
4	Quantum Theory of Atom Field Coupling Near Absorbing Dielectrics	58
4.1	Field quantization	58
4.1.1	Commutation relations and vacuum correlations	61
4.2	Light interactions with a quantum oscillator	62
4.2.1	Heisenberg equations of motion	63
4.2.2	Decay rate and the Lamb Shift	65
4.2.3	Lamb shift: Renormalized interaction with a quantum oscillator	67
4.3	Summary	69
5	Single Photon Excitation	71
5.1	Outline of the proposed experiment	73
5.2	Theoretical model	74
5.3	Excitation by a time-reversed spontaneously emitted pulse	77
5.4	Results	79
5.5	Summary	83
6	Conclusion	85
A	Green's Functions of Layered Dielectrics	88
A.1	General relations for the Green's functions	88
A.2	Bulk dielectric dyadic Green's function	89
A.2.1	Lossless homogeneous medium	90
A.3	Reflection and transmission Green's function	91
B	Stationary Phase Method	98
C	Spontaneous Decay of the Harmonic Oscillator	102
D	Excitation Probability for a Single-Photon Pulse	105
	Bibliography	109

List of Figures

2.1	A comparison of the a) real and b) imaginary parts of the dielectric constant for Au, for both experimental values (dotted) and the Drude model (line) . The Drude model is evaluated from Eq. (2.38) with the parameters $\omega_p = 1.38 \times 10^{16} s^{-1}$ and $\tau = 1.2 \times 10^{14} s^{-1}$ [1, 2].	21
2.2	The dispersion relations for surface plasmons and light. The dispersion relation for light in a vacuum is given by $\omega = ck$ and the projection of the wave vector of light in a prism along the metal film is given by $\omega = \frac{c}{n}k \sin \theta$ indicates a projection of the wave vector along the metal film. For large values of k_{sp} , the surface plasmon frequency approaches the bulk plasma frequency of $\frac{\omega_p}{\sqrt{2}}$. The index of refraction n is taken for glass. Note that only the the real part of the dispersion relation is displayed for the surface plasmon.	24
2.3	The optical excitation of surface plasmons in the so called Kretschmann configuration, where light is incident at the surface plasmon resonance angle θ_{sp} with a wavevector k_{light} and a transverse component k_p . The transverse component matches the wavevector of the surface plasmon k_{sp}	26
2.4	The reflectivity $ R_{1,2}^{TM} $ from a 56nm gold film in a Kretschmann configuration, showing the near perfect attenuated reflection at a wavelength of 800nm, where $\varepsilon_2 = -23.0 + 1.99i$	29
2.5	The reflectance $ R_{1,2}^{TM} $ from a gold film for varying thickness in a Kretschmann configuration (Red d=65nm, Blue d=46nm, Black d=56nm). The vacuum wavelength is 800nm.	30
2.6	The transmission $ T_{1,3}^{TM} $ from a gold film for varying thickness in a Kretschmann configuration (Red d=65nm, Blue d=46nm, Black d=56nm).	31
3.1	Kretschmann configuration of a thin metal film interface between a prism and vacuum used to couple emitters to surface plasmon modes. Region 1 consists of a prism ($\varepsilon_1 = 2.28$), region 2 corresponds to a thin metal film ($\varepsilon_2 = -22 + 1.99i$), and region 3 is the vacuum. . . .	34
3.2	The amplitude response in z -direction of two emitters in (a) free space (b) and placed at a distance of $\Delta z = 100\text{nm}$ from the metal interface and separated a distance Δx from each other. Both emitters are driven in the z -direction by an electric field that is detuned by $\delta\omega$ from a resonance frequency of $\omega_0 = 2.36 \times 10^{15} s^{-1}$	40

3.3	The z -amplitude $x_{0,3}$ (a) and x -amplitude $x_{0,1}$ (b) of two emitters near a metal film (solid line) and a perfect mirror (dashed line). The emitters are driven by a field that is detuned by $\delta\omega$. They are separated by $\Delta x = 80\text{nm}$ from each other and $\Delta z = 100\text{nm}$ from the metal interface.	41
3.4	Electric field lines in the near field of two dipoles driven on the primary resonance (a), and the secondary resonance (b) near a metal interface at $z = 0$. The bold arrows indicate the dipole location and orientation of the emitters.	42
3.5	The decay rate of a single oscillator placed within the vicinity of a thin metal film, at a separation distance of Δz . The decay rates are given for a dipole oriented parallel (solid) and perpendicular (dotted) relative to the plane of the interface.	46
3.6	The intensity profile of an emitter oriented parallel to the interface in the positive x -coordinate, combined with arrows indicating the electric field direction. The intensity scales from low (blue) to high (red). The red hues near the equator are numerical artifacts.	48
3.7	Four different collective eigenmodes: (a) superradiant mode, (b) subradiant mode, (c) and (d) are suppressed superradiant modes for which all real dipole moments are in phase but all mirror images are out of phase. Shown is the orientation of the dipole moment for real emitters (above the interface) and their mirror images (dashed, below the interface).	49
3.8	The far-field emission pattern of 8 oscillators in the superradiant mode at a distance of $\Delta z = 200\text{nm}$ from the interface (solid) and in free space (dashed). Shown is the ratio of the radiation intensity S and the maximum intensity S_0 produced by a single emitter in free space. The emitters are placed parallel to the horizontal axis.	52
3.9	(a) Scaling of the collective decay rate with the number N of oscillators. Circles correspond to the superradiant mode, squares and triangles to the suppressed superradiant modes displayed in Fig. 3.7 (c) and (d), respectively, and diamonds to the subradiant mode displayed in Fig. 3.7 (b). The distance between adjacent oscillators is 50 nm. Each oscillator is a distance $\Delta z = 100\text{nm}$ away from the interface. In (b) the scaling of the maximum intensity of the peak at the surface plasmon resonance angle with the number N of oscillators. In the superradiant case the results are reduced by a factor of 10 for presentational purposes.	55

5.1	a) Sketch of proposed experiment: a single-photon pulse passes through a ring shaped mirror and a prism that sits on a thin metal film. The photon excites an atom on the other side of the film. See Sec. 5.1 for more details. b) Cross section of prism (ε_1), metal film (ε_2), and vacuum (ε_0), with the atom at a height Δz above the metal film. The time-reversed spontaneously emitted light pulse arrives at the metal film from below. It has a conical spatial profile, exponentially increasing temporal shape, and enters at the surface plasmon resonance angle θ_{sp} .	72
5.2	Excitation probability (5.12) in a lossless homogeneous dielectric. The incoming single-photon pulse (5.9) has the structure of an electric dipole field, which is confined to a cone of width $\delta\theta$ around the inclination angle $\theta = \pi/2$.	80
5.3	Excitation probability P_e of a harmonic oscillator as a function of its distance Δz_A from the metal film and of the frequency width γ_ε of the incoming single-photon pulse. a) P_e for the case when the oscillator's decay rate is kept at the free-space decay rate γ_0 . b) The variation of the oscillator's decay rate $\gamma(\Delta z_A)$ with the distance is taken into account. The solid line on the front displays the value of $0.1\gamma(\Delta z_A)/\gamma_0$. The factor of 0.1 has been included for presentational purposes only.	82

Chapter 1

Introduction

1.1 Surface plasmons

Surface plasmon polaritons, commonly known as just surface plasmons (SPs) have become a hot research topic, promising advances in numerous technologies. Surface plasmons are transverse electromagnetic fields that accompany charge density waves which propagate along a metal-dielectric interface. There are two fundamental properties of surface plasmons that make them attractive for applications. First, the strong spatial confinement of oscillating surface modes results in a strong enhancement of electromagnetic fields, allowing the use of surface plasmons in processes that require high field intensities. Second, the strong confinement makes surface plasmons a possibility for hybrid devices smaller than purely optical systems.

First I will review many of milestones leading to modern research concerning surface plasmons, and then discuss the current state of research.

1.1.1 Surface Plasmon Historical Milestones

The theoretical existence and understanding of surface plasmons began with Ritchie in his paper *Plasma Losses by Fast Electrons in Thin Films* in 1957 [3]. Ritchie showed that fast electrons traveling through thin metal films not only lost energy to the excitation of volume plasmons, but an additional loss corresponding to plasmons confined to the surface occurred. The following year it was shown that the surface

plasmons were coupled to surface electromagnetic radiation giving the full name surface plasmon polariton [4]. Ferrel would, for the first time, derive the dispersion relations for surface electromagnetic fields at a metal surface [5]. In 1960, Swan and Powell would first observe surface plasmons by firing electrons at magnesium and aluminum films, observing the surface plasmon energy loss [6].

Prior to the development by Ritchie, phenomena associated with surface plasmons were known. In 1908, Sommerfeld theoretically established that at the boundary of two media where one medium is a loss free medium and the other lossy dielectric, such as a metal, there existed electromagnetic waves at the surface [7]. It wasn't until 1936 when the surface electromagnetic fields were first associated to a phenomena, which was related to the diffraction spectra of a metal grating [8]. The oldest known phenomena concerning surface plasmons is the practice of creating stained glass by infusing the glass with metallic substances, such as the stained windows of Sainte Chapelle in Paris [9]. The glass produces deep red and yellow glow when sunlight is incident at oblique angles, the light exciting the optical resonances of surface plasmons on the metal particles. The interaction of light with metal nano-particles, even today, remains a relevant topic of research. While research by this point provided insight into past phenomena, surface plasmons would later motivate a wide range of topics.

The earliest optical excitation of surface plasmons in experiments would be conducted by Otto in 1968, through a method generally known as attenuated total reflection (ATR) [10]. By bringing a glass prism close to a metal surface in a vacuum, light incident through the prism would couple evanescently across the vacuum to the metal generating surface plasmons. The prism was necessary to create the

simultaneous momentum and energy conservation required to achieve light coupling to surface plasmons. The so called Otto configuration would soon be modified by Kretschmann and Raether, where the metal film is deposited on the prism and the surface plasmons are generated on the exposed metal surface [11]. Because of the easy implementation, the Kretschmann configuration proved to be more useful than the Otto configuration. For this reason, the Kretschmann configuration was chosen for the thesis.

A further discovery involving surface plasmons involves their large field intensities, and enhancement of effects. The signal from the Raman scattering of light from individual molecules, where the light is emitted at a frequency different than the excitation frequency, is typically weak. By adsorbing molecules onto a rough silver surface, the Raman scattered signal was found to have a enhancements of up to 10^6 [12]. A part of the enhancement was caused by the large electric fields of surface plasmons, and the effect would come to be known as Surface Enhanced Raman Scattering (SERS) [13, 14, 15].

Because surface plasmons are sensitive to the metal properties and neighbouring materials, the ATR method of surface plasmon excitation would lead to various applications as a biological and chemical sensor [16, 17, 18]. Research involving surface plasmons would mature in the 1980s and companies like Pharmacia began developing commercial biosensor devices to meet the needs of scientists [19], and performing tasks such as detection of contamination and monitoring chemical processes. However, new developments with respect to the physics of SPs only emerged in the late 1990s.

1.1.2 Modern studies of surface plasmons: Nanoplasmonics

Current technology research related to computation and communication involves various photonic devices such as waveguides and photonic crystals [20, 21], as well as electronic devices such as single-electron transistors and quantum dots for information processing applications [22, 23]. Currently, managing data requires data to be frequently transferred between electronic and optical devices, the desire being to replace electronic devices with faster optical ones. Light can be processed at frequencies higher than electronics, increasing bandwidth, but requires optical fibres which limits the scale of optical circuitry [24]. On the other hand, electronics can be confined to very small dimensions, but are lossy at high frequencies, thus limiting bandwidth. Because surface plasmons have a smaller wavelength than the photons used to excite them, plasmonics can shrink optical technologies and potentially maintain a larger bandwidth, combining the strengths of optical and electronic systems [25, 26].

Surface plasmons have consequently become a focus of research in the past decade, particularly in the recently developed fields of nanoplasmonics and nano-photonics. A large part of current surface plasmon research is tailoring the dimensions and shapes of metal geometries to manipulate surface plasmon resonances. The last decade has seen various nanofabrication methods to construct geometries on the nanometre scale, such as nanoimprint lithography [27, 28] and electron beam lithography [29, 30]. Other techniques are based on the chemical synthesis of metals [31, 32]. The emergence of these techniques has made it possible to engineer the electromagnetic response of metals that eased the development of surface plasmon

technologies.

Because surface plasmons combine features of both electronics and optics, this serves as motivation for their use in overcoming the expected bottlenecks in electronic circuits [33]. Being able to confine surface plasmons has already led to numerous sub-wavelength scale devices such as waveguides [34, 35, 36], ring resonators [37, 38], surface plasmon based switches [39], surface plasmon based lasers (SPASERS) [40, 41], and even super-resolution sensors used to read storage media [42].

Nanoplasmonics are potentially the fastest processes in optics, with short relaxation and evolution times [43, 44, 45]. Based on the idea of time-reversal, which is central to the concept of focusing waves [46, 47], the plasmonic system plays the role of a focusing antenna. A time reversed pulse leads to a concentration of the optical energy at the location of an emitter and, by directing the radiation along multiple modes, interference leads to ultra fast optical control [48].

SPASERS (surface plasmon amplification by stimulated emission of radiation), are a prospective nanoplasmonic device that is used to generate coherent plasmonic fields. First proposed by Stockman [40], the first developments towards a SPASER involved the placement of a gain medium consisting of organic dye molecules next to a metal film in an ATR configuration [49]. This development relied on optically pumping a dye layer for optical gain, but this method lacked the feedback mechanism for a SPASER. Metallic nanoparticles would provide a resonant cavity for amplification, whereby multiple atoms surrounding the nanoparticle are optically pumped and subsequently decay into the nanoparticles surface plasmon modes [50]. The configuration of atoms generates dark states through image effects within the particle that prevents radiative decay of the surface plasmons. The surface plasmon modes

can then be resonantly populated. The SPASER functions as a nanoscale equivalent of a laser, generating and amplifying highly localized fields.

Although a great deal of research deals with nanofabricated environments that confine surface plasmons due to the geometric bounds of the environment, the realization of Airy waves have led to directed propagation of surface plasmons on open surfaces. Airy waves are waves that resist diffraction and experience transverse acceleration of the wave packet [51, 52]. The Airy plasmons are "relatively unaffected by surface roughness and defects" and potentially offer a means to effectively transfer energy across metallic surfaces [53], and alternate methods to guide surface plasmons through varying linear potentials [54]. The Airy plasmons can be generated in the Kretschmann configuration, where the metal surface is etched to shape an incoming light pulse into an Airy wave [55].

1.2 Optical phenomena extended to surface plasmons

The motivation of this research is understanding how optical emitters like atoms, which are used to store and process information, behave in the presence of a lossy metal film that supports surface plasmons. This thesis focuses on the ideal excitation of a single emitter using a single photon coupled to a surface plasmon, and the collective dynamics of emitters in the presence of surface plasmons. Both these studies use the Kretschmann configuration, owing to its widespread availability and simplicity.

1.2.1 Superradiant emission

Superradiance is a cooperative effect in which the radiation emitted by N scatterers is substantially enhanced compared to isolated scatterers. For this effect to occur the distance between the emitters needs to be much smaller than the wavelength of the radiation. The field amplitudes of the emitters then interfere constructively so that the radiation intensity is increased by a factor of N^2 compared to a single emitter. Furthermore, light emitted by one of the scatterers can induce stimulated emission for another scatterer so that the collective decay rate is enhanced by a factor of N if all emitters are initially excited. These two defining properties of superradiant emission are consequences of phasing and back-reaction which can occur both in classical and in quantum systems [56]. Radiation reaction is generally affected by any surrounding dielectric material. In particular, when atom-sized dipolar emitters are placed within a wavelength of a metal interface, surface plasmons can be generated. Because of the increased intensity of surface plasmon fields, an emitter reacts strongly with surface plasmon modes when placed near a metal film and the radiative properties of the emitter are significantly affected [2].

The spontaneous emission rate of individual atoms also depends on the presence of neighbouring resonant atoms and their corresponding positions. An emitter is influenced by radiation reaction of additional emitters giving rise to cooperative emission effects, such as super- and sub-radiant emission. These cooperative emission effects have been predicted for many physical systems, from blackholes to dielectric cylinders [57]. In acoustic systems, the musical tones produced by two neighbouring tuning forks decay more rapidly unless the frequency of each fork is slightly detuned

from each other[58]. In atomic systems, so called 'Dicke states' give rise to a spontaneous coherence in an excited atomic ensemble that creates superradiant emission [59].

The topic of superradiance has received renewed interest with the development of nanotechnologies and quantum information [60]. In quantum optics, superradiance can be used to create entanglement between atoms and light [61]. Entanglement within a superradiant system is also being used to understand phase transitions in quantum systems [62]. For this reason there is strong interest in methods that affect the interactions in cooperative emission.

The radiation from an ensemble of atoms depends upon the dielectric environment that composes the system [63, 64], and the positions of the atoms in the case of inhomogeneous dielectrics[65, 66, 67, 68]. While spontaneous emission is well understood for isolated emitters, emission from a system of emitters varies extensively with their interaction, depending on the state of nearby emitters and the image state induced in the surrounding media. The influence of dipole images can modify superradiant states into subradiant states when placed adjacent to a conductor, and only by understanding the role of interactions between the emitters and their images can the state be reliably determined. While the existence of superradiant surface plasmons has been established [69], the role of these image states in the super- and sub-radiant emission of surface plasmons into the far field needs to be determined and is studied within this thesis. A classical description will suffice for determining the influence of surface plasmons on the radiation intensity and spontaneous emission rate, where a quantum mechanical description is necessary for the timing of a superradiant pulse [70].

1.2.2 Single-photon excitation of atoms

Along with the creation of single photon sources [71, 72, 73], the absorption of single photons and the transport of such photons is extensively studied in quantum information sciences [74, 75, 76]. In an ideal situation a processing device would emit a photon to send information to another device for further processing. Such devices could consist of trapped atoms and quantum dots [77, 78, 79], so it is desirable to couple a single photon to an emitter with unit probability, but such couplings require large light-matter interactions that are typically associated with focused beams [80] and high finesse cavities [81, 82]. The scale of devices that use focused beams and cavities are limited in scale by the wavelength of radiation.

For lossless media, the invariance of Maxwell's equations under time inversion implies that an emitter can be excited into a specific state by directing a photon through the same modes associated with radiation emitted from the desired state. The perfect excitation of an atom in free space requires a photon that matches the time-reversal of the photon state corresponding to spontaneous decay [83]. The excitation is caused by a rephasing of the incoming pulse that cancels the phase terms occurring due to spontaneous emission and the uncertainty of the zero mean electromagnetic fields. Ideal excitation of the atom would require the entirety of the time-reversed evolution, corresponding to an infinitely long pulse. A finite pulse length would decrease the excitation probability. However, because the excitation probability grows exponentially fast, near unity excitation probabilities are possible for reasonable pulse lengths. Another effect that decreases the excitation rate is a reduction of the angular profile of the incoming photon pulse, which reduces the

overlap with the time-inverted mode of spontaneously emitted light. However, if the angular dispersion of spontaneously emitted radiation could be reduced, the angular profile of the optimal exciting photon pulse could be succinctly different.

The inclusion of a thin metal film in the Kretschmann configuration reduces the angular dispersion of a radiating system and would be easy to implement. Although an incoming photon pulse would see an increase in interaction strength due to the conversion to a surface plasmon mode, the increase in noise due to the metal film may prevent unit probability in single photon excitation. By accounting for all radiation modes and losses, the feasibility of single photon excitation of a single emitter can be determined.

Sub-wavelength (super) resolution

Excitation by a single photon is also relevant for other applications such as beating the diffraction limit, because of its relation to time reversal. Fink accomplished sub-wavelength resolution by time reversing and reflecting transmitted electric fields from multiple antennae, where the signal was refocused on individual antennae separated by distances smaller than the diffraction limit [84] [85]. A time-reversed signal propagates backwards through a time independent medium following the same path, undergoing the reflections and scattering that occurs in the forward direction [86]. The signal then refocuses on the originator, at a resolution better than the diffraction limit. The time-reversal is key not only in sub-wavelength resolution, but also in the perfect excitation of atoms with a single photon.

Evanescent fields are a key component to high resolution devices such as scanning tunnelling microscopes, where propagating light is limited by the diffraction limit.

The ability to resolve an emitter is limited by near-field information not being present in the produced radiation. By coupling the near field to the far-field with scatterers, the radiation can then be used to resolve objects below the diffraction limit.

1.3 Outline for the Thesis

Chapter 1 establishes the historical background of surface plasmon research and current topics in nanoplasmonics. The motivation for researching superradiant surface plasmons and single photon excitation via surface plasmons along with the background is given.

Chapter 2 reviews the electrodynamics of surface plasmons and their physical properties, including their theoretical derivation. The complex dielectric function of metals based on the Drude model is also discussed, along with the derivation of the Fresnel coefficients and the electromagnetic Green's function for layered media. The physical properties of surface plasmons are presented and a discussion of the transmission and reflection characteristics of thin metal films in the Kretschmann configuration is given.

Chapter 3 deals with the influence of a metal film supporting surface plasmons on the collective behaviour of optical emitters and their cooperative behaviour. The optical emitters are modelled as charged harmonic oscillators, and the sub- and super-radiant behaviour of the emission rates are understood in terms of a mirror effect of the charges in the metal surface. The radiation profiles of the radiant system are obtained by applying approximations on the Green's function.

Chapter 4 discusses the quantization of the electromagnetic field in the presence of

a metal, which is an example of an absorbing and dispersive dielectric. The losses are characterized by noise currents that are added to Maxwell's equations, and the QED formalism is constructed around the classical Green's function of Chapter 2. The equations of motion for the atomic and electromagnetic field operators are derived and renormalized.

Chapter 5 analyzes the excitation of a quantum harmonic oscillator near the interface by a single photon pulse. We determine a suitable ansatz for the time reversal of a photon emitted by the emitter through the metal film. We then analyze the influence of losses on the excitation probability by comparing the results of the full theory to the case when non-radiative decay into the metal is ignored.

Chapter 6 contains summarizing remarks of our work and the final conclusion of this dissertation.

Chapter 2

Electrodynamics of Surface Plasmon Polaritons

Plasmons are charge density oscillations that occur in a plasma, such as the conduction electrons in a metal. A surface plasmon is confined to the surface of usually a metal, and a surface plasmon polariton refers specifically to the coupling of an electromagnetic wave to a surface plasmon. Both terms are used interchangeably, although surface plasmon is more commonly used .

In this chapter, the fundamental concepts of electromagnetism that form the basis for the study of surface plasmon phenomena are outlined. The macroscopic Maxwell equations and the notation are introduced in Sec. 2.1, along with the construction of the Green's function formalism that is later necessary for the QED formalism in Chapter 4. The Drude model, which is the dielectric function for metals, is discussed in Sec. 2.2, and then the creation of surface plasmons is covered in Sec. 2.3. Furthermore, we discuss how surface plasmon resonance in the Kretschmann configuration is affected by physical parameters such as the wavelength and film thickness. We then determine the optimal parameters for surface plasmon generation, which will be necessary for our studies of superradiance and single photon excitation.

2.1 Electromagnetic fields and dielectrics

Provided that the surface plasmon wavelength is greater than the mean free path of the electron oscillations, a macroscopic description for dielectric media can be used

[87]. The macroscopic Maxwell equations for electromagnetic fields are

$$\nabla \cdot \mathbf{D}(\mathbf{r}, t) = \rho(\mathbf{r}, t) \quad (2.1)$$

$$\nabla \times \mathbf{E}(\mathbf{r}, t) = -\partial_t \mathbf{B}(\mathbf{r}, t) \quad (2.2)$$

$$\nabla \cdot \mathbf{B}(\mathbf{r}, t) = 0 \quad (2.3)$$

$$\nabla \times \mathbf{H}(\mathbf{r}, t) = \mathbf{j}(\mathbf{r}, t) + \partial_t \mathbf{D}(\mathbf{r}, t), \quad (2.4)$$

where \mathbf{E} is the electric field, \mathbf{D} the electrical displacement, \mathbf{B} and \mathbf{H} are the magnetic induction and magnetic field respectively. The terms ρ and \mathbf{j} denote the charge and current densities respectively. The constitutive fields \mathbf{D} and \mathbf{H} for a non-magnetic isotropic inhomogeneous media are defined as

$$\mathbf{D}(\mathbf{r}, t) = \varepsilon_0 \mathbf{E}(\mathbf{r}, t) + \mathbf{P}(\mathbf{r}, t) \quad (2.5)$$

$$\mathbf{B}(\mathbf{r}, t) = \mu_0 \mathbf{H}(\mathbf{r}, t), \quad (2.6)$$

where the polarization is given by \mathbf{P} . Assuming the polarization of the media responds linearly to the electric field, the polarization becomes causally related to the electric field via the dielectric susceptibility $\chi(\mathbf{r}, t)$ with the relation

$$\mathbf{P}(\mathbf{r}, t) = \int_t^\infty dt' \chi(\mathbf{r}, t - t') \mathbf{E}(\mathbf{r}, t'). \quad (2.7)$$

Inserting Eq. (2.7) into the constitutive relation Eq. (2.5) and taking the Fourier transform gives

$$\mathbf{D}(\mathbf{r}, \omega) = \varepsilon_0 \varepsilon(\mathbf{r}, \omega) \mathbf{E}(\mathbf{r}, \omega), \quad (2.8)$$

where the relative permittivity $\varepsilon(\mathbf{r}, \omega)$ is

$$\varepsilon(\mathbf{r}, \omega) = 1 + \int_t^\infty dt' e^{i\omega(t-t')} \chi(\mathbf{r}, t'). \quad (2.9)$$

The real and imaginary part of the permittivity (ε' and ε'' respectively) are interrelated by the analytic properties of the dielectric susceptibility. where causality provides the condition that $\chi(\mathbf{r}, t - t')$ is zero for times of $t < t'$. The permittivity $\varepsilon(\mathbf{r}, \omega)$ is then an analytic function of ω in the upper complex plane and the real and imaginary parts are related through the Kramers-Kronig relations

$$\varepsilon'(\mathbf{r}, \omega) = 1 - \frac{1}{\pi} \mathcal{P} \int d\omega' \frac{\varepsilon''(\mathbf{r}, \omega')}{\omega - \omega'}, \quad (2.10)$$

$$\varepsilon''(\mathbf{r}, \omega) = \frac{1}{\pi} \mathcal{P} \int d\omega' \frac{\varepsilon'(\mathbf{r}, \omega') - 1}{\omega - \omega'}. \quad (2.11)$$

The imaginary part is out of phase with the real part and corresponds to absorption and losses in the media. For metals, the complex dielectric function accounts for induced currents within the metal and follows naturally from the Drude model, which will be discussed later.

The macroscopic Maxwell equations in the frequency domain are, upon using Eq. (2.8),

$$\nabla \cdot (\varepsilon(\mathbf{r}, \omega) \mathbf{E}(\mathbf{r}, \omega)) = \rho(\mathbf{r}, \omega) \quad (2.12)$$

$$\nabla \times \mathbf{E}(\mathbf{r}, \omega) = i\omega \mathbf{B}(\mathbf{r}, \omega) \quad (2.13)$$

$$\nabla \cdot \mathbf{B}(\mathbf{r}, \omega) = 0 \quad (2.14)$$

$$\nabla \times \mathbf{B}(\mathbf{r}, \omega) = \mu_0 \mathbf{j}(\mathbf{r}, \omega) - i \frac{\omega}{c^2} \varepsilon(\mathbf{r}, \omega) \mathbf{E}(\mathbf{r}, \omega), \quad (2.15)$$

From the combination of the Maxwell equations, the electric field $\mathbf{E}(\mathbf{r}, \omega)$ obeys the inhomogeneous wave equation

$$\left(\frac{\omega^2}{c^2} \varepsilon(\mathbf{r}, \omega) - \nabla \times \nabla \times \right) \mathbf{E}(\mathbf{r}, \omega) = -i\omega \mu_0 \mathbf{j}(\mathbf{r}, \omega), \quad (2.16)$$

where the solution can be expressed in terms of the retarded dyadic Green's function $\mathbf{G}(\mathbf{r}, \mathbf{r}', \omega)$, a rank two tensor, which is the solution to the Helmholtz equation

$$\left(\nabla_{\mathbf{r}} \times \nabla_{\mathbf{r}} \times - \frac{\omega^2}{c^2} \epsilon(\mathbf{r}, \omega) \right) \mathbf{G}(\mathbf{r}, \mathbf{r}', \omega) = \mathbb{1} \delta(\mathbf{r} - \mathbf{r}'). \quad (2.17)$$

The Green's function then propagates the effect of the current densities to the electromagnetic field. Solving the Green's function is a classical problem, describing the propagation of radiation accounting for varying boundary conditions, although deriving its explicit form is rather involved. Once the Green's function is derived, however, all propagation modes for electromagnetic radiation are accounted for and the electric field for an arbitrary source current can be determined from the Green's function through the relation

$$\mathbf{E}(\mathbf{r}, \omega) = i\omega\mu_0 \int d^3\mathbf{r}' \mathbf{G}(\mathbf{r}, \mathbf{r}', \omega) \mathbf{j}(\mathbf{r}', \omega). \quad (2.18)$$

The Green's function solution for bulk dielectrics and the terms associated with reflection and transmission of radiation are necessary to acquire the entire electric field.

2.1.1 Green's function solution - bulk dielectric

Consider a bulk dielectric where the dielectric permittivity does not vary with position such that $\epsilon(\mathbf{r}, \omega) = \epsilon(\omega)$. The solution to Eq. (2.17) is then [88]

$$G_{\mu\nu}(\mathbf{r}, \mathbf{r}', \omega) = \left[q(\omega)^{-2} \frac{\partial}{\partial r_\mu} \frac{\partial}{\partial r_\nu} + \delta_{\mu\nu} \right] \frac{e^{iq(\omega)|\mathbf{r}-\mathbf{r}'|}}{4\pi|\mathbf{r}-\mathbf{r}'|}, \quad (2.19)$$

where the indices indicate the appropriate cartesian coordinates and $q(\omega) = \sqrt{\epsilon(\omega)} \frac{\omega}{c}$. In momentum (\mathbf{k}) space, the dyadic Green function $G_{\mu\nu}(\mathbf{k}, \omega)$ is given by the trans-

form

$$G_{\mu\nu}(\mathbf{k}, \omega) = \left(\delta_{\mu\nu} - \frac{k_\mu k_\nu}{q^2(\omega)} \right) \frac{1}{k^2 - q^2(\omega)}. \quad (2.20)$$

In addition to describing solutions for a bulk dielectric, this term is also necessary for determining the fields in the case of interfaces.

2.1.2 Green's function solution - planar interfaces

The Green's functions corresponding to the reflected and transmitted fields are obtained by solving the homogeneous equation

$$\left[\frac{\partial}{\partial r_\gamma} \frac{\partial}{\partial r_\mu} - \delta_{\gamma\mu} \left(\Delta + \varepsilon_3 \frac{\omega^2}{c^2} \right) \right] G_{\mu\nu}(\mathbf{r}, \mathbf{r}', \omega) = 0. \quad (2.21)$$

Using the method from Ref. [89] (See also Ref. [90]), the dyadic Green's functions of a multiple layered planar dielectric are solved. Due to the translational invariance of the problem of a planar dielectric interface, it is useful to decompose the Green's function into transverse and normal components through the Fourier transform

$$G_{\mu\nu}(\mathbf{r}, \mathbf{r}', \omega) = \int \frac{d^2 \mathbf{k}_p}{(2\pi)^2} e^{i\mathbf{k}_p \cdot (\mathbf{r}_p - \mathbf{r}'_p)} \tilde{G}_{\mu\nu}(\mathbf{k}_p, \omega; z, z'), \quad (2.22)$$

where \mathbf{k}_p is the wave vector component tangential to the interface and \mathbf{r}_p is the corresponding position component.

Together with the Fourier transform, the differential equation Eq. (2.17) is

$$\begin{pmatrix} k_y^2 - \epsilon \frac{\omega^2}{c^2} - \frac{\partial^2}{\partial z^2} & -k_x k_y & ik_x \frac{\partial}{\partial z} \\ -k_x k_y & k_x^2 - \epsilon \frac{\omega^2}{c^2} - \frac{\partial^2}{\partial z^2} & ik_y \frac{\partial}{\partial z} \\ ik_x \frac{\partial}{\partial z} & ik_y \frac{\partial}{\partial z} & k_p^2 - \epsilon \frac{\omega^2}{c^2} \end{pmatrix} \begin{pmatrix} \tilde{G}_{xx} & \tilde{G}_{xy} & \tilde{G}_{xz} \\ \tilde{G}_{yx} & \tilde{G}_{yy} & \tilde{G}_{yz} \\ \tilde{G}_{zx} & \tilde{G}_{zy} & \tilde{G}_{zz} \end{pmatrix} = \delta(\mathbf{r} - \mathbf{r}') \begin{pmatrix} 1 & 0 & 0 \\ 0 & 1 & 0 \\ 0 & 0 & 1 \end{pmatrix} \quad (2.23)$$

The coupled differential equations produced by the wave equation can be simplified by rotating about the z -axis such that k_x becomes k_p . The rotation has the effect

that all transverse electric fields are tied to the y -axis and the transverse magnetic components are associated with x and z . The rotation is given by

$$\tilde{\mathbf{D}}(\mathbf{k}_p, \omega; z, z') = \mathbf{U}(k_p) \tilde{\mathbf{G}}(\mathbf{k}_p, \omega; z, z') \mathbf{U}^{-1}(k_p) \quad (2.24)$$

where the matrix \mathbf{U} is defined as

$$\mathbf{U}(k_p) = \frac{1}{k_p} \begin{pmatrix} k_x & -k_y & 0 \\ k_y & k_x & 0 \\ 0 & 0 & k_p \end{pmatrix}. \quad (2.25)$$

The transformed differential equation is

$$\begin{pmatrix} -\epsilon \frac{\omega^2}{c^2} - \frac{\partial^2}{\partial z^2} & 0 & ik_p \frac{\partial}{\partial z} \\ 0 & k_p^2 - \epsilon \frac{\omega^2}{c^2} - \frac{\partial^2}{\partial z^2} & 0 \\ ik_p \frac{\partial}{\partial z} & 0 & k_p^2 - \epsilon \frac{\omega^2}{c^2} \end{pmatrix} \begin{pmatrix} \tilde{D}_{xx} & \tilde{D}_{xy} & \tilde{D}_{xz} \\ \tilde{D}_{yx} & \tilde{D}_{yy} & \tilde{D}_{yz} \\ \tilde{D}_{zx} & \tilde{D}_{zy} & \tilde{D}_{zz} \end{pmatrix} = \delta(\mathbf{r} - \mathbf{r}') \begin{pmatrix} 1 & 0 & 0 \\ 0 & 1 & 0 \\ 0 & 0 & 1 \end{pmatrix}. \quad (2.26)$$

From Eq. (2.26) we have the following differential equations:

$$-\left(\epsilon \frac{\omega^2}{c^2} + \partial_z^2\right) \tilde{D}_{xx}(\mathbf{k}_p, \omega; z, z') + ik_p \partial_z \tilde{D}_{zx}(\mathbf{k}_p, \omega; z, z') = \delta(\mathbf{r} - \mathbf{r}') \quad (2.27)$$

$$-\left(\epsilon \frac{\omega^2}{c^2} + \partial_z^2\right) \tilde{D}_{xy}(\mathbf{k}_p, \omega; z, z') + ik_p \partial_z \tilde{D}_{zy}(\mathbf{k}_p, \omega; z, z') = 0 \quad (2.28)$$

$$-\left(\epsilon \frac{\omega^2}{c^2} + \partial_z^2\right) \tilde{D}_{xz}(\mathbf{k}_p, \omega; z, z') + ik_p \partial_z \tilde{D}_{zz}(\mathbf{k}_p, \omega; z, z') = 0 \quad (2.29)$$

$$\left(k_p^2 - \epsilon \frac{\omega^2}{c^2} - \partial_z^2\right) \tilde{D}_{yx}(\mathbf{k}_p, \omega; z, z') = 0 \quad (2.30)$$

$$\left(k_p^2 - \epsilon \frac{\omega^2}{c^2} - \partial_z^2\right) \tilde{D}_{yy}(\mathbf{k}_p, \omega; z, z') = \delta(\mathbf{r} - \mathbf{r}') \quad (2.31)$$

$$\left(k_p^2 - \epsilon \frac{\omega^2}{c^2} - \partial_z^2\right) \tilde{D}_{yz}(\mathbf{k}_p, \omega; z, z') = 0 \quad (2.32)$$

$$ik_p \partial_z \tilde{D}_{xx}(\mathbf{k}_p, \omega; z, z') + \left(k_p^2 - \epsilon \frac{\omega^2}{c^2}\right) \tilde{D}_{zx}(\mathbf{k}_p, \omega; z, z') = 0 \quad (2.33)$$

$$ik_p \partial_z \tilde{D}_{xy}(\mathbf{k}_p, \omega; z, z') + (k_p^2 - \epsilon \frac{\omega^2}{c^2}) \tilde{D}_{zy}(\mathbf{k}_p, \omega; z, z') = 0 \quad (2.34)$$

$$ik_p \partial_z \tilde{D}_{xz}(\mathbf{k}_p, \omega; z, z') + (k_p^2 - \epsilon \frac{\omega^2}{c^2}) \tilde{D}_{zz}(\mathbf{k}_p, \omega; z, z') = \delta(\mathbf{r} - \mathbf{r}') \quad (2.35)$$

Note that $\tilde{D}_{xy}(\mathbf{k}_p, \omega; z, z')$ and $\tilde{D}_{zy}(\mathbf{k}_p, \omega; z, z')$ are coupled together by homogeneous equations (see Eq. (2.28) and (2.34)). Additionally, $\tilde{D}_{yx}(\mathbf{k}_p, \omega; z, z')$ and $\tilde{D}_{yz}(\mathbf{k}_p, \omega; z, z')$ independently satisfy homogeneous equations as seen in Eq. (2.30) and (2.32). Consequently, the terms $\tilde{D}_{xy}(\mathbf{k}_p, \omega; z, z')$, $\tilde{D}_{zy}(\mathbf{k}_p, \omega; z, z')$, $\tilde{D}_{yx}(\mathbf{k}_p, \omega; z, z')$ and $\tilde{D}_{yz}(\mathbf{k}_p, \omega; z, z')$ are all zero. Furthermore, $\tilde{D}_{zx}(\mathbf{k}_p, \omega; z, z')$ and $\tilde{D}_{zz}(\mathbf{k}_p, \omega; z, z')$ can be obtained from $\tilde{D}_{xx}(\mathbf{k}_p, \omega; z, z')$ and $\tilde{D}_{xz}(\mathbf{k}_p, \omega; z, z')$ respectively, leaving only three Green's function terms which need to be solved for explicitly.

The boundary conditions derived from Maxwell's equations are then re-expressed in terms of the dyadic components of the Green's function. The x and y components correspond to the tangential fields and z to the perpendicular fields. Because the second index ν corresponds to the orientation of source terms, the boundary conditions are applied in terms of the first index μ . Because of the continuity of electromagnetic fields at the boundary of an interface, the following components of $\tilde{G}_{\mu\nu}(\mathbf{k}_p, \omega; z, z')$ need to be continuous:

Condition 1: Tangential component of \mathbf{E} is continuous.

$$\tilde{D}_{x\nu}(\mathbf{k}_p, \omega; z, z')$$

$$\tilde{D}_{y\nu}(\mathbf{k}_p, \omega; z, z')$$

Condition 2: Tangential component of \mathbf{H} is continuous.

$$\partial_z \tilde{D}_{y\nu}(\mathbf{k}_p, \omega; z, z')$$

$$\partial_z \tilde{D}_{x\nu}(\mathbf{k}_p, \omega; z, z') - ik_p \tilde{D}_{z\nu}(\mathbf{k}_p, \omega; z, z')$$

Condition 3: Normal component of \mathbf{D} is continuous.

$$\varepsilon(\mathbf{r}, \omega) \tilde{D}_{z\nu}(\mathbf{k}_p, \omega; z, z')$$

Condition 4: Normal component of \mathbf{H} is continuous.

$$ik_p \tilde{D}_{y\nu}(\mathbf{k}_p, \omega; z, z').$$

The explicit derivation of the individual Green's function terms for a 3 layered system is detailed in Appendix A. The derivation results in the generalized reflection and transmission coefficients for a multi-layered system. The reflection coefficient R^{TM} for transverse magnetic waves reflecting from a single interface is given by

$$R_{i,i-1}^{\text{TM}} = \frac{\varepsilon_{i-1}\beta_i - \varepsilon_i\beta_{i-1}}{\varepsilon_{i-1}\beta_i + \varepsilon_i\beta_{i-1}}, \quad (2.36)$$

where $\beta_i \equiv \sqrt{\varepsilon_i \frac{\omega^2}{c^2} - k_x^2}$. The first index indicates the region the radiation is incident from, and the second is the second region that makes up the interface. For multiple interfaces, the reflection coefficient has the general form

$$\tilde{R}_{i,i-1}^{\text{TM}} = \frac{R_{i,i-1}^{\text{TM}} + \tilde{R}_{i-1,i-2}^{\text{TM}} e^{i2\beta_{i-1}(d_{i-1}-d_{i-2})}}{1 + R_{i,i-1}^{\text{TM}} \tilde{R}_{i-1,i-2}^{\text{TM}} e^{i2\beta_{i-1}(d_{i-1}-d_{i-2})}}. \quad (2.37)$$

These Fresnel coefficients will be utilized in the following discussion on surface plasmon generation.

2.2 Drude Model

The study of surface plasmons focuses on two types of materials that have a qualitatively different dielectric function $\varepsilon(\omega)$, dielectrics and metals, where the function

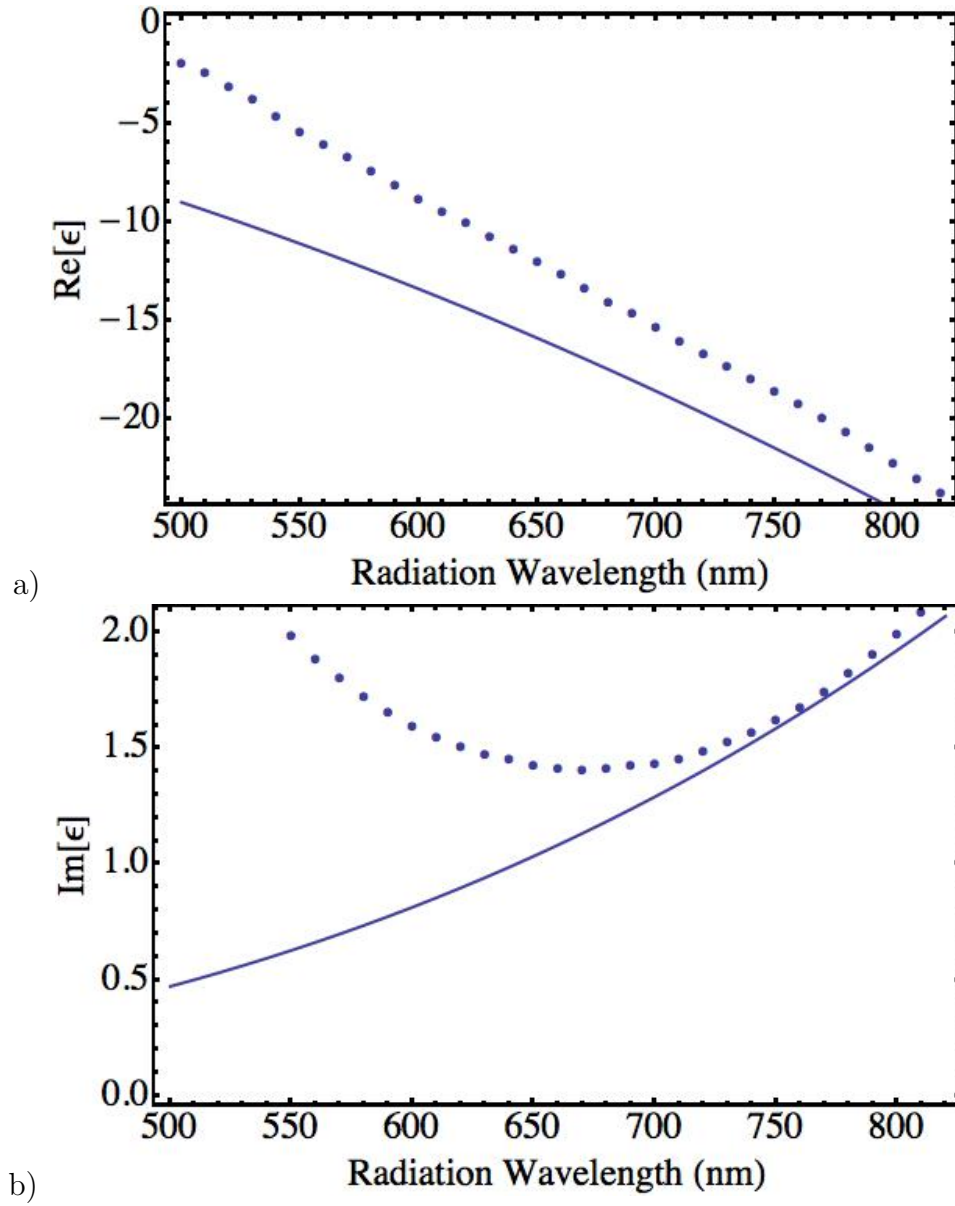


Figure 2.1: A comparison of the a) real and b) imaginary parts of the dielectric constant for Au, for both experimental values (dotted) and the Drude model (line) . The Drude model is evaluated from Eq. (2.38) with the parameters $\omega_p = 1.38 \times 10^{16} s^{-1}$ and $\tau = 1.2 \times 10^{14} s^{-1}$ [1, 2].

describes the response of the medium to electromagnetic radiation. For dielectrics, the electrons are tightly bound to the nuclei and losses are negligible, giving a real and positive dielectric function. A sufficient approximation of a metal is a free electron gas that are easily moved by an applied electric field, where a phenomenological collision rate is introduced to provide the associated losses. The Drude model is derived from considering electrons driven by an electric field with an impulse dependent on the mean free-time between electron collisions [91]. The dielectric function is

$$\varepsilon(\omega) = 1 - \frac{\omega_p^2}{\omega(\omega + i\tau)} \quad (2.38)$$

where τ is the average collision rate determined from the mean free path of electrons, and ω_p is the plasma frequency. The plasma frequency is given as

$$\omega_p = \sqrt{\frac{n_e e^2}{m_e \varepsilon_0}} \quad (2.39)$$

where n_e is the electron density of the conductor, and m_e is the mass of the electron. In Figure 2.1 the measured values for the dielectric function of gold is compared to the Drude model in the optical regime. Gold and silver are typical materials chosen for studying surface plasmons due to their reflective properties. In the numerical evaluations, a wavelength 800nm is chosen, which is typical for many atomic systems and within the frequency range of tunable Titanium-Sapphire lasers [92].

In general, for metals at optical frequencies result in a negative real part and small imaginary part ($\omega < \omega_p$), corresponding to fields that can propagate and decay over short distances. For frequencies much lower than optical frequencies the negative real part dominates and becomes large, resulting in only the presence of exponentially decaying fields. For frequencies larger than the plasma frequency the

real part becomes positive, corresponding to a transparency of the material at that frequency.

2.3 Surface Plasmon resonance

The existence of surface plasmons can be derived by an analysis of the reflection of radiation on a planar metal-dielectric interface, where radiation is neither transmitted or reflected. This electromagnetic field decays exponentially away from the interface into the dielectric and metal and is transverse magnetic, or rather the magnetic field \mathbf{H} is parallel to the interface.

By equating R^{TM} to 0, the dispersion relation of surface plasmons are determined from the boundary conditions of a nonreflecting electromagnetic field at the interface. The resulting dispersion relation is given by

$$c^2 k_{sp}^2 = \left(\frac{\omega}{c}\right)^2 \frac{\varepsilon_0 \varepsilon_m}{\varepsilon_0 + \varepsilon_m}, \quad (2.40)$$

$$k_z^2 = \varepsilon_{0,1} \left(\frac{\omega}{c}\right)^2 - k_{sp}^2. \quad (2.41)$$

Because k_x^2 is always greater than $\varepsilon_{0,1} \left(\frac{\omega}{c}\right)^2$, the wavevector component k_z is always imaginary resulting in an electromagnetic field that decays exponentially from the interface as z increases. The surface plasmon propagates along the interface with a wavevector component k_x . One important observation of Eq. (2.40) is that both dielectric constants must be of opposite signs to produce a purely imaginary z -component of the wavevector.

Figure 2.2 indicates that the surface plasmon dispersion relation is never equal to that of light in free space. Consequently, surface plasmons cannot be resonantly

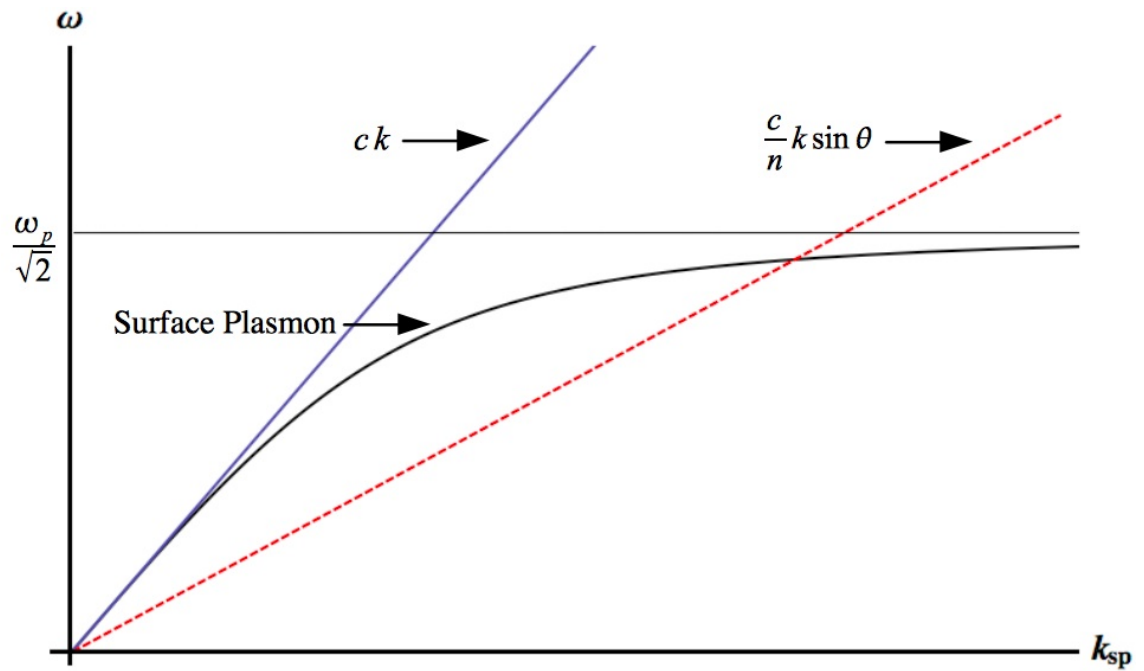


Figure 2.2: The dispersion relations for surface plasmons and light. The dispersion relation for light in a vacuum is given by $\omega = ck$ and the projection of the wave vector of light in a prism along the metal film is given by $\omega = \frac{c}{n}k \sin \theta$ indicates a projection of the wave vector along the metal film. For large values of k_{sp} , the surface plasmon frequency approaches the bulk plasma frequency of $\frac{\omega_p}{\sqrt{2}}$. The index of refraction n is taken for glass. Note that only the the real part of the dispersion relation is displayed for the surface plasmon.

excited by a field incident on the vacuum-metal interface. A similar situation where direct coupling is not possible exists for the metal-prism interface. The physical reason is that the in-plane momentum and energy conservation are not simultaneously possible between incident radiation and the surface plasmon. To excite surface plasmons with free space radiation, schemes that involve additional dielectric layers or affect the “structure” of the metal surface are necessary.

2.3.1 Optical Excitation of Surface Plasmons

The crudest and simplest method of SP excitation is to roughen the metal surface, which creates irregular boundary conditions on the surface [93]. For light illuminating a surface, there will be surface features the size of k_0^{-1} . This allows momentum matching for a given frequency between radiative and SP modes. The propagation of SPs are sensitive to boundary conditions of the adjacent media, and are easily scattered by the same surface structures used to couple light into the surface plasmon. A method of more finesse is creating a periodic structure with a length scale of the free space radiation [94]. The surface plasmons are free to propagate provided there are no irregularities. While more reliable for creating propagating surface plasmon modes, the wavelength of light is restricted in such geometries.

The more flexible method is sending light through an additional medium in the so called attenuated total reflection configuration, also known as the Kretschmann configuration [11]. When light is incident on an interface of different dielectric properties below the critical angle, an evanescent field is generated that decays exponentially away from the interface. The evanescent field decays on the order of the wavelength of the light and has a propagating momentum component parallel to the interface.

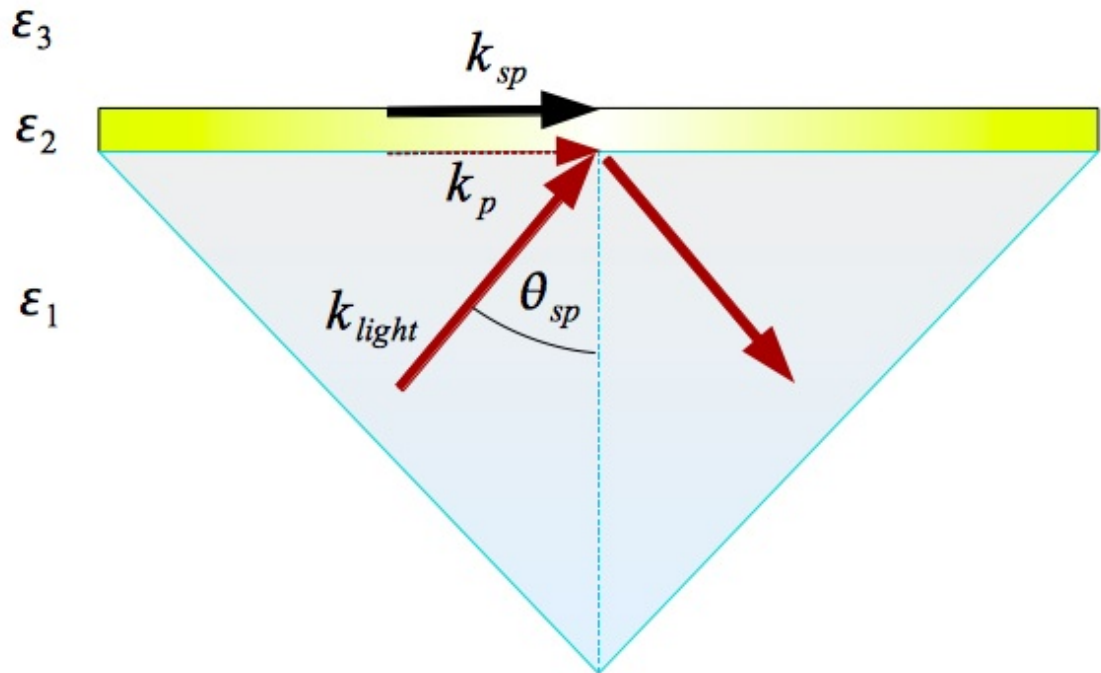


Figure 2.3: The optical excitation of surface plasmons in the so called Kretschmann configuration, where light is incident at the surface plasmon resonance angle θ_{sp} with a wavevector k_{light} and a transverse component k_p . The transverse component matches the wavevector of the surface plasmon k_{sp} .

For a given angle θ_i , the parallel momentum component is

$$k_p = \sqrt{\varepsilon_1} \frac{\omega}{c} \sin \theta_i. \quad (2.42)$$

The parallel momentum component is limited by the critical angle θ_c , where the momentum of the incident light cannot be supported in the adjacent media and produces a purely evanescent field with no propagating component. Varying θ_i results in a range of parallel momentum limited to $\sqrt{\varepsilon_1} \frac{\omega}{c} > k_p > k_p = \sqrt{\varepsilon_1} \frac{\omega}{c} \sin \theta_c$.

If the intermediate medium is thin enough, the evanescent electric field generates density oscillations of electrons at the surface of the adjacent metal-air interface. Because $\varepsilon_1 > \varepsilon_3$, a simultaneous matching of the energy (frequency) and the wavevectors k_p and k_{sp} occurs (The crossing is illustrated in Fig. 2.2). Surface plasmon resonance occurs at the angle where $k_p = k_{sp}$ (θ_{sp}), and is marked by the attenuated total reflection of the incoming light. Figure 2.3 illustrates the reflectance of the interface as the angle of incidence is varied. At the surface plasmon resonance angle nearly all radiation is coupled into surface plasmons.

It is worth noting that a common treatment of surface plasmon resonance is determining the resonance angle through the relations given in Eq. (2.42) and Eq. (2.40). Equating the two expressions gives the resonance condition

$$\theta_{sp} = \sin^{-1} \sqrt{\frac{\varepsilon_0 \varepsilon_m}{\varepsilon_1 (\varepsilon_0 + \varepsilon_m)}}. \quad (2.43)$$

The resonance angle determined from the expression, while a good approximation, does not take into account the additional interface has on the dispersion of the surface plasmon [2]. The dispersion relation Eq. (2.40) is obtained from the Fresnel coefficient for a single interface (See Eq. (2.36)), and to obtain the dispersion relation for a

double interface the generalized Fresnel coefficient Eq. (2.37) is used. Specifically when

$$1 + R_{0,1}^{TM} \tilde{R}_{1,2}^{TM} e^{i2k_{zm}d} = 0. \quad (2.44)$$

where k_{zm} is the evanescent wavevector in the metal film.

By expanding the normal wavevector components around k_{sp}^0 , the surface plasmon wavevector for a single interface, an expression for the deviation Δk_{sp} can be obtained. The shift is small when $e^{i2k_{zm}d} \ll 1$, which indicates for a dielectric-metal interface consisting of vacuum ($\varepsilon_0 = 1$) and gold ($\varepsilon_m = -23.0 + 1.99i$ at a wavelength of 800 nm) occurs at about 200 nm.

$$\Delta k_x = \frac{R_{0,1}^{TM} e^{i2k_{zm}d}}{\varepsilon_0 - \varepsilon_m} \left(\frac{\omega}{c} \right) \left(\frac{\varepsilon_0 \varepsilon_m}{\varepsilon_0 + \varepsilon_m} \right)^{3/2} \quad (2.45)$$

The shift Δk_{sp} is necessarily complex indicating that not only is k_{sp} shifted from k_{sp}^0 , but there is additional loss in the propagating surface plasmon modes. These losses are due to the surface plasmon coupling back through the metal film into region 1. The radiation can not couple into the vacuum because there is no crossover between the dispersion relations. The energy momentum conservation that prevents a direct coupling to surface plasmons with incident light forbids the surface plasmon from coupling into that region.

2.3.2 Surface plasmon coupling and electromagnetic field enhancement

The prism-metal film geometry of the Kretschmann method lends itself well to analysis through the connection between the Fresnel coefficients and reflection and transmission. Attenuated total reflection characterizes the excitation of surface plasmons,

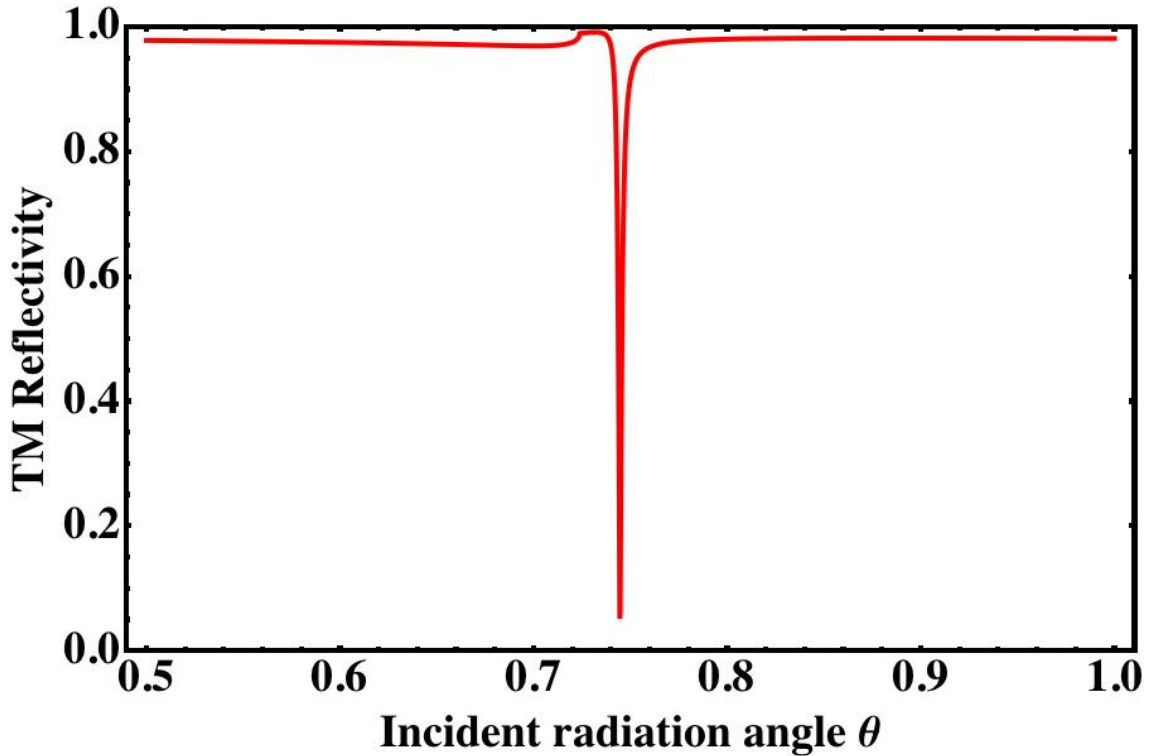


Figure 2.4: The reflectivity $|R_{1,2}^{TM}|$ from a 56nm gold film in a Kretschmann configuration, showing the near perfect attenuated reflection at a wavelength of 800nm, where $\varepsilon_2 = -23.0 + 1.99i$.

and this corresponds to a dip in the reflectance of transverse magnetic light at angles greater than the critical angle for total internal reflection. The reflectance is defined as the magnitude of the reflection Fresnel coefficient. The efficiency of coupling to surface plasmons in ATR schemes depends not only on the metal film thickness and the dielectric constants $\varepsilon_1/\varepsilon_2/\varepsilon_0$ of the three regions, but also the wavelength of the radiation. These parameters also have a significant impact on the nature of the surface plasmon fields.

The reflection coefficient for a TM wave reflecting from the interface between

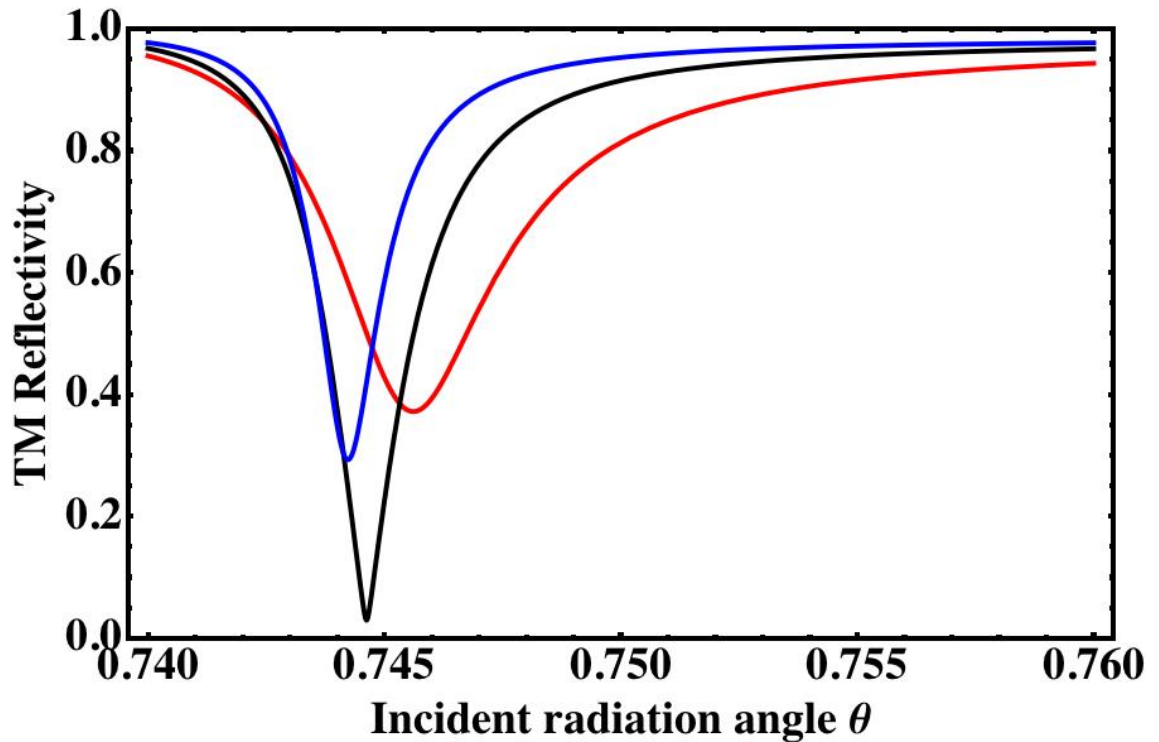


Figure 2.5: The reflectance $|R_{1,2}^{TM}|$ from a gold film for varying thickness in a Kretschmann configuration (Red $d=65\text{nm}$, Blue $d=46\text{nm}$, Black $d=56\text{nm}$). The vacuum wavelength is 800nm .

regions 1 and 2 in a 3-layered system is given by Eq. (2.37). In Fig. 2.4 the magnitude of the reflection coefficient is plotted for a varying incident angle, showing attenuated total reflection due to the generation of surface plasmons. The dip occurs when light partially reflected back into the metal film and prism from the vacuum metal interface destructively interferes with the incident radiation producing a near zero minima in reflectivity.

There is a critical thickness for the generation of surface plasmons, as the incident field penetrates the film evanescently. If the thickness d of the film increases,

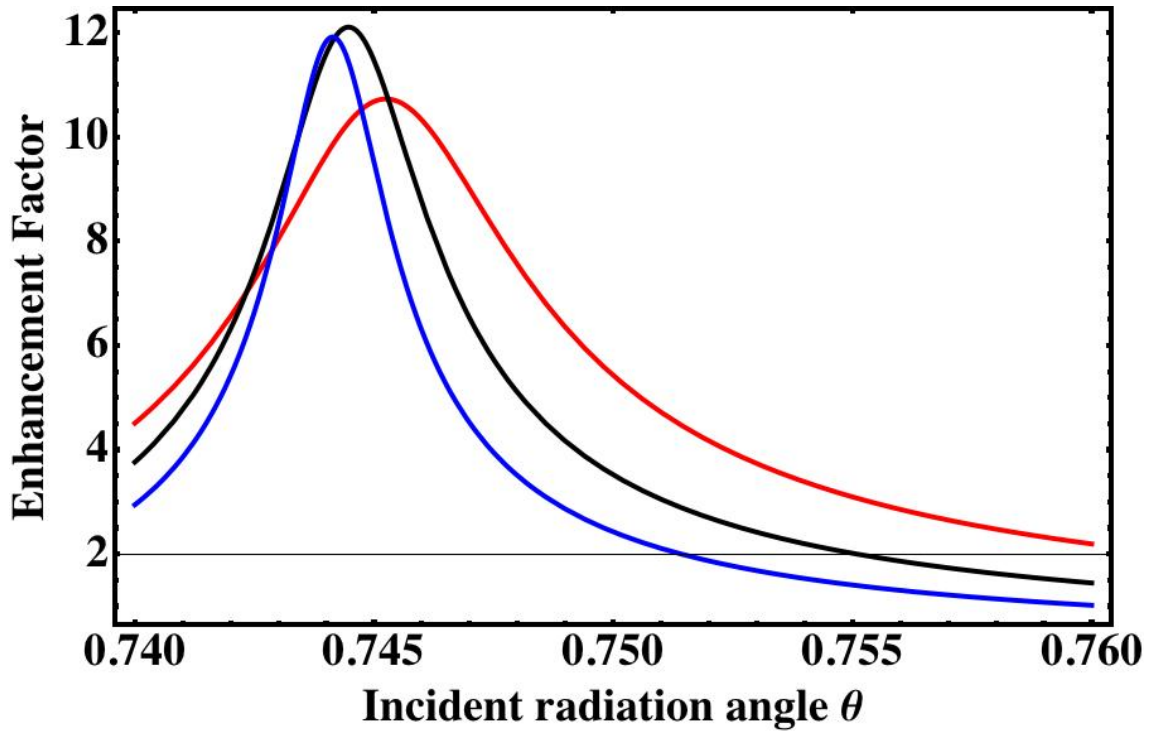


Figure 2.6: The transmission $|T_{1,3}^{\text{TM}}|$ from a gold film for varying thickness in a Kretschmann configuration (Red $d=65\text{nm}$, Blue $d=46\text{nm}$, Black $d=56\text{nm}$).

the strength of oscillations at the vacuum-metal interface are reduced and produces weaker reflections (See Fig. 2.5)). The consequence is incomplete destructive interference and the reflectivity increases. As the film thickness is increased, the behaviour becomes that of a silver mirror. If the film thickness is decreased then the induced oscillations at metal interface increase. While increased coupling to surface plasmons is expected, the radiative rate of surface plasmons as determined from $\text{Im}\Delta k_x$ back into the prism increases and results in an increase in reflectivity, as determined from $\text{Im}\Delta k_x$.

At the surface plasmon resonance angle with the appropriate wavelength or film

thickness, radiation is entirely coupled to the surface. Because the surface plasmon modes are confined within a small distance of the interface [95], much smaller than the wavelength of the light wave, the electromagnetic energy is confined to a smaller volume and the associated field intensity is enhanced. The enhancement of the electric field is seen in the transmission coefficients (see Eq. (A.54)) illustrated in Fig. 2.6, where the transmitted field will have an electric field amplitude an order of magnitude larger than the incoming field. The increased field strength of the surface plasmons allows for larger couplings to nearby atoms and molecules, causing an enhancement of field related effects.

2.4 Summary

The following chapters discuss the generation of surface plasmons by superradiant ensembles of emitters and exciting an emitter by a surface plasmon generated by a single photon. The physical parameters, such as emitter wavelength and fill thickness, have been chosen to create maximum coupling between emitters and radiation through surface plasmons.

Chapter 3

Collective Radiation in the Presence of Surface Plasmons

When several emitters are located within a fraction of the emitted radiation wavelength, their dynamic dipole-dipole interaction can significantly alter the radiation dynamics as compared to a single emitter. Collective emission can potentially demonstrate super- and sub-radiant behaviour, where the interactions either drive or damp neighbouring dipoles. Because of the strength of the surface plasmon modes in the metal film, additional collective effects can occur. In this chapter, we discuss the influence of surface plasmons on the radiation from a single dipole and the collective radiation of multiple dipoles.

In Sec. 3.1 we discuss how we acquire the electromagnetic field from multiple emitters using Green's functions, where the formalism is applied to harmonically oscillating emitters that are driven by a light field in Sec. 3.2. We demonstrate that their collective dynamics can be changed from super- to sub-radiant behaviour by varying the frequency of the driving field. In Sec. 3.3, the collective decay of initially excited harmonic oscillators are studied and we give a detailed description of super- and sub-radiant decay modes, their decay rates, and emission patterns. We then discuss how well superradiant emission is realized in these modes.

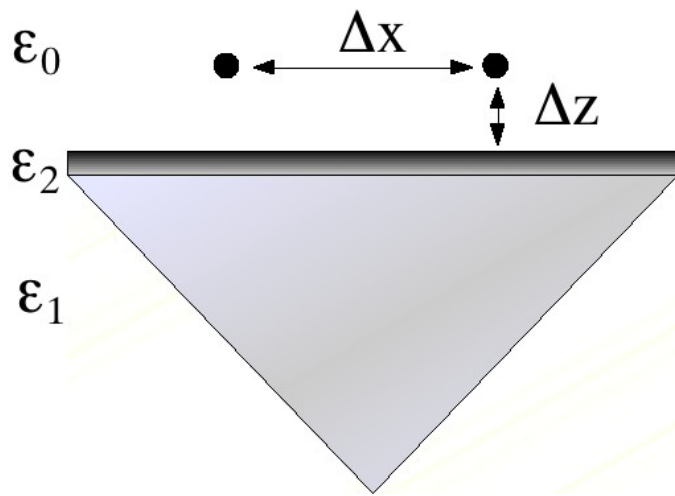


Figure 3.1: Kretschmann configuration of a thin metal film interface between a prism and vacuum used to couple emitters to surface plasmon modes. Region 1 consists of a prism ($\epsilon_1 = 2.28$), region 2 corresponds to a thin metal film ($\epsilon_2 = -22 + 1.99i$), and region 3 is the vacuum.

3.1 Radiation of oscillating emitters near an interface

We consider the behavior of N atomic dipoles that are located near a thin metallic interface that supports surface plasmon modes, see Fig. 3.1. To simplify the considerations we study an infinite planar interface so that the prism, which is needed in experiments for phase-matching, can be replaced by an infinite half-space filled with a non-absorbing dielectric. The dipoles are located at positions $\mathbf{r}^{(1)}, \dots, \mathbf{r}^{(N)}$ in region 3 above the interface.

To describe the system of emitters, each dipole is modeled as a charged classical harmonic oscillator with charge q , mass m , and resonance frequency ω_0 . The restoring force associated with the harmonic motion originates from the attraction by a stationary charge distribution of opposite sign (the “nucleus”) located at the point $\mathbf{r}^{(i)}$. Charge i oscillates about the point $\mathbf{r}^{(i)}$ with an amplitude $\mathbf{x}^{(i)}$ that is of the order of Bohr’s radius and much smaller than the individual separation distance between emitters Δx . The equation of motion for the harmonic oscillators affected by an external electric field $\mathbf{E}(\mathbf{r}, t)$ is given by,

$$\ddot{\mathbf{x}}_0^{(j)} + \omega_0^2 \mathbf{x}_0^{(j)} = \frac{q}{m} \left(\mathbf{E}(\mathbf{r}^{(j)}, t) + \sum_{i=1}^N \mathbf{E}^{(i)}(\mathbf{r}^{(j)}, t) \right). \quad (3.1)$$

The term in parentheses can be interpreted as the local electric field at the position $\mathbf{r}^{(j)}$ of the j th oscillator. It consists of the external applied field $\mathbf{E}(\mathbf{r}^{(j)}, t)$ in region 3 (e.g., a laser beam) plus the superposition of the fields $\mathbf{E}^{(i)}(\mathbf{r}^{(j)}, t)$ that are created by emitter i .

The propagation of an electric field $\mathbf{E}(\mathbf{r}, t)$ in the presence of multiple interfaces is solved using a Green’s Function approach. The electric field due to a current

source of $\mathbf{j}(\mathbf{r}, t)$ is determined by the well known differential wave equation

$$\left(\frac{1}{c^2} \varepsilon(\mathbf{r}) \left(\frac{\partial}{\partial t} \right)^2 + \nabla \times \nabla \times \right) \mathbf{E}(\mathbf{r}, t) = -\mu_0 \frac{\partial}{\partial t} \mathbf{j}(\mathbf{r}, t), \quad (3.2)$$

where $\varepsilon(\mathbf{r})$ is the complex relative permittivity of a dielectric. We assume here for simplicity that the permittivity of the interfaces does not depend on the radiation frequency, which is the case for the interface that we are studying. This method has a much broader range of validity. The constants c and μ_0 are the speed of light and permeability of free space respectively. The solution to Eq. (3.2) in terms of the dyadic Green's function $\mathbf{G}(\mathbf{r}, t; \mathbf{r}', t')$ is

$$\mathbf{E}(\mathbf{r}, t) = -\mu_0 \iint dt' d^3 \mathbf{r}' \mathbf{G}(\mathbf{r}, t; \mathbf{r}', t') \frac{\partial}{\partial t'} \mathbf{j}(\mathbf{r}', t'), \quad (3.3)$$

where $\mathbf{G}(\mathbf{r}, t; \mathbf{r}', t')$ is a retarded solution to

$$\left(\frac{1}{c^2} \varepsilon(\mathbf{r}) \left(\frac{\partial}{\partial t} \right)^2 + \nabla \times \nabla \times \right) \mathbf{G}(\mathbf{r}, t; \mathbf{r}', t') = \mathbf{I} \delta(\mathbf{r} - \mathbf{r}') \delta(t - t'). \quad (3.4)$$

We assume that each emitter consists of a charge q (the ‘‘electron’’) that performs small oscillations of amplitude $\mathbf{x}^{(j)}(t)$ around a fixed position $\mathbf{r}^{(j)}$ at which a charge $-q$ (the ‘‘nucleus’’) is placed. The current density $\mathbf{j}(\mathbf{r}', t')$ produced by emitter j can then be written as

$$\mathbf{j}(\mathbf{r}', t') = q \delta(\mathbf{r}' - \mathbf{r}^{(j)}) \dot{\mathbf{x}}^{(j)}(t'). \quad (3.5)$$

This current density contains the complete information about the radiation field produced by both the electron and the resting nucleus and determines the radiative electric field through Eq. (3.3). In addition one generally needs to include the electric Coulomb field of a charge distribution. However, because the oscillation amplitudes of the electron are small and the total charge of the emitter is zero, each oscillator

essentially describes a point dipole with dipole moment $\mathbf{p} = q\mathbf{x}(t)$. We then can ignore the Coulomb contribution so that each emitter can be thought of as an oscillating point dipole. Inserting Eq. (3.5) into Eq. (3.3) then yields the electric field produced by emitter j ,

$$\mathbf{E}^{(j)}(\mathbf{r}, t) = -\mu_0 q \int_{-\infty}^{\infty} dt' \mathbf{G}(\mathbf{r}, \mathbf{r}^{(j)}, t - t') \ddot{\mathbf{x}}^{(j)}(t'). \quad (3.6)$$

Within the Green's function formalism, the effect of surface plasmons are included through the Fresnel coefficients, i.e., the complex ratio of the reflected ($R_{i,i-1}^{\text{TM}}$) or transmitted ($T_{i,i-1}^{\text{TM}}$) electric field and the incident field, where i is region in consideration and $i-1$ the neighbouring region. The surface plasmons generate characteristic resonances in these coefficients.

To acquire a general solution for the oscillator amplitude, let us now assume that emitter j oscillates according to

$$\mathbf{x}^{(j)}(t) = \mathbf{x}^{(j)}(0) e^{-i\omega t - \Gamma t} \quad (3.7)$$

for some frequency ω and a real, positive decay parameter $\Gamma \ll \omega$. To simplify the derivations we use a complex amplitude $\mathbf{x}(t)$ for the oscillators. The use of complex solutions is possible because for harmonic oscillators interacting via the electromagnetic field the equations of motions are linear second-order differential equations. Real and imaginary part of $\mathbf{x}(t)$ then correspond to two linearly independent, real solutions of the equations of motion. For the field intensity we use the quantity $|\mathbf{E}|^2$ which is proportional to the intensity for real oscillators amplitudes averaged over

one cycle $2\pi/\omega$. Eq. (3.6) then becomes

$$\begin{aligned} \mathbf{E}^{(j)}(\mathbf{r}, t) &= -\mu_0 q \int_{-\infty}^{\infty} dt' \mathbf{G}(\mathbf{r}, \mathbf{r}^{(j)}, t-t') (\Gamma + i\omega)^2 \mathbf{x}^{(j)}(0) e^{-i\omega t' - \Gamma t'} \\ &= -\mu_0 q (\Gamma + i\omega)^2 e^{-i\omega t - \Gamma t} \mathbf{G}(\mathbf{r}, \mathbf{r}^{(j)}, \omega - i\Gamma) \mathbf{x}^{(j)}(0), \end{aligned} \quad (3.8)$$

where $\mathbf{G}(\mathbf{r}, \mathbf{r}^{(j)}, \omega - i\Gamma)$ is the analytic continuation of the temporal Fourier transform of $\mathbf{G}(\mathbf{r}, \mathbf{r}^{(j)}, t)$ into the lower half plane.

Noting the pole at $\omega_1 = \omega - i\Gamma$ and applying calculus of residues, the electric field is then

$$\mathbf{E}^{(j)}(\mathbf{r}, t) = -\mu_0 q \mathbf{G}(\mathbf{r}, \mathbf{r}^{(j)}, \omega - i\Gamma) (\Gamma + i\omega)^2 \mathbf{x}^{(j)}(0) e^{-i\omega t - \Gamma t}. \quad (3.9)$$

Inserting Eq. (3.9) and Eq. (3.7) into Eq. (3.1) gives

$$[(\Gamma + i\omega)^2 + \omega_0^2] \mathbf{x}^{(j)}(t) = \frac{q}{m} \left\{ \mathbf{E}(\mathbf{r}^{(j)}, t) - \mu_0 q \sum_{i=1}^N \mathbf{G}(\mathbf{r}^{(j)}, \mathbf{r}^{(i)}, \omega - i\Gamma) (\Gamma + i\omega)^2 \mathbf{x}^{(i)}(t) \right\}, \quad (3.10)$$

where these coupled equations can then be used to describe driven and decaying systems of charged harmonic oscillators.

3.2 Driving oscillators between super- and sub-radiant emission

If the emitters are driven by an external electric field of the form $\mathbf{E}(\mathbf{r}, t) = \mathbf{E}_0 e^{i\mathbf{k}\cdot\mathbf{r}} e^{-i\omega t}$ they will eventually settle into a state where each dipole oscillates with the frequency ω of the driving field, so that $\mathbf{x}(t) = \mathbf{x}_0 e^{-i\omega t}$. This ansatz, combined with Eq. (3.10)

transforms Eq. (3.1) into the algebraic equation ¹

$$\begin{aligned} \mathbf{E}_0^{(i)} = e^{-i\mathbf{k}\cdot\mathbf{r}} & \left[\frac{m}{q}(\omega_0^2 - \omega^2)\delta_{ij}\mathbb{1} - \text{Im}\mathbf{G}(\mathbf{r}^{(i)}, \mathbf{r}^{(i)}, \omega) \right. \\ & \left. \times \delta_{ij} \frac{\mu_0\omega^2q}{2\pi} - \frac{\mu_0\omega^2q}{2\pi} \sum_{j \neq i}^N \mathbf{G}(\mathbf{r}^{(i)}, \mathbf{r}^{(j)}, \omega) \right] \mathbf{x}_0^{(j)}, \end{aligned} \quad (3.11)$$

and forms a set of $3N$ coupled equations for the Cartesian components of N oscillators. The indices i, j run from 1 to N and $\mathbb{1}$ denotes the unit matrix in three dimensions. To find the total electric field emitted by all N sources we need to solve these equations for $\mathbf{x}^{(i)}$ and then superpose the fields produced by all sources.

Figure 3.2(a) shows the amplitude response $x_{0,3}$, i.e., the z -component of the amplitude vector \mathbf{x}_0 of the oscillators, for two nearby emitters in free space driven by an electric field polarized in the z direction. For separation distances Δx less than 50 nm the resonance frequency begins to shift considerably due to dynamic dipole-dipole coupling between the emitters. Because in free space the dyadic Green's function is diagonal with respect to radiation polarization, and because the emitters are only driven along the z -axis, there is only coupling between the z -components of oscillations.

Placing the two emitters close to the metal interface leads to a dramatic change in the emitter dynamics. In Fig. 3.2(b) the z -amplitude of two scatterers that are a distance $\Delta z = 100\text{nm}$ away from the interface is displayed. It has a similar overall shape as the amplitude response in free space, but an additional narrow resonance peak appears on the tail of the primary resonance. This narrow feature is more prominent in Fig. 3.3(a) which displays the same quantity for a fixed distance

¹ Eq. (3.11) corresponds to Eq. (3.10) in the limit of stationary amplitudes, i.e., $\Gamma = 0$ in Eq. (3.10).

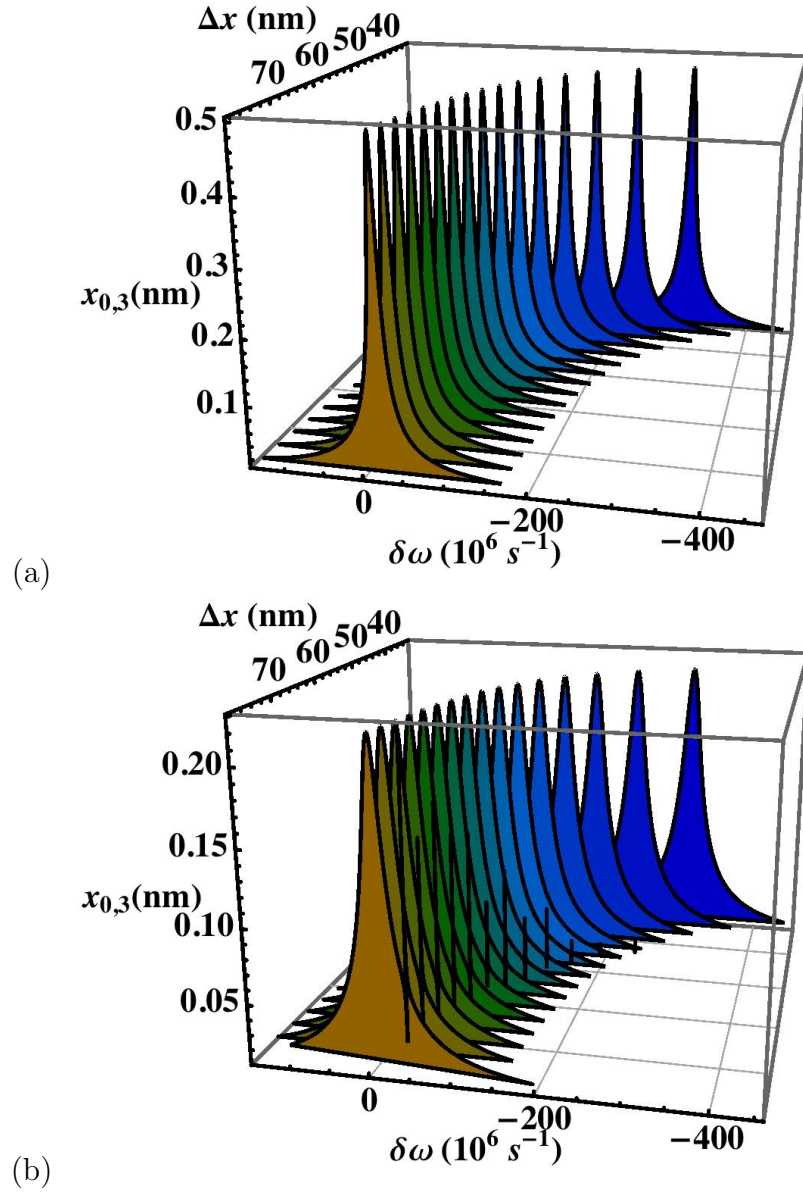


Figure 3.2: The amplitude response in z -direction of two emitters in (a) free space (b) and placed at a distance of $\Delta z = 100\text{nm}$ from the metal interface and separated a distance Δx from each other. Both emitters are driven in the z -direction by an electric field that is detuned by $\delta\omega$ from a resonance frequency of $\omega_0 = 2.36 \times 10^{15}\text{s}^{-1}$.

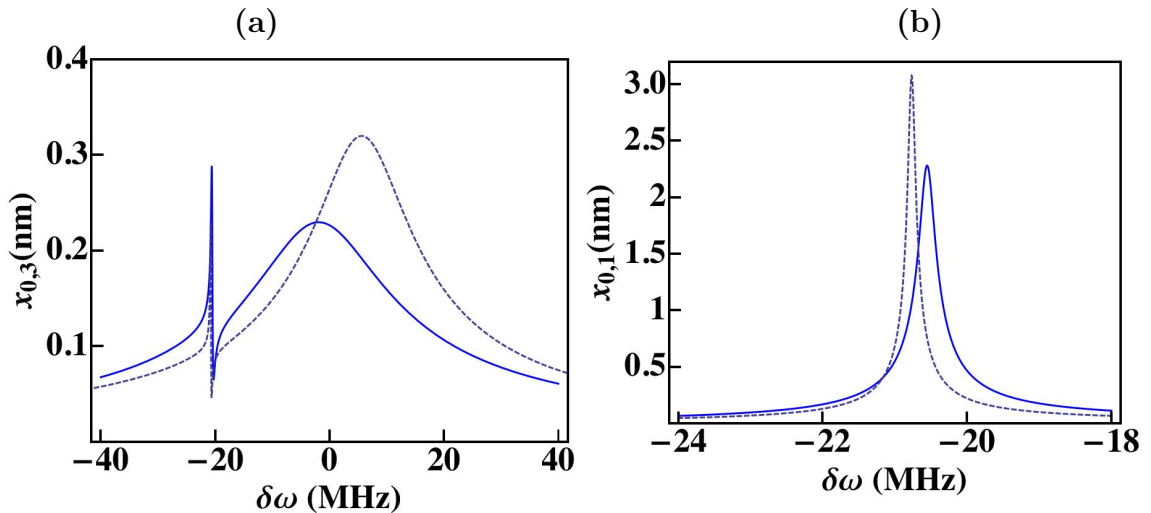


Figure 3.3: The z -amplitude $x_{0,3}$ (a) and x -amplitude $x_{0,1}$ (b) of two emitters near a metal film (solid line) and a perfect mirror (dashed line). The emitters are driven by a field that is detuned by $\delta\omega$. They are separated by $\Delta x = 80\text{nm}$ from each other and $\Delta z = 100\text{nm}$ from the metal interface.

$\Delta x = 80\text{nm}$ between the scatterers.

The origin of the secondary resonance is the reflection of light emitted by one oscillator from the interface and its subsequent absorption by the other oscillator. In free space light emitted by one oscillator necessarily has the same polarization as the external driving field. Therefore, the emitters are collectively oscillating along the z -direction. However, light that is reflected by the interface can have a different polarization. In the case under consideration it induces a coupling between the x - and z -components of the oscillators; mathematically this is related to the G_{13} terms in Eq. (3.11).

Figure 3.3(b) indicates that at the secondary resonance the dipole orientation changes from normal to almost parallel to the interface. Because the two dipoles are

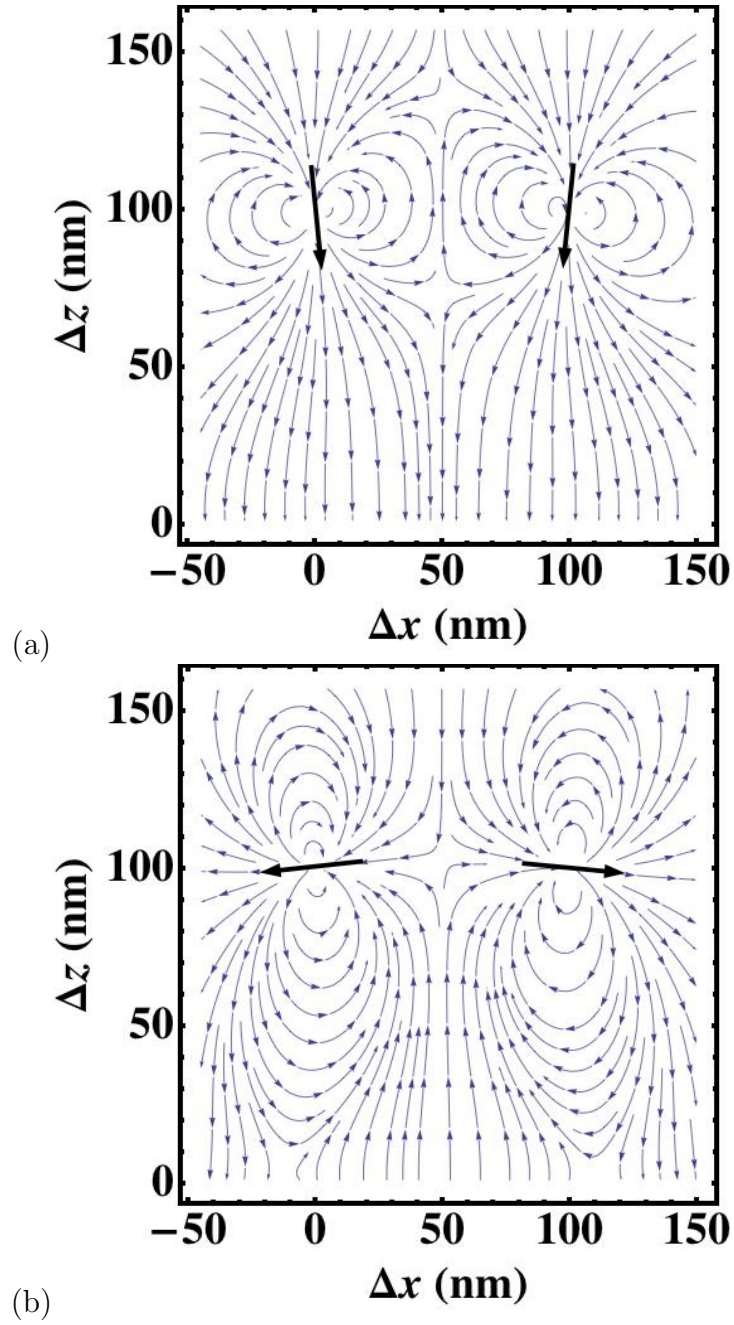


Figure 3.4: Electric field lines in the near field of two dipoles driven on the primary resonance (a), and the secondary resonance (b) near a metal interface at $z = 0$. The bold arrows indicate the dipole location and orientation of the emitters.

nearly anti-parallel to each other their emitted radiation interferes destructively. This implies that the system changes from superradiant behaviour around the primary resonance to a subradiant behaviour around the secondary resonance. Figure 3.4 displays the electric near-field and the dipole orientation at the two resonances. An intuitive explanation of the secondary resonance can be given as follows. For most driving field frequencies the coupling between the x and z components of the oscillators is weak. However, at the resonance frequency of sub-radiant modes this coupling can transfer most of the energy of the oscillator from the z to the x components because the latter only lose very little energy energy through radiative emission and thus decay slowly. The secondary resonance therefore has to be narrow because its linewidth is inversely proportional to the large decay time of the x -oscillations.

To improve our understanding we compare in Figs. 3.3(a) and (b), a numerical evaluation of the oscillation amplitudes for two emitters near the metal film with a corresponding calculation for two emitters near a perfect mirror. The latter case can be described by taking the dielectric constant ϵ_2 of the metal film to be infinite, which corresponds to a perfect conductor. While the mirror images explain the qualitative features very well, the narrow resonance is greater in the case of the mirror. We attribute this difference to the existence of surface plasmons, which are not present in the case of a perfect mirror. The dispersion and decay of surface plasmons cause the emitter energy to be dissipated more quickly and this is represented by a corresponding decrease and broadening in the narrow resonance.

With increasing distance from the interface the narrow resonance falls off exponentially because of the decreasing strength of the reflected near field at the interface. Presumably for the same reason the resonance frequencies are shifted by a larger

amount near the metal film.

3.3 Collective decay of classical emitters

We model the collective decay of initially excited oscillators near the interface by assuming that there is no driving field and that the emitters perform a simple damped harmonic motion $\mathbf{x}^{(j)}(t) = \mathbf{x}^{(j)}(0)e^{-i\omega t - \Gamma t}$, with ω and Γ the collective oscillation frequency and decay rate, respectively. Using Eq. (3.10), we can transform Eq. (3.1) into a transcendental equation for the collective parameters ω and Γ ,

$$[(\Gamma + i\omega)^2 + \omega_0^2] \mathbf{x}^{(j)}(t) = -\frac{\mu_0 q^2}{m} (\Gamma + i\omega)^2 \sum_{i=1}^N \mathbf{x}^{(i)}(t) \mathbf{G}(\mathbf{r}^{(j)}, \mathbf{r}^{(i)}, \omega - i\Gamma). \quad (3.12)$$

For optical emission it is safe to assume that $\Gamma \ll \omega$, i.e., the duration of the emitted light pulse is much longer than the inverse frequency. Because $\mathbf{G}(\mathbf{r}^{(j)}, \mathbf{r}^{(i)}, \omega)$, is a meromorphic function of Ω in the lower half plane, and because its poles are determined by the properties of the metal interface and are unrelated to Γ , we can approximate $\mathbf{G}(\mathbf{r}, \mathbf{r}^{(j)}, \omega - i\Gamma)$ by $\mathbf{G}(\mathbf{r}, \mathbf{r}^{(j)}, \omega - i\epsilon)$, where $\epsilon > 0$ is infinitesimally small. This reduces the transcendental equation (3.12) to a linear eigenvalue problem

$$\left[(i\Gamma + \delta)\mathbb{1} - \frac{\mu_0 q^2 \omega_0}{2m} \sum_{i=1}^N \mathbf{G}(\mathbf{r}^{(j)}, \mathbf{r}^{(i)}, \omega) \right] \mathbf{x}^{(i)}(0) = 0, \quad (3.13)$$

with frequency shift $\delta \equiv \omega_0 - \omega \ll \omega_0$. The decay parameter Γ and the frequency shift δ relate to the imaginary and real part of the eigenvalue problem (3.13), respectively. Generally, Γ characterizes the collective decay rate of the all oscillators.

3.3.1 Decay rate

It is instructive to first study the decay of a single oscillator $\mathbf{x}(t)$ at position \mathbf{r} . In free space the Green's function takes the form [96]

$$\mathbf{G}(\mathbf{r}, \mathbf{r}, \omega) = \left(G' + i \frac{\omega_0}{6\pi c} \right) \mathbb{1}. \quad (3.14)$$

The real part G' is related to the Lamb shift of atomic resonance lines. It is formally divergent and would need to be renormalized [70]. However, because we are only interested in the decay rate, we can ignore the line shift and assume it is absorbed in the definition of the detuning. Because the Lamb shift is much smaller than the optical resonance frequency this will result in an excellent approximation for the decay rate. As we are dealing with free space, the matrix in Eq. (3.13) is proportional to the identity and the corresponding eigenvalue problem is trivially solved and yields the well-known decay rate of a single oscillator,

$$\Gamma_0 = \frac{\mu_0 q^2 \omega_0}{2m} \text{Im} G_{\mu\mu}(\mathbf{r}, \mathbf{r}, \omega_0) \quad (3.15)$$

$$= \frac{\mu_0 q^2 \omega_0^2}{12\pi m c}. \quad (3.16)$$

The decay rate near the interface can be derived in a similar way as long as Γ is much smaller than the optical frequency and varies little for frequency variations on the order of the Lamb shift. These assumptions should be satisfied as long as the emitter is not too close to the interface. We remark, however, that these approximations are not universally valid and fail in the case of photonic band gap materials [97], for instance. The Green's function $G_{\mu\nu}(\mathbf{r}, \mathbf{r}, \omega)$ evaluated at a single point \mathbf{r} near the interface is diagonal in Cartesian coordinates (see App. A). We therefore can use Eq. (3.15) to find the decay rate.

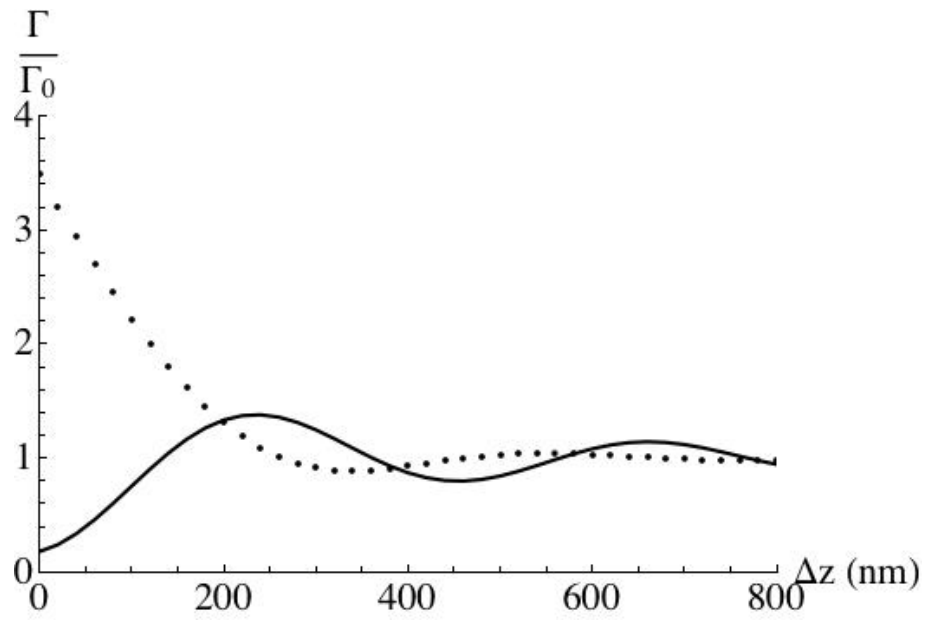


Figure 3.5: The decay rate of a single oscillator placed within the vicinity of a thin metal film, at a separation distance of Δz . The decay rates are given for a dipole oriented parallel (solid) and perpendicular (dotted) relative to the plane of the interface.

Fig. 3.5 depicts the decay rate of an emitter as a function of the distance Δz of the emitter from the metal film as illustrated in Fig. 3.1. It demonstrates that the decay rate is enhanced (suppressed) if the emitter oscillates perpendicular (parallel) to the interface, respectively. This can be understood using the concept of mirror images with each emitter considered as an electric dipole. If a dipole is oriented perpendicular to the interface, its mirror image is in phase and thus can enhance the emission of the dipole. On the other hand, dipoles that oscillate in the plane of the interface have mirror images that are 180° out of phase so that the radiation reaction causes damping of the dipole. Hence, if the mirror images were composed of real charges these two situations would just correspond to superradiant and subradiant collective emission of two emitters, respectively.

The energy lost by emitters during the decay is partly used to heat the metal (non-radiative decay). Another significant part is turned into radiation that couples to surface plasmons that then propagates into the prism. This radiative coupling is the reciprocal process of illuminating the metal film at the surface plasmon resonance angle and exciting an emitter. An excited emitter thus couples radiation into a narrow solid angle, with a corresponding increase in radiation intensity. Furthermore, the coupling of an emitter to surface plasmons only occurs in directions in which TM waves are generated. In Figure 3.6 we show the intensity pattern for an emitter that is oriented in the x -coordinate direction parallel to the metal film in the $x - y$ plane. In the y direction, perpendicular to the emitter orientation, TE waves are generated and a corresponding minimum in the transmitted radiation is detected.

We now turn to the collective decay of $N > 1$ emitters. In this case there are $3N$ eigenstate solutions of Eq. (3.13). Fig. 3.7 displays four out of 24 numerically

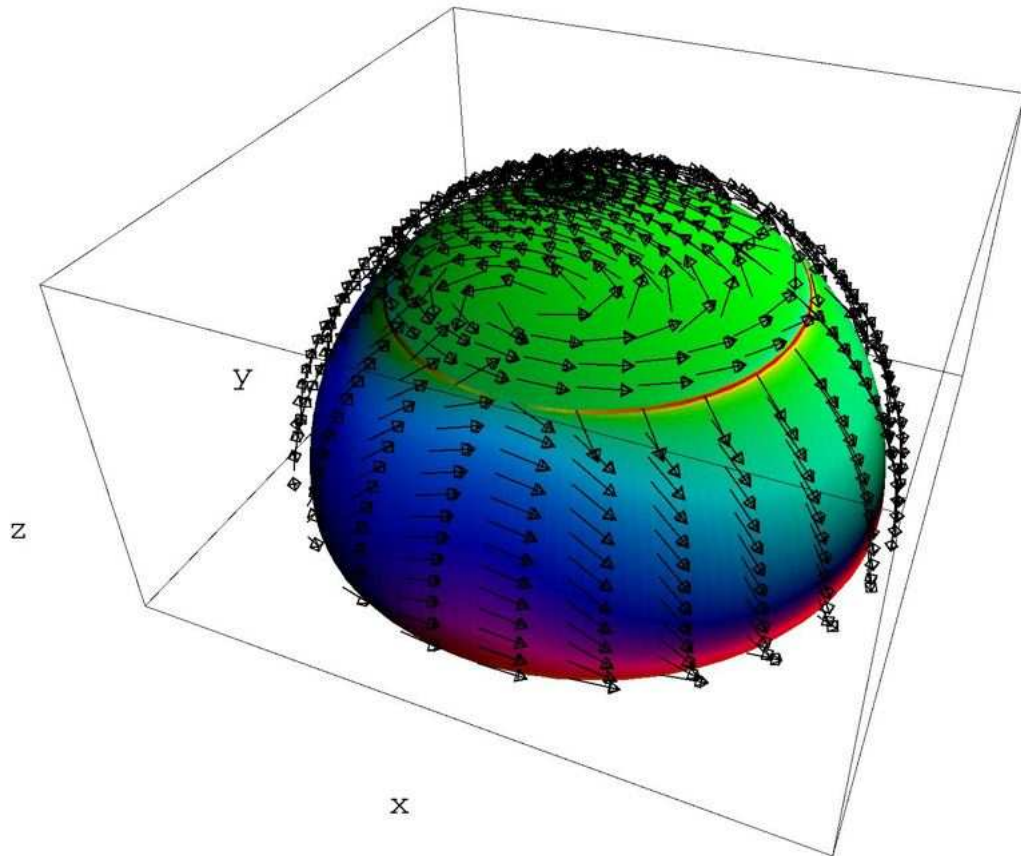


Figure 3.6: The intensity profile of an emitter oriented parallel to the interface in the positive x -coordinate, combined with arrows indicating the electric field direction. The intensity scales from low (blue) to high (red). The red hues near the equator are numerical artifacts.

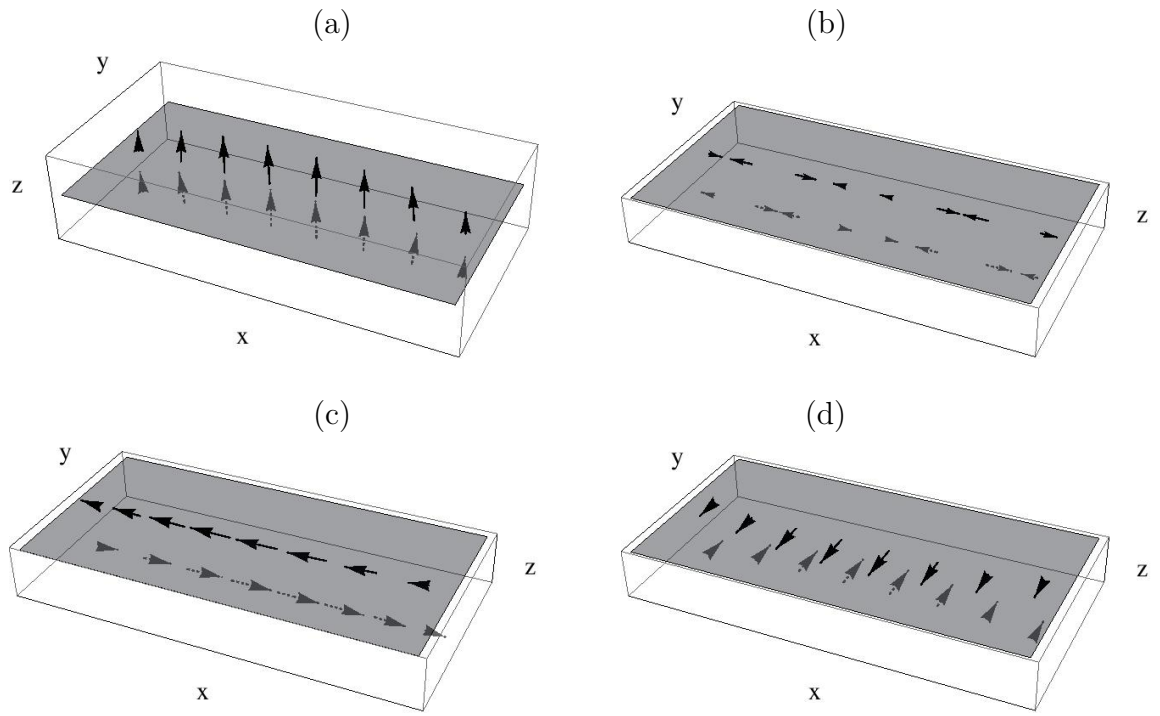


Figure 3.7: Four different collective eigenmodes: (a) superradiant mode, (b) subradiant mode, (c) and (d) are suppressed superradiant modes for which all real dipole moments are in phase but all mirror images are out of phase. Shown is the orientation of the dipole moment for real emitters (above the interface) and their mirror images (dashed, below the interface).

determined eigenmodes for $N = 8$ which each are examples for a particular collective behaviour. In free space a state where all emitters oscillate in phase and in the same direction is superradiant. The presence of the interface breaks the axial symmetry and oscillations in the plane of the interface are suppressed because the corresponding mirror images trigger subradiant behaviour. Fig. 3.7(a) shows the superradiant mode where the emitters oscillate in phase along the z-axis. In this case their mirror images are also in phase and enhance the radiation intensity. Fig. 3.7(b) shows a subradiant mode where the emitted fields of the individual emitters interfere destructively. Fig. 3.7(c) and (d) display a very different state which we call suppressed superradiant states. All oscillators are in phase and in free space it would be a superradiant state. However, the mirror images are out of phase so that the intensity of the emitted radiation is strongly reduced as compared to the superradiant state. In Fig. 3.9(a), which will be discussed below, we display the collective decay rate of these modes as a function of the number of oscillators.

3.3.2 Far-field radiation

A simple way to learn about the dynamics of a collection of emitters is to observe their emission pattern in the far field. The radiation intensity is determined by the (time averaged) Poynting vector

$$\mathbf{S}(\mathbf{r}, t) = \frac{1}{2\mu_0 c} |\mathbf{E}(\mathbf{r}, t)|^2 \hat{\mathbf{r}}. \quad (3.17)$$

The electric field of each emitter is determined by Eq. (3.6) and the total field $\mathbf{E}(\mathbf{r}, t)$ is the superposition of the individual fields. To evaluate Eq. (3.6) in the far field we have to compute the radiative Green's function (2.22) in the far-field limit,

$kr \rightarrow \infty$, which can be accomplished using the method of stationary phase described in Appendix B.

For a source in the region $z' > d$ and observation of the field at position \mathbf{r} in the region $z < 0$, the dyadic Green's function can be approximated as

$$G_{\mu\nu}(\mathbf{r}, \mathbf{r}', \omega) = \frac{i}{2\pi} \left(\frac{k_1 z}{r r'} \right) e^{ik_1 r} e^{-ik_1 \sin \phi (\cos \theta x' + \sin \theta y')} \\ \times \tilde{G}_{\mu\nu}(k_1 \sin \phi \cos \theta, k_1 \sin \phi \sin \theta, \omega; z'), \quad (3.18)$$

with the unwieldy coefficients $\tilde{G}_{\mu\nu}$ defined in Eqs. (A.41) - (A.49). A similar expression can be derived for an observation point in region 3. The direction from the emitters to the observation point is given by $(\sin \phi \cos \theta, \sin \phi \sin \theta, \cos \phi)$. The radiation profiles are determined from the positive frequency components of the electric field in the far field. For emitters that are equidistant from the interface, the Poynting vector can be represented as

$$|\mathbf{S}(\mathbf{r}, \mathbf{t})| = \frac{\mu_0 \omega^4}{8\pi^2 c} \left(\frac{kz}{r^2} \right)^2 |\tilde{G}_{\mu\nu}(k_i \sin \phi \cos \theta, k_i \sin \phi \sin \theta, \omega; z')|^2 \\ \times \left| \sum_i^N e^{-ik \sin \phi (\cos \theta x^{(i)} + \sin \theta y^{(i)})} e^{-\Gamma t} x^{(i)} \right|^2, \quad (3.19)$$

with $j = 1, 3$ for the observation point in region 1 or 3, respectively.

The last term is the relevant phasing term which determines the N^2 -gain in intensity that is associated with superradiance. The superradiant decay modes must be in phase, i.e., $k \sin \phi (\cos \theta x^{(i)} + \sin \theta y^{(i)}) + \arg(x_{\mu}^{(i)}) = n_i 2\pi$ for each emitter i , then the sum becomes proportional to N^2 . In other words, constructive interference between the emitted radiation of all emitters is one condition for observing superradiance.

The transmitted radiation profile (3.19) for the superradiant state in the plane of the emitters ($\theta = 0$) is illustrated in Fig. 3.8 for a linear arrangement of 8 emitters

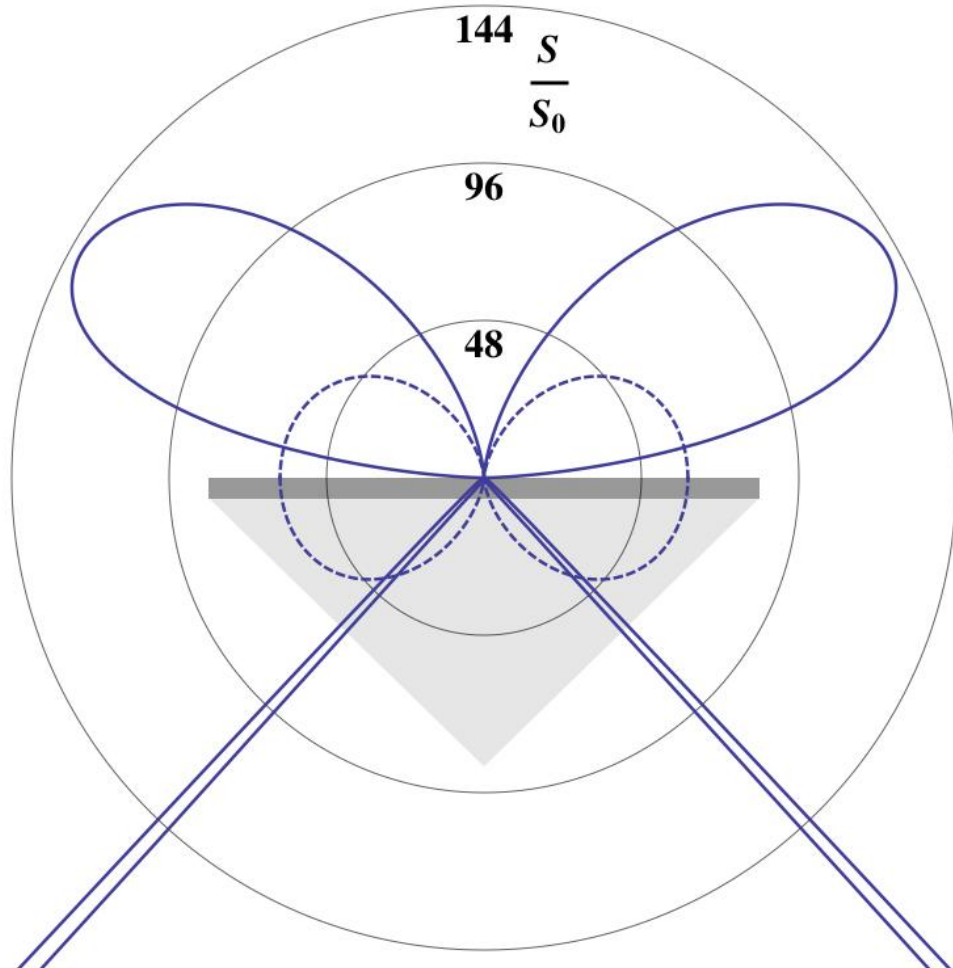


Figure 3.8: The far-field emission pattern of 8 oscillators in the superradiant mode at a distance of $\Delta z = 200\text{nm}$ from the interface (solid) and in free space (dashed). Shown is the ratio of the radiation intensity S and the maximum intensity S_0 produced by a single emitter in free space. The emitters are placed parallel to the horizontal axis.

periodically separated within a distance of $\lambda/2$, with $\lambda = 800\text{nm}$ and $\omega = 2\pi c/\lambda$. The dashed curve shows the emission pattern in free space. For perfect superradiance its maximum intensity (along the horizontal axis) should scale like $S = AN^2S_0$, with S_0 is the maximum intensity for a single emitter in free space and with the superradiance prefactor $A = 1$ in free space. Because the outermost oscillators are a distance $\lambda/2$ apart so that their emitted fields are out of phase, the N^2 scaling is only roughly fulfilled.

For emitters near the interface (solid curve in Fig. 3.8) surface plasmons lead to the narrow but extremely large peaks in the lower half of Fig. 3.8 at the plasmon resonance angle with a width of about 0.01 radian. Emission into the radiative modes around this peak is superradiant (see below) with $A \approx 240$. The value of A depends on the separation distance of the emitters from the interface and the Fresnel coefficient $\tilde{T}_{3,2}^{\text{TM}}$ defined in Appendix A. A will decrease exponentially as the separation distance between emitter and interface increases due to decreased near field coupling of the emitter to surface plasmon modes. For given dielectric constants ε_i and emission wavelength λ there is an optimum film thickness for which A is maximized. The values used in this paper correspond to an optimum film thickness of 56nm for $\lambda = 800\text{nm}$. Hence, the radiation from multiple emitters transmitted into the surface plasmon resonance angle (the spikes in Fig. 3.8) combines the enhancement A and the N^2 gain of superradiance. For the case $N = 8$ the peaks have a maximum of almost 15000 times the maximum intensity S_0 for a single emitter in free space.

3.3.3 Suppressed superradiance

We conclude this section with a discussion of the main indicators for superradiance in the superradiant and the suppressed superradiant states. In Fig. 3.9(a) we display the scaling of the collective decay parameter with the number of oscillators, which is a measure for how strongly light emitted from one oscillator can drive emission from another oscillator. Because of the growing size of the arrangement of oscillators, which varies from 50 nm for $N = 2$ to 550 nm for $N = 12$, we expect superradiant phenomena to decrease with N . This is indeed the case for the superradiant state (circles), but for the suppressed superradiant states collective decay ($\Gamma \sim N$) (triangles and squares) is preserved.

Interestingly, we observe the opposite situation with respect to the N^2 dependence of the peak intensity at the surface plasmon resonance angle, which is shown in Fig. 3.9(b). For the superradiant state the peak intensity can well be described by $S \approx AN^2S_0$, indicating constructive interference of the emitted radiation despite the growing size of the sample. For the suppressed superradiant states the ability to constructively interfere depends on the dipole orientation: the N^2 scaling is significantly affected only if the dipoles are aligned as in Fig. 3.7(c).

Clearly the two suppressed superradiant states fulfill the criteria for superradiance as well, or better, than the superradiant state itself. We use the notion “suppressed” to characterize their behaviour because their decay rate is reduced by a factor of 6 and their peak intensity by a factor of 25 as compared to the superradiant state. We can understand suppressed superradiant behavior by considering each dipole and its mirror image as one entity. The dipole moment of this entity vanishes, but

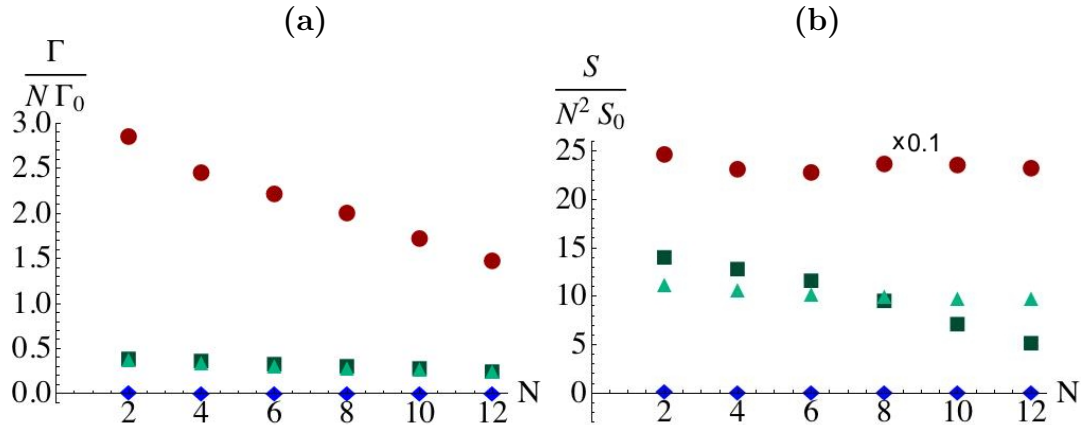


Figure 3.9: (a) Scaling of the collective decay rate with the number N of oscillators. Circles correspond to the superradiant mode, squares and triangles to the suppressed superradiant modes displayed in Fig. 3.7 (c) and (d), respectively, and diamonds to the subradiant mode displayed in Fig. 3.7 (b). The distance between adjacent oscillators is 50 nm. Each oscillator is a distance $\Delta z = 100\text{nm}$ away from the interface. In (b) the scaling of the maximum intensity of the peak at the surface plasmon resonance angle with the number N of oscillators. In the superradiant case the results are reduced by a factor of 10 for presentational purposes.

it can emit (a weaker) quadrupole radiation. Because all N quadrupoles are in phase their emitted fields interfere constructively and the intensity scales like N^2 . Furthermore, similar to how a neighbouring dipole in phase can increase the decay rate, a quadrupole can drive the neighbour when in phase. Hence, the suppressed superradiant state can be considered a superradiant state for quadrupoles.

The different behaviour of the states of Fig. 3.7 can be understood by considering the mirror images as real charges. For suppressed superradiant states the spatial size of each quadrupole, $2\Delta z = 200\text{nm}$, is larger than the distance $\Delta x = 50\text{nm}$ between

adjacent quadrupoles. Hence, they interact with their respective near field so that cooperative decay can still grow like N . On the other hand, for the superradiant state each dipole interacts with the far field of other dipoles so that the deviation from the linear scaling with N is more pronounced, albeit the overall interaction energy is much larger.

The N^2 scaling of the peak intensity can be understood by taking into account that the maximum peak appears at the surface plasmon resonance angle, i.e., in a direction that is different from the axis along which the oscillators are aligned. Generally, surface plasmons can only be generated in the direction of the polarization of the emitted radiation because it is the latter's electric field that generates electron density oscillations. For the suppressed superradiant state 3.7(c) there are significant deviations from the N^2 law because the dipoles oscillate in the plane of the interface parallel to the x -axis. This means that most radiation is emitted into a surface plasmon mode that propagates in the x -direction, but in this direction phase variations have a very pronounced effect. For the suppressed superradiant state 3.7(d), as for the superradiant state, most radiation is emitted into a plasmon that propagates in the y -direction, i.e., parallel to the alignment of emitters. Therefore their emitted radiation fields can still constructively interfere.

3.4 Summary

In this paper we give a detailed account of how super- and sub-radiant emission by oscillating dipoles is affected by surface plasmons. It was shown that the interface generates an indirect coupling between the emitters through light that is reflected by

the interface. In the superradiant mode the peak intensity of the emitted radiation is two orders of magnitude larger than a similar arrangement of emitters in free-space. The decay rate of the system is increased by the presence of mirror dipoles at the interface. Applying a driving field to the emitters can induce super- and sub-radiant emitter modes by a suitable choice of frequency.

The collective decay eigenmodes of initially excited oscillators showed that certain modes, which naively would be expected to behave in a sub-radiant fashion, are actually superradiant modes, albeit with a strongly suppressed overall intensity. These suppressed superradiant modes are also a consequence of the additional coupling between oscillators that is generated by the interface. An intuitive picture explains this effect as superradiance of quadrupole radiation.

Chapter 4

Quantum Theory of Atom Field Coupling Near Absorbing Dielectrics

To develop a full quantum theory of light-atom interactions in the presence of surface plasmons, both the atom and electromagnetic field need to be quantized. Because surface plasmons require an absorbing and dispersive medium, theoretical predictions will be inaccurate if losses are not appropriately accounted for. When a photon is absorbed into a lossy medium, additional noise is generated. To account for this noise, the electromagnetic field operators must contain information about the losses.

In this chapter, we first review a Green's function approach to the quantization of the electromagnetic field in Sec. 4.1, where the usual creation operators of the field are coupled to the medium to create a new bosonic field operator. In Sec. 4.2 we then derive the equations of motion for the new field operators interacting with an atom, which is modeled as a quantized harmonic oscillator.

4.1 Field quantization

To describe the quantization of the radiation field in the presence of absorbing dielectrics, we use a Green's function method [96, 88]. The losses appear in the Maxwell equations as a coupling of the electromagnetic field to phenomenological noise currents. These noise currents are related to the canonical variables that are used to describe the field dynamics. We begin with Maxwell's equations in operator form

and frequency domain,

$$\nabla \cdot \hat{\mathbf{B}}(\mathbf{r}, \omega) = 0, \quad (4.1)$$

$$\nabla \times \hat{\mathbf{E}}(\mathbf{r}, \omega) = i\omega \hat{\mathbf{B}}(\mathbf{r}, \omega), \quad (4.2)$$

$$\nabla \times \hat{\mathbf{B}}(\mathbf{r}, \omega) = -i\frac{\omega}{c^2}\epsilon(\mathbf{r}, \omega)\hat{\mathbf{E}}(\mathbf{r}, \omega) + \mu_0\hat{\mathbf{j}}(\mathbf{r}, \omega), \quad (4.3)$$

$$\nabla \cdot \left(\epsilon_0\epsilon(\mathbf{r}, \omega)\hat{\mathbf{E}}(\mathbf{r}, \omega) \right) = \hat{\rho}(\mathbf{r}, \omega), \quad (4.4)$$

where the dielectric permittivity is a complex function of position and frequency given by $\epsilon(\mathbf{r}, \omega) = \epsilon'(\mathbf{r}, \omega) + i\epsilon''(\mathbf{r}, \omega)$. As a result of the analytical properties of the electric field and the fluctuation-dissipation theorem, the real and complex parts are related by the Kramers-Kronig relations to ensure causality [98]. The (positive-frequency part of the) electric field operator $\hat{\mathbf{E}}(\mathbf{r}, \omega)$ is determined from the inhomogeneous wave equation

$$\left(-\frac{\omega^2}{c^2}\epsilon(\mathbf{r}, \omega) + \nabla \times \nabla \times \right) \hat{\mathbf{E}}(\mathbf{r}, \omega) = i\omega\mu_0\hat{\mathbf{j}}(\mathbf{r}, \omega). \quad (4.5)$$

The solution can be expressed in terms of the retarded dyadic Green's function $\mathbf{G}(\mathbf{r}, \mathbf{r}', \omega)$ given by Eq. (3.4)

The Green's function then describes the retarded coupling between the noise current operator and the electromagnetic field. Solving the Green's function is essentially a classical problem. We use the same Kretschmann configuration of dielectrics as in Chapter 3, where the Green's function details are contained in Appendix A [99].

Once the Green's function is known, all propagation modes for electromagnetic radiation are accounted for, and the frequency component of the electric field oper-

ator is expressed as

$$\hat{\mathbf{E}}(\mathbf{r}, \omega) = i\omega\mu_0 \int d^3\mathbf{r}' \mathbf{G}(\mathbf{r}, \mathbf{r}', \omega) \hat{\mathbf{j}}(\mathbf{r}', \omega), \quad (4.6)$$

and the magnetic induction as

$$\hat{\mathbf{B}}(\mathbf{r}, \omega) = (i\omega)^{-1} \nabla \times \hat{\mathbf{E}}(\mathbf{r}, \omega). \quad (4.7)$$

The dynamic variables in this quantization method are bosonic field operators $\hat{\mathbf{f}}$, which are related to the noise current term $\hat{\mathbf{j}}$ through

$$\hat{\mathbf{j}}(\mathbf{r}, \omega) = \omega \sqrt{\frac{\hbar\epsilon_0}{\pi}} \epsilon''(\mathbf{r}, \omega) \hat{\mathbf{f}}(\mathbf{r}, \omega). \quad (4.8)$$

The field operators are given as

$$\hat{\mathbf{E}}(\mathbf{r}) = \int_0^\infty d\omega \hat{\mathbf{E}}(\mathbf{r}, \omega) + \text{H. c.} \quad (4.9)$$

$$\hat{\mathbf{B}}(\mathbf{r}) = \int_0^\infty d\omega \hat{\mathbf{B}}(\mathbf{r}, \omega) + \text{H. c.} \quad (4.10)$$

The Hamiltonian of the coupled electromagnetic field is

$$\hat{H}_{\text{EM}} = \int d^3\mathbf{r} \int_0^\infty d\omega \hbar\omega \hat{\mathbf{f}}^\dagger(\mathbf{r}, \omega) \hat{\mathbf{f}}(\mathbf{r}, \omega), \quad (4.11)$$

and can be used to derive Maxwell's equations from the Heisenberg equations of motion. The field operators obey the commutation relations

$$\left[\hat{\mathbf{f}}(\mathbf{r}, \omega), \hat{\mathbf{f}}^\dagger(\mathbf{r}', \omega') \right] = \delta(\mathbf{r} - \mathbf{r}') \delta(\omega - \omega') \mathbb{1}, \quad (4.12)$$

$$\left[\hat{\mathbf{f}}^{(\dagger)}(\mathbf{r}, \omega), \hat{\mathbf{f}}^{(\dagger)}(\mathbf{r}', \omega') \right] = 0. \quad (4.13)$$

Using the field variables \mathbf{f} to describe the quantization guarantees that all equal-time commutation relations are preserved for absorbing media.

A useful and important result derived from Eq. (3.4) is the integral relation

$$\int d^3\mathbf{x} \frac{\omega^2}{c^2} \epsilon''(\mathbf{r}', \omega) \mathbf{G}(\mathbf{r}, \mathbf{x}, \omega) \mathbf{G}^*(\mathbf{x}, \mathbf{r}', \omega) = \text{Im} \mathbf{G}(\mathbf{r}, \mathbf{r}', \omega), \quad (4.14)$$

which frequently appears in commutators involving the electromagnetic field operators.

4.1.1 Commutation relations and vacuum correlations

The equal time commutation relations for the electric field and magnetic induction can be shown to give the free space commutation relations [100],

$$\left[\hat{E}_i(\mathbf{r}), \hat{E}_j(\mathbf{r}') \right] = 0 = \left[\hat{B}_i(\mathbf{r}), \hat{B}_j(\mathbf{r}') \right] \quad (4.15)$$

$$\left[\hat{E}_i(\mathbf{r}), \hat{B}_j(\mathbf{r}') \right] = -i \frac{\hbar}{\epsilon_0} \epsilon_{jkl} \partial_k \delta(\mathbf{r} - \mathbf{r}'), \quad (4.16)$$

by using Eq. (4.6) and Eqs. (4.7). The general expression for commutation relation between $\hat{\mathbf{E}}(\mathbf{r})$ and $\hat{\mathbf{B}}(\mathbf{r})$ after using Eq. (4.14) gives

$$\left[\hat{E}_i(\mathbf{r}), \hat{B}_j(\mathbf{r}') \right] = \frac{\hbar}{\pi \epsilon_0} \epsilon_{jkl} \partial_k \int_{-\infty}^{\infty} d\omega \frac{\omega}{c^2} G_{il}(\mathbf{r}, \mathbf{r}', \omega). \quad (4.17)$$

The effect of the physical environment on vacuum noise is given by the correlation function

$$\begin{aligned} \langle 0 | \hat{E}_i(\mathbf{r}, \omega) \hat{E}_i^\dagger(\mathbf{r}', \omega') | 0 \rangle &= \langle 0 | \left[\hat{E}_i(\mathbf{r}, \omega), \hat{E}_i^\dagger(\mathbf{r}', \omega') \right] | 0 \rangle \\ &= \frac{\hbar}{\pi \epsilon_0} \left(\frac{\omega}{c} \right)^2 \text{Im} G_{ii}(\mathbf{r}, \mathbf{r}', \omega) \delta(\omega - \omega'). \end{aligned} \quad (4.18)$$

Equation (4.18) relates the vacuum fluctuations of the electromagnetic field to the imaginary part of the Green's function. Because the Green's function describes how fields of a given frequency ω are distributed, the Green's function and hence the vacuum fluctuations are related to the density of states [101]. Furthermore, the statistical fluctuations are related to the dielectric constant $\epsilon(\mathbf{r}, \omega)$ of the medium.

4.2 Light interactions with a quantum oscillator

The quantization of the electromagnetic field in Sec. (4.1) leads to a description of light coupled to an absorbing medium. To describe the evolution of individual atoms in the presence of the medium assisted electromagnetic field, we need to describe the atom-light interaction. In this thesis, the atoms are modeled as harmonic oscillators where oscillating electrons are bound by a heavier positively charged nucleus. For a stationary nucleus, the non-relativistic Hamiltonian for an oscillating electron of charge q_{charge} and mass m is given as

$$\hat{H}_A = \frac{\hat{p}^2}{2m} + \frac{1}{2}m\omega_0\hat{x}^2, \quad (4.19)$$

where \hat{p} and \hat{x} are the canonical momentum and coordinate operators respectively, with an oscillation frequency of ω_0 . Defining the harmonic oscillator annihilation operator as \hat{b} , the position and momentum operator in the annihilation operator basis are then given by

$$\hat{x} = \sqrt{\frac{\hbar}{2m\omega_0}} (\hat{b}^\dagger + \hat{b}), \quad (4.20)$$

$$\hat{p} = i\sqrt{\frac{\hbar m\omega_0}{2}} (\hat{b}^\dagger - \hat{b}). \quad (4.21)$$

The emitter's Hamiltonian is then expressed as

$$\hat{H}_A = \hbar\omega_0\hat{b}^\dagger\hat{b}, \quad (4.22)$$

with energy eigenvalues $E_n = n\hbar\omega_0$.

Provided that the radiation wavelength is much larger than the electron displacement from the nucleus, such that light cannot distinguish the individual charges, the

atom-light interaction can be described using electric dipole coupling. The atomic dipole operator is given by

$$\hat{\mathbf{d}} = q_{\text{charge}} \hat{x} \hat{\mathbf{e}}, \quad (4.23)$$

where $\hat{\mathbf{e}}$ is the oscillation direction of the electron. The coupling of the emitter to the medium-assisted field in the electric dipole approximation produces an interaction term

$$\hat{H}_{\text{int}} = \hat{\mathbf{d}} \cdot \hat{\mathbf{E}}(\mathbf{r}_A). \quad (4.24)$$

The corresponding total Hamiltonian of the atom-light system takes the form

$$\hat{H} = \hat{H}_{\text{EM}} + \hat{H}_A + \hat{H}_{\text{int}}, \quad (4.25)$$

Applying the rotating wave approximation results in the Hamiltonian

$$\bar{H} = \int d^3\mathbf{r} \int_0^\infty d\omega \hbar\omega \hat{\mathbf{f}}^\dagger(\mathbf{r}, \omega) \cdot \hat{\mathbf{f}}(\mathbf{r}, \omega) + \hbar\omega_0 b^\dagger b - \hbar g \left(\hat{b}^\dagger \hat{\mathbf{e}} \cdot \hat{\mathbf{E}}(\mathbf{r}_A) + \hat{\mathbf{e}} \cdot \hat{\mathbf{E}}^\dagger(\mathbf{r}_A) \hat{b} \right), \quad (4.26)$$

where

$$g \equiv \frac{q_{\text{charge}}}{\hbar} \sqrt{\frac{\hbar}{2m\omega_0}} \quad (4.27)$$

is the coupling constant between field and emitter.

4.2.1 Heisenberg equations of motion

The operators of the atom-field system evolve dynamically according to the Heisenberg equations of motion

$$i\hbar\partial_t \hat{O} = [\hat{O}, \hat{H}]. \quad (4.28)$$

The equation of motion for the bosonic field operators, upon using the commutation relation Eq. (4.12) and the Hamiltonian Eq. (4.26), are found to be

$$\partial_t \hat{\mathbf{f}}(\mathbf{r}, \omega, t) = -i\omega \hat{\mathbf{f}}(\mathbf{r}, \omega, t) + ig \left[\hat{\mathbf{f}}(\mathbf{r}, \omega), \hat{\mathbf{E}}^\dagger(\mathbf{r}_A) \cdot \mathbf{e} \right] \hat{b} \quad (4.29)$$

and likewise for the harmonic oscillator

$$\partial_t \hat{b} = -i\omega_0 \hat{b} + ig \mathbf{e} \cdot \hat{\mathbf{E}}(\mathbf{r}_A, t). \quad (4.30)$$

The two equations of motion Eq. (4.30) and (4.29) are coupled first-order differential equations that fully describe light interactions with an emitter near an absorbing dielectric. Due to the non-diagonal elements of the Green's function, separating and fully solving the two equations can be difficult. The system dynamics for an initially excited atom has been solved using the Markov approximation [96]. In this thesis, we wish to describe a system involving an initial photon pulse.

We will use a Laplace transformation to algebraically separate the first-order differential equations. After this transformation the equations of motion take the form

$$\hat{\mathbf{f}}(\mathbf{r}, \omega, s) = \frac{1}{s + i\omega} \left(\hat{\mathbf{f}}(\mathbf{r}, \omega) + ig \left[\hat{\mathbf{f}}(\mathbf{r}, \omega), \hat{\mathbf{E}}^\dagger(\mathbf{r}_A) \cdot \mathbf{e} \right] \hat{b}(s) \right), \quad (4.31)$$

$$\hat{b}(s) = \frac{1}{s + i\omega_0} \left(\hat{b}_0 + ig \mathbf{e} \cdot \hat{\mathbf{E}}(\mathbf{r}_A, s) \right), \quad (4.32)$$

where the operators taken at $t = 0$, $\hat{\mathbf{f}}(\mathbf{r}, \omega)$ and \hat{b}_0 , are the usual Schrödinger operators. By using Eq. (4.6), the commutator in Eq. (4.31) becomes

$$\begin{aligned} \left[\hat{f}_i(\mathbf{r}, \omega), \hat{\mathbf{E}}^\dagger(\mathbf{r}_A) \cdot \mathbf{e} \right] &= -i\sqrt{\hbar\pi\epsilon_0} \int_0^\infty d\omega' \int d^3\mathbf{r}' \sqrt{\epsilon''(\mathbf{r}', \omega')} \frac{\omega'^2}{c^2} G_{jk}^*(\mathbf{r}_A, \mathbf{r}', \omega') \\ &\times \left[\hat{f}_i(\mathbf{r}, \omega), \hat{f}_k^\dagger(\mathbf{r}', \omega') \right] e_j \end{aligned} \quad (4.33)$$

$$= -i\sqrt{\frac{\hbar}{\pi\epsilon_0}} \sqrt{\epsilon''(\mathbf{r}, \omega)} \frac{\omega^2}{c^2} G_{ij}^*(\mathbf{r}, \mathbf{r}_A, \omega') e_j. \quad (4.34)$$

Inserting Eq. (4.32) into Eq. (4.7) and using the integral relation (4.14) gives an electric field operator of the form

$$\hat{\mathbf{E}}(\mathbf{r}, s) = \hat{\mathbf{E}}_{\text{free}}(\mathbf{r}, s) + i\mathbf{M}(\mathbf{r}, s)\hat{b}(s). \quad (4.35)$$

$$\hat{\mathbf{E}}_{\text{free}}(\mathbf{r}, s) = \int_0^\infty \frac{d\omega}{s + i\omega} \hat{\mathbf{E}}(\mathbf{r}, \omega) \quad (4.36)$$

$$\mathbf{M}(\mathbf{r}, s) \equiv \frac{\hbar g}{\pi \varepsilon_0} \int_0^\infty \frac{d\omega}{s + i\omega} \frac{\omega^2}{c^2} \text{Im} \mathbf{G}(\mathbf{r}, \mathbf{r}_A, \omega) \cdot \hat{\mathbf{e}}. \quad (4.37)$$

The equation of motion for $\hat{b}(t)$ is coupled to the electric field at the position of the oscillator \mathbf{r}_A . Consequently, the oscillator solution is found to be

$$\hat{b}(s) = \frac{\hat{b}_0 + ig\hat{\mathbf{e}} \cdot \hat{\mathbf{E}}_{\text{free}}(\mathbf{r}_A, s)}{s + i\omega_0 + g\hat{\mathbf{e}} \cdot \mathbf{M}(\mathbf{r}_A, s)}, \quad (4.38)$$

The explicit expression electric field is then found from Eq. (4.35) by inserting the oscillator solution Eq. (4.38),

$$\hat{E}_i(\mathbf{r}, s) = \hat{E}_{\text{free},i}(\mathbf{r}, s) + i\mathbf{M}(\mathbf{r}, s) \frac{\hat{b}_0 + ig\hat{\mathbf{e}} \cdot \hat{\mathbf{E}}_{\text{free}}(\mathbf{r}_A, s)}{s + i\omega_0 + g\hat{\mathbf{e}} \cdot \mathbf{M}(\mathbf{r}_A, s)} \quad (4.39)$$

The first term in the expression describes the free evolution of the radiation field, while the second term consists of radiation emitted from an excited oscillator and free field radiation scattered from the oscillator. To further simplify these expressions, the dynamics of an emitting source, specifically the spontaneous emission of radiation, is considered.

4.2.2 Decay rate and the Lamb Shift

The spontaneous decay rate and frequency shift of a classical emitter are related to the radiative Green's function. By assuming that the excited state amplitude of emitter decays exponentially, the lowest order perturbation is calculated by using

the Wigner-Weisskopf approximation[102]. The explicit expressions of the Lamb shift and decay rate for a quantum oscillator are determined from the Wigner-Weisskopf approximation by replacing $\mathbf{M}(\mathbf{r}_A, s)$ with $\mathbf{M}(\mathbf{r}_A, -i\omega_0)$. Defining two real parameters $\Gamma_{ij}(\mathbf{r}, s)$ and $\Delta_{ij}(\mathbf{r}, s)$ through

$$\Gamma_{ij}(\mathbf{r}, s) + i\Delta_{ij}(\mathbf{r}, s) \equiv \frac{g^2\hbar}{\pi\epsilon_0} \int_0^\infty \frac{d\omega}{s + i\omega} \frac{\omega^2}{c^2} \text{Im}G_{ij}(\mathbf{r}, \mathbf{r}_A, \omega), \quad (4.40)$$

we can reduce the solution to

$$\hat{b} = \frac{1}{s + i\omega'_0 + \gamma} \left(\hat{b}_0 + ig\hat{\mathbf{e}} \cdot \hat{\mathbf{E}}_{\text{free}}(\mathbf{r}_A, s) \right) \quad (4.41)$$

$$\hat{E}_i(\mathbf{r}, s) = \hat{E}_{i,\text{free}}(\mathbf{r}, s) + \frac{i}{g} (\Gamma_{ij}(\mathbf{r}, s) + i\Delta_{ij}(\mathbf{r}, s)) \hat{e}_j \hat{b}(s). \quad (4.42)$$

In these expressions, we have introduced the spontaneous emission rate and the Lamb shift of the oscillator's resonance frequency

$$\Delta\omega_L = \omega'_0 - \omega_0 = g^2 \frac{\hbar}{\pi\epsilon_0} \text{Im} \left[\int_0^\infty \frac{d\omega}{i(\omega - \omega_0)} \mathbf{e} \cdot \text{Im}\mathbf{G}(\mathbf{r}_A, \mathbf{r}_A, \omega) \cdot \mathbf{e} \right] \quad (4.43)$$

$$\gamma = g^2 \frac{\hbar}{\pi\epsilon_0} \text{Re} \left[\int_0^\infty \frac{d\omega}{i(\omega - \omega_0)} \mathbf{e} \cdot \text{Im}\mathbf{G}(\mathbf{r}_A, \mathbf{r}_A, \omega) \cdot \mathbf{e} \right] \quad (4.44)$$

for a single oscillator in an arbitrary dielectric. For an oscillator in the presence of a planar interface oriented along the z -axis, it corresponds to the real part of the zz -component of Eq. (4.40). The Lamb shift is formally divergent, so that the theory needs to be renormalized.

For a homogenous lossless dielectric only the electromagnetic field is transverse and only the transverse part of \mathbf{G} needs to be considered. By using the relation Eq. (A.9), the well known expression for the spontaneous rate is recovered,

$$\gamma = \frac{\hbar g^2 \omega_0^3}{6\pi\epsilon_0 c^3} n \quad (4.45)$$

where n is the index of refraction.

4.2.3 Lamb shift: Renormalized interaction with a quantum oscillator

To avoid problems with infinite terms, we need to renormalize the system by considering a harmonic oscillator of finite size. This can be done by smearing out the electric field in the interaction part of the Hamiltonian in Eq. (4.24), by replacing the electric field operator with

$$\hat{\mathcal{E}}(\mathbf{r}) = \int d^3\mathbf{x} \mathcal{S}(\mathbf{x}) \hat{\mathbf{E}}(\mathbf{r} - \mathbf{x}), \quad (4.46)$$

where $\mathcal{S}(\mathbf{x})$ is a smearing function that is a real test function, centred on the origin, with a width typically equated to the size of a real atom.

The most significant change in introducing the smearing function appears in the vector $\mathbf{M}(\mathbf{r}, s)$, which we introduced in the calculation of spontaneous emission rate and Lamb shift. In the smeared out-case it is replaced by

$$\mathcal{M}(\mathbf{r}_A, s) \equiv \frac{\hbar g}{\pi \epsilon_0} \int_0^\infty \frac{d\omega}{s + i\omega} \frac{\omega^2}{c^2} e_k \int d^3\mathbf{x} d^3\mathbf{x}' \mathcal{S}(\mathbf{x}) \mathcal{S}(\mathbf{x}') \text{Im}\mathbf{G}(\mathbf{r}_A - \mathbf{x}, \mathbf{r}_A - \mathbf{x}', \omega). \quad (4.47)$$

Applying the Wigner-Weisskopf approximation to the dynamics of a harmonic oscillator, the quantity $\mathcal{M}(\mathbf{r}_A, -i\omega_0 + i\varepsilon)$ allows the introduction of the decay rate and Lamb shift by

$$\begin{aligned} \gamma + i\Delta\omega_{\text{Lamb}} &= g \hat{\mathbf{e}} \cdot \mathcal{M}(\mathbf{r}_A, -i\omega_0 + i\varepsilon) \quad (4.48) \\ &= \frac{\hbar g^2}{\epsilon_0} \frac{\omega_0^2}{c^2} \left(\int d^3\mathbf{x} d^3\mathbf{x}' \mathcal{S}(\mathbf{x}) \mathcal{S}(\mathbf{x}') \hat{\mathbf{e}} \cdot \text{Im}\mathbf{G}(\mathbf{r}_A - \mathbf{x}, \mathbf{r}_A - \mathbf{x}', \omega_0) \cdot \hat{\mathbf{e}} \right. \\ &\quad - \frac{i}{\pi} \int_0^\infty d\omega \frac{\mathcal{P}}{\omega - \omega_0} \int d^3\mathbf{x} d^3\mathbf{x}' \mathcal{S}(\mathbf{x}) \mathcal{S}(\mathbf{x}') \\ &\quad \left. \times \hat{\mathbf{e}} \cdot \text{Im}\mathbf{G}(\mathbf{r}_A - \mathbf{x}, \mathbf{r}_A - \mathbf{x}', \omega) \cdot \hat{\mathbf{e}} \right). \quad (4.49) \end{aligned}$$

The divergent terms in the Green's function occur in its real part, which contains contributions from non-reflected radiation and from radiation that is reflected by the interface. The latter contribution is dominant for distances less than 20 nm. Because the real part of the Green's function arises from the evaluation of the principal value in the second term in Eq. (4.49), for a lossless and homogeneous medium the contributing divergent term is expressed using Eq. (A.12),

$$\begin{aligned} \mathcal{I}(\mathbf{r}) &\equiv \int d^3\mathbf{x} d^3\mathbf{x}' \mathcal{S}(\mathbf{x}) \mathcal{S}(\mathbf{x}') \text{Im} \mathbf{G}(\mathbf{r} - \mathbf{x}, \mathbf{r}_A - \mathbf{x}', \omega) \\ &= \frac{\pi}{2q(\omega)} \int d^3\mathbf{k} e^{i\mathbf{k}\cdot(\mathbf{r}-\mathbf{r}_A)} \left(\mathbb{1} - \frac{\mathbf{k} \otimes \mathbf{k}}{k^2} \right) \delta(k - q(\omega)) \mathcal{S}(\mathbf{k}) \mathcal{S}(-\mathbf{k}). \end{aligned} \quad (4.50)$$

If the smearing function is isotropic, $\mathcal{S}(\mathbf{x}) = \mathcal{S}(|\mathbf{x}|)$ and $\mathcal{S}(\mathbf{k}) = \mathcal{S}(k)$, this expression reduces to

$$\mathcal{I}(\mathbf{r}_A) = \frac{4\pi^2 q}{3} |\mathcal{S}(q)|^2 \mathbb{1}. \quad (4.51)$$

Hence, from Eq. (4.48) the Lamb shift takes the finite value

$$\Delta\omega_{\text{Lamb}} = -\frac{4\pi}{3} \frac{\hbar g^2}{\epsilon_0} \int_0^\infty d\omega q(\omega) |\mathcal{S}(q(\omega))|^2 \frac{\mathcal{P}}{\omega - \omega_0} \frac{\omega^2}{c^2}. \quad (4.52)$$

The main effect of smearing out the interaction therefore amount to introducing the factor $|\mathcal{S}(q(\omega))|^2$ in the above integral. Without this factor, the integral would diverge for large values of ω . However, a smooth smearing function with a finite width (e.g., a Gaussian) has a Fourier transform that obeys $|\mathcal{S}(q(\omega))| \rightarrow 0$ for $\omega \rightarrow \infty$. The smearing procedure is therefore equivalent to a smooth cut-off of the integral in frequency space.

As an example, we now consider a double Lorentzian smearing function $\mathcal{S}(\mathbf{x}) = w/(\pi^2(r^2 + w^2)^2)$, which has the Fourier transform

$$\mathcal{S}(\mathbf{k}) = \frac{e^{-kw}}{(2\pi)^{3/2}}. \quad (4.53)$$

For optical resonance frequencies we have $k \sim 10^7 \text{ m}^{-1}$. The cutoff should be around the size of an atom, so $w \sim 10^{-10} \text{ m}$. Consequently, $|\mathcal{S}(q(\omega))|^2 \approx (2\pi)^{-3/2}$. The factor $(2\pi)^{-3/2}$ is simply a consequence of the Fourier transformation and should be the same for any smearing function \mathcal{S} . Furthermore, all meaningful smearing functions should have a value that approaches $(2\pi)^{-3/2}$ for optical frequencies because the smearing should not be noticeable on scales of the resonance wavelength.

To evaluate Eq. (4.52), the integral is separated into three pieces based on the Lamb shifted frequencies ω'_0 . The integral has the structure

$$\Delta\omega_{\text{Lamb}} \propto \int_0^\infty d\omega h(\omega) \frac{\mathcal{P}}{\omega - \omega_0}. \quad (4.54)$$

In a narrow interval $I_2 = [\omega'_0 - \Omega, \omega'_0 + \Omega]$, with $\gamma \ll \Omega \ll \omega'_0$, the contribution vanishes due to the principal value. Below this interval, in $I_1 = [0, \omega'_0 - \Omega]$, we can approximate the denominator by $-\omega'_0$. Above the resonant region, in $I_3 = [\omega'_0 + \Omega, \infty]$, we can approximate the denominator by ω . Furthermore, we can set $|\mathcal{S}(q)|^2 \approx (2\pi)^{-3/2}$ in I_1 . The integral then becomes

$$\Delta\omega_{\text{Lamb}} \approx \frac{\gamma}{4\pi} \frac{\omega_0'^3}{\omega_0^3} - \frac{8\pi^2\gamma}{\omega_0^3} \int_{\omega'_0}^\infty d\omega \omega^2 |\mathcal{S}(q(\omega))|^2. \quad (4.55)$$

The Lamb shift can then be calculated exactly,

$$\Delta\omega_{\text{Lamb}} = \frac{\gamma}{\pi\xi^3} \frac{\omega_0'^3}{\omega_0^3} (e^{-\xi}\xi^3 \text{Ei}(\xi) - \xi^2 - \xi - 2) \quad (4.56)$$

$$\xi \equiv \frac{2nw\omega'_0}{c}. \quad (4.57)$$

4.3 Summary

We have developed a theoretical basis for studying the dynamics of quantum harmonic oscillators affected by a lossy and dispersive medium. The developed method

is general and applies to any configuration of dielectrics. In the following chapter, we apply it to study the excitation of a single quantum oscillator by a single photon.

Chapter 5

Single Photon Excitation

In this chapter, we investigate whether SPs can be used to excite atoms in the vicinity of a metal film via a single-photon pulse. Optimizing the single-photon excitation probability P_e is important for applications in quantum information. However, excitation by a single photon is also relevant for other applications such as beating the diffraction limit [84, 85, 86] because of its relation to time reversal.

To shed light on this relation we consider optimal excitation of an atom in free space. Stobińska *et al.* [83] suggested that the time reversal of a spontaneously emitted photon would be the perfect pulse shape for this problem. Spontaneous emission, i.e., the emission of a single photon by an initially excited atom, is a unitary process if both atomic and radiative degrees of freedom are taken into account. Therefore, the perfect time reversal of a spontaneously emitted photon pulse would excite the atom with certainty.

In free space, a time-reversed spontaneously emitted pulse covers the full solid angle, a geometry that is difficult to produce. Furthermore, confining light to a small volume is advantageous for both sub-wavelength resolution and optimal excitation. If an atom is placed in the vicinity of a metal surface, the generation of SP during the excitation process concentrates the photon pulse near the metal surface. In addition, light emanating from a point near the surface will be predominantly emitted into a narrow cone θ_{sp} (see Sec. 3.3.2). A time-reversed spontaneously emitted photon pulse would therefore have a conical, rather than spherical, geometry.

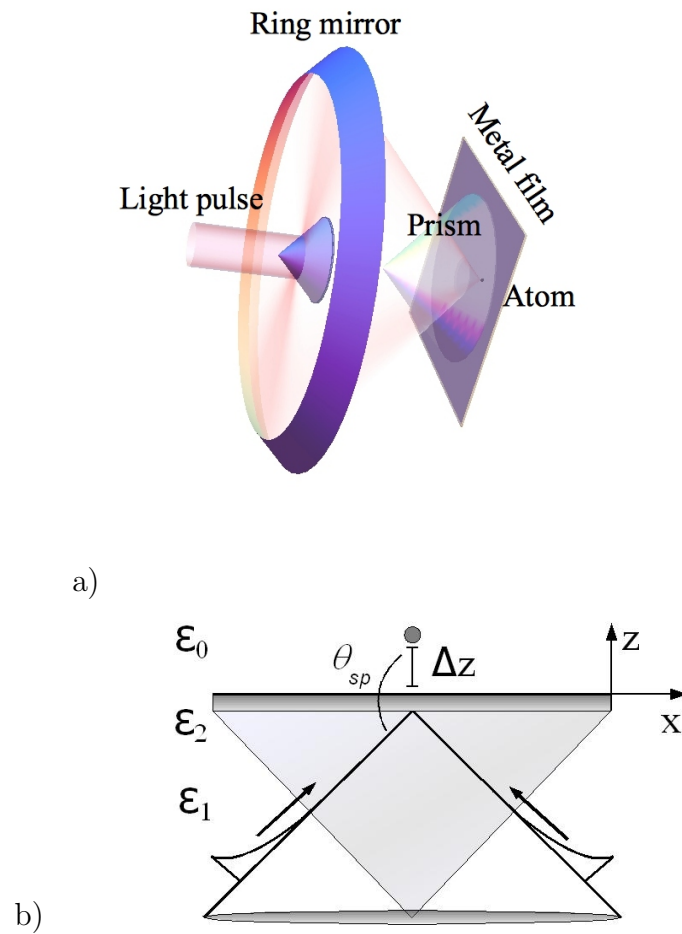


Figure 5.1: a) Sketch of proposed experiment: a single-photon pulse passes through a ring shaped mirror and a prism that sits on a thin metal film. The photon excites an atom on the other side of the film. See Sec. 5.1 for more details. b) Cross section of prism (ϵ_1), metal film (ϵ_2), and vacuum (ϵ_0), with the atom at a height Δz above the metal film. The time-reversed spontaneously emitted light pulse arrives at the metal film from below. It has a conical spatial profile, exponentially increasing temporal shape, and enters at the surface plasmon resonance angle θ_{sp} .

To study SP-assisted single-photon excitation, we consider the specific experimental setup depicted in Fig. 5.1, which is described in Sec. 5.1. In Sec. 5.2, a simplified method is proposed to construct single-photon creation operators in the presence of lossy dielectrics. This method is employed in Sec. 5.3 to find the atomic excitation probability. In Sec. 5.4, we present our main results and analyze how losses in the metal film affect the excitation probability.

5.1 Outline of the proposed experiment

We again consider a prism with dielectric constant $\varepsilon_1 = n_1^2 = 1.51^2$ and a metal film of thickness $d = 44$ nm with dielectric constant $\varepsilon_2 = -23.0 + 1.99i$. For these parameters the SP resonance angle takes the value $\theta_{\text{sp}} \approx 137.3^\circ$, which is inside the range of total-reflection and close to the total reflection angle of 138.5° .

To excite the atom with a time-reversed spontaneously emitted single-photon pulse, we first need to discuss the form of an ordinary spontaneously emitted pulse in the presence of SPs. We focus on atoms that are polarized along the z -direction because they emit TM-polarized light. The radiation intensity then has a dipole characteristic, i.e., it is modulated with a factor of $\sin^2 \phi$, where ϕ is the azimuthal angle in spherical coordinates. In free space, the radiation is symmetric under inversion of the z -direction, but the generation of SPs breaks this symmetry. For an atom located in the region above the metal film in Fig. 5.1b), most of the radiation is emitted into a narrow cone around the SP resonance angle θ_{sp} (see Sec. 3.3.2). The temporal shape of the pulse is a decaying exponential, corresponding to the decrease of atomic excitation over time.

In the proposed experiment, we suggest to use the time-reversal of this pulse to excite the atom. Because most of the radiation is emitted into a narrow cone around θ_{sp} , we can restrict the time-reversed pulse to this cone, which considerably simplifies the geometry for optimal excitation. A sketch of the setup is shown in Fig. 5.1a). A single-photon pulse with a dipolar ($\sin^2 \phi$) intensity distribution is incident on a conical mirror, which reflects the pulse towards a ring shaped mirror. The latter converts the pulse into a conical mode that enters the prism with a narrow angular width $\delta\theta$ around the SP resonance angle θ_{sp} . The pulse then passes through the metal film and excites an atom on the other side of the film.

5.2 Theoretical model

Because a single photon can only trigger a single excitation process in an atom or molecule, the details of the atom are not relevant as long as the photon is nearly resonant with one (dipole-allowed) atomic transition and off-resonant processes can be neglected. We then can model the atom by a quantum harmonic oscillator and utilize the theory we developed in Chapter 4.

To describe a time-reversed spontaneously emitted single-photon pulse, we first have to solve the problem of spontaneous emission in the presence of SPs. This has recently been accomplished by Archambault *et al.* [103], who also addressed a point of considerable practical relevance. The formalism presented in Refs. [96, 88] requires that the dielectric permittivity obeys the Kramers-Kronig relations, which in particular demands that the permittivity converges to unity as $|\omega| \rightarrow \infty$. This makes it necessary to consider frequency-dependent permittivities which are

analytical functions of ω . However, for pulses with narrow frequency width it appears unduly complicated to require knowledge of the permittivity for all frequencies.

In Ref. [103], the problem of frequency dependent permittivities was overcome using an expansion in momentum space. Here, we suggest a more general solution to the problem, which may help to simplify the application of the theory of Refs. [96, 88]. We propose to introduce a mode annihilation operator \hat{a} , which annihilates a photon in a specific field mode $\mathcal{E}(\mathbf{r})$.

The initial state of a photon with this field mode can then be expressed as $|\psi\rangle = \hat{a}^\dagger|\text{vac}\rangle$. For a general single-photon state $|\psi\rangle$, the field mode corresponds to the vacuum field amplitude

$$\mathcal{E}(\mathbf{r}) = \langle \text{vac} | \hat{\mathbf{E}}(\mathbf{r}) | \psi \rangle. \quad (5.1)$$

We have found that the field mode and the annihilation operator are connected through the following relation,

$$\hat{a} = \frac{2\epsilon_0\epsilon_\infty}{\hbar} \int d^3r \int_0^\infty \frac{d\omega}{\omega} \mathcal{E}^*(\mathbf{r}) \cdot \hat{\mathbf{E}}(\mathbf{r}, \omega), \quad (5.2)$$

with $\epsilon_\infty \equiv \lim_{|\omega| \rightarrow \infty} \epsilon(\mathbf{r}, \omega)$. The proof is as follows. Using the commutator from Eq. (4.18), it is easy to see that the electric field amplitude in a single-photon state $\hat{a}^\dagger|\text{vac}\rangle$ is given by

$$\begin{aligned} \langle \text{vac} | \hat{\mathbf{E}}_i(\mathbf{r}) \hat{a}^\dagger | \text{vac} \rangle &= [\hat{\mathbf{E}}_i(\mathbf{r}), \hat{a}^\dagger] \\ &= \frac{2\epsilon_\infty}{\pi} \int d^3r' \mathcal{E}_j(\mathbf{r}') \int_0^\infty d\omega \frac{\omega}{c^2} \text{Im} G_{ij}(\mathbf{r}, \mathbf{r}', \omega). \end{aligned} \quad (5.3)$$

The integral over the Green's function can be evaluated using

$$\begin{aligned} \int_0^\infty d\omega \frac{\omega}{c^2} \text{Im} G_{ik}(\mathbf{r}, \mathbf{r}', \omega) &= \frac{1}{2ic^2} \int_{-\infty}^\infty d\omega \omega G_{ik}(\mathbf{r}, \mathbf{r}', \omega) \\ &= \frac{\pi}{2\epsilon_\infty} \delta_{ik} \delta(\mathbf{r} - \mathbf{r}'). \end{aligned} \quad (5.4)$$

A very similar relation is given by Eq. (B 13) of Ref. [96] for $\epsilon_\infty = 1$. It can be derived using the residue theorem by employing that the Green's function is holomorphic in the upper half plane and

$$\lim_{|\omega| \rightarrow \infty} q^2(\mathbf{r}, \omega) G_{ik}(\mathbf{r}, \mathbf{r}', \omega) = -\delta_{ik} \delta(\mathbf{r} - \mathbf{r}') , \quad (5.5)$$

with $q(\mathbf{r}, \omega) = \sqrt{\epsilon(\mathbf{r}, \omega)} \omega / c$ (see Eq. (A 30) of Ref. [96]). The electric field amplitude in a single-photon state thus becomes

$$\begin{aligned} \langle \text{vac} | \hat{\mathbf{E}}_i(\mathbf{r}) a^\dagger | \text{vac} \rangle &= \int d^3x \mathbf{E}_k(\mathbf{x}) \delta_{ik} \delta(\mathbf{r} - \mathbf{x}) \\ &= \mathbf{E}_i(\mathbf{r}). \end{aligned} \quad (5.6)$$

which verifies Eq. (5.2).

To ensure that the mode annihilation operator obeys the usual commutation relation $[\hat{a}, \hat{a}^\dagger] = 1$, we use Eqs. (5.2) and (4.18) to arrive at the normalization condition

$$1 = \frac{4\epsilon_0\epsilon_\infty^2}{\hbar\pi c^2} \int d^3r \int d^3r' \mathbf{E}_i^*(\mathbf{r}) \mathbf{E}_j(\mathbf{r}') \int_0^\infty d\omega \text{Im} G_{ij}(\mathbf{r}, \mathbf{r}', \omega) . \quad (5.7)$$

In a lossless homogeneous medium, this can be simplified to

$$1 = \frac{2\epsilon_0\epsilon_\infty^2}{\hbar c^2} \int d^3k |\mathbf{E}(\mathbf{k})|^2 \frac{v_{\text{gr}}(\mathbf{k})}{k} , \quad (5.8)$$

where $v_{\text{gr}}(k)$ is the group velocity of light.

Obviously, if the Kramers-Kronig relations hold, $\epsilon_\infty = 1$. However, if the frequency width of the light pulse is so narrow that we can consider ϵ to be constant over the frequency range of the pulse, the dielectric medium can be modelled using a constant permittivity, such that $\epsilon_\infty = \epsilon \neq 1$. While this procedure is not exact, it should give an excellent approximation for near-resonant pulses interacting

with atoms. For off-resonant phenomena, where a wide range of frequencies can contribute, the full formalism of QED in absorbing dielectrics needs to be employed.

5.3 Excitation by a time-reversed spontaneously emitted pulse

Our goal is to find the probability $P_e(t)$ for the harmonic oscillator to be excited by an incoming single-photon pulse in the configuration outlined in Sec. 5.1. The optimal mode of the single-photon pulse should correspond to the time-reversal of a spontaneously emitted photon.

Spontaneous emission in the presence of absorbing dielectrics has been studied in Refs. [104, 105, 106, 107, 108, 109]. We reconsider this problem in App. C to obtain the emitted field amplitude in the presence of SPs, which is given by Eq. (C.7). However, the actual time-reversal of this pulse is inconvenient to work with and may be difficult to prepare in an experiment. We therefore consider the following ansatz for the initial field amplitude in momentum space,

$$\boldsymbol{\mathcal{E}}(\mathbf{k}) = \left(\mathbf{e} - \mathbf{k} \frac{\mathbf{e} \cdot \mathbf{k}}{k^2} \right) \mathcal{A} \quad (5.9)$$

$$\mathcal{A} = \mathcal{N} \frac{e^{i\omega_k t \varepsilon - i\mathbf{k} \cdot \mathbf{r} \varepsilon}}{-i(\omega'_0 - \omega_k) + \gamma \varepsilon} h(\theta), \quad (5.10)$$

which provides an excellent approximation to the exact cone (see below). The physical interpretation of the field $\boldsymbol{\mathcal{E}}(\mathbf{k})$ is as follows. The term in parentheses ensures that the electric field is transverse and generates the same intensity distribution as an electric dipole oriented along the unit vector \mathbf{e} . For a dipole orientation \mathbf{e} along the z -axis, the radiation is transverse magnetic with respect to the interface, so that radiation can couple into SP modes.

The amplitude \mathcal{A} of the pulse contains a Lorentzian factor of width $\gamma_{\mathcal{E}}$, centered around the (Lamb-shifted) oscillator's resonance frequency ω'_0 , with $\omega_k = kc/n_1$. In position space, this Lorentzian generates an amplitude that increases exponentially with the distance from the origin. The exponential $\exp(i\omega_k t_{\mathcal{E}} - i\mathbf{k} \cdot \mathbf{r}_{\mathcal{E}})$ ensures that the pulse is incoming. In free space, its focal point would be given by $\mathbf{r}_{\mathcal{E}}$, but in the presence of the interface the actual focal point is at a different position. Nevertheless, the parameter $\mathbf{r}_{\mathcal{E}}$ can be used to optimize P_e . The exponential factor containing $t_{\mathcal{E}} \gg \gamma^{-1}$ cuts the field off at a distance $r = ct_{\mathcal{E}}/n_1$. The time $t_{\mathcal{E}}$ can be interpreted as the time at which the spontaneously decaying pulse is inverted, and produces a field amplitude as drawn on the lower cone in Fig. 5.1b). The function

$$h(\theta) = e^{-\frac{(\theta - \theta_{\text{sp}})^2}{\delta\theta^2}} \quad (5.11)$$

is a Gaussian envelope for the inclination angle $\theta = \cos^{-1}(k_z/k)$, which confines the pulse to a narrow cone of width $\delta\theta$ around the SP resonance angle θ_{sp} . The confinement mimics the effect of the Fresnel coefficients, which are contained in the Green's function in Eq. (C.7). Finally, the normalization factor \mathcal{N} makes sure that the field amplitude satisfies the normalization condition (5.8). It needs to be evaluated numerically.

For a given single-photon amplitude, the excitation probability can be found by solving the equations of motions and calculating the probability $P_e(t)$ to find the oscillator in the first excited state. In the Heisenberg picture, this dynamical problem is very similar to that of spontaneous emission. The only difference is the initial state, which can be written as $|\psi_0\rangle = \hat{a}^\dagger|\text{vac}\rangle \otimes |0\rangle$, with \hat{a} of Eq. (5.2) and the field amplitude of Eq. (5.9). The solution of the dynamical problem is presented

in App. D. The resulting excitation probability can be expressed as

$$P_e(t) = \left| [\hat{b}(t), \hat{a}^\dagger] \right|^2, \quad (5.12)$$

where the commutator in the presence of the interface is given by

$$\begin{aligned} [\hat{b}(t), \hat{a}^\dagger] &= \sqrt{\frac{2}{\pi}} \frac{n_1^4}{c^4} \int_0^\pi d\theta \cos\theta \sin^3\theta \int_0^\infty d\omega \frac{\omega^3 e^{-i\omega t}}{\omega - \omega'_0 + i\gamma} \\ &\times \frac{2g \mathcal{A} \beta_2 \epsilon_1 \epsilon_2 e^{i(\beta_2 d - \beta_3(d-z_A))}}{e^{2i\beta_2 d} (\beta_2 \epsilon_1 - \beta_1 \epsilon_2)(\beta_2 \epsilon_3 - \beta_3 \epsilon_2) - (\beta_2 \epsilon_1 + \beta_1 \epsilon_2)(\beta_3 \epsilon_2 + \beta_2 \epsilon_3)}. \end{aligned} \quad (5.13)$$

In this expression, $\beta_i = \sqrt{\epsilon_i \omega^2 / c^2 - \vec{k}_\parallel^2}$. The spontaneous emission rate γ of the oscillator in the presence of the interface is given by Eq. (4.44). In the following section, we will analyze this result for specific situations.

5.4 Results

The excitation probability $P_e(t)$ of Eq. (5.12) is maximized for $t = t_\mathcal{E}$, when the incoming pulse corresponds to a completely reversed spontaneous decay. We will focus on this case, but we have numerically verified that the excitation probability decreases if $t \neq t_\mathcal{E}$.

In a lossless homogenous dielectric the dynamics of the oscillator-radiation system is unitary. We then should have $P_e \approx 1$ for an inverted decay, which provides a test of ansatz (5.9). This situation can be modeled by setting all dielectric constants ϵ_i equal to ϵ_1 in Eq. (5.13). The resulting excitation probability is shown in Fig. 5.2 and demonstrates that P_e approaches unity for $\delta\theta \rightarrow \infty$ in Eq. (5.11). This limit describes the situation when the restriction of the pulse to a narrow cone is removed. In the opposite limit of very narrow pulse width, P_e approaches zero because of

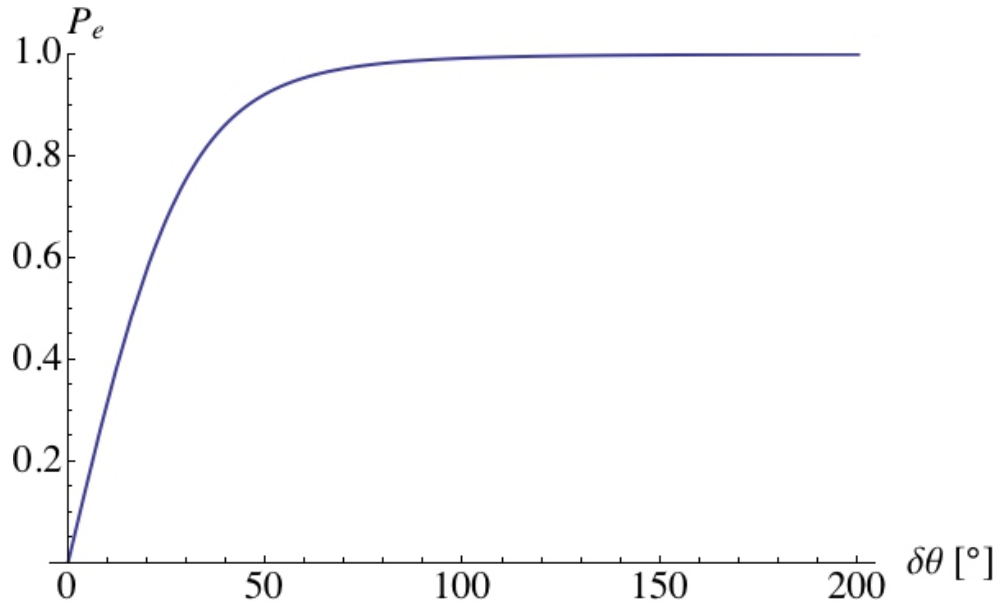


Figure 5.2: Excitation probability (5.12) in a lossless homogeneous dielectric. The incoming single-photon pulse (5.9) has the structure of an electric dipole field, which is confined to a cone of width $\delta\theta$ around the inclination angle $\theta = \pi/2$.

the mode mismatch between the cone-like single-photon pulse and the actual time-inversion of a spontaneously emitted photon pulse in a homogeneous medium. To avoid misunderstandings, we emphasize that the energy contained in the pulse does not depend on $\delta\theta$, because the single-photon pulse is always normalized according to Eq. (5.8).

For the Kretschmann configuration described in Sec. 5.1, the excitation profile has a very different character. Because the SP resonance angle is only 1.2° away from the total reflection angle, only a very narrow cone of width $\delta\theta = 0.17^\circ$ can be used to excite the oscillator. Because this cone has a large overlap with the time-inverted mode of a spontaneously emitted photon, one would expect high excitation

probabilities P_e . However, this argument ignores losses in the metal film, which lead to a significant reduction of P_e .

To isolate the effect of losses, we first disregard the variation of the oscillator's spontaneous emission rate near the interface by replacing γ in Eq. (5.13) by the free-space decay rate γ_0 . The resulting excitation probability is shown in Fig. 5.3 a) as a function of the pulse frequency width $\gamma_\mathcal{E}$ and the distance Δz_A between the oscillator and the metal film. Not surprisingly, the excitation probability is largest for $\gamma_\mathcal{E} = \gamma_0$. The excitation probability decreases exponentially with the distance Δz_A because of the evanescent nature of the electromagnetic field generated by SPs.

Fig. 5.3 a) suggests that, if γ was equal to γ_0 , excitation probabilities close to 70% would be possible for atoms close to the interface. On the other hand, the amount of energy that is emitted into the cone around the SP resonance angle when an atom decays is also about 70% of the total emitted energy. Hence, the result $P_e < 0.7$ reflects the fact (i) the pulse amplitude (5.9) is a very good approximation for the conical part of the time-inversion of spontaneously emitted light, and (ii) the excitation probability cannot be close to unity because the cone only contains 70% of the emitted radiation.

Losses in the metal film lead to a further reduction of the excitation probability. Fig. 5.3 b) displays P_e when the variation of γ with the distance Δz_A is taken into account. Figs. 5.3 a) and b) display similar values for P_e only in regions where $\gamma \approx \gamma_0$, i.e., for $\Delta z_A > 300$ nm. For smaller distances, the increasing spontaneous emission rate suppresses the excitation rate, even when the pulse's frequency width is held at the optimal value $\gamma_\mathcal{E} = \gamma$. The maximal excitation probability of 35% is achieved for $\gamma_\mathcal{E} = \gamma$ at a distance $\Delta z_A \approx 250$ nm.

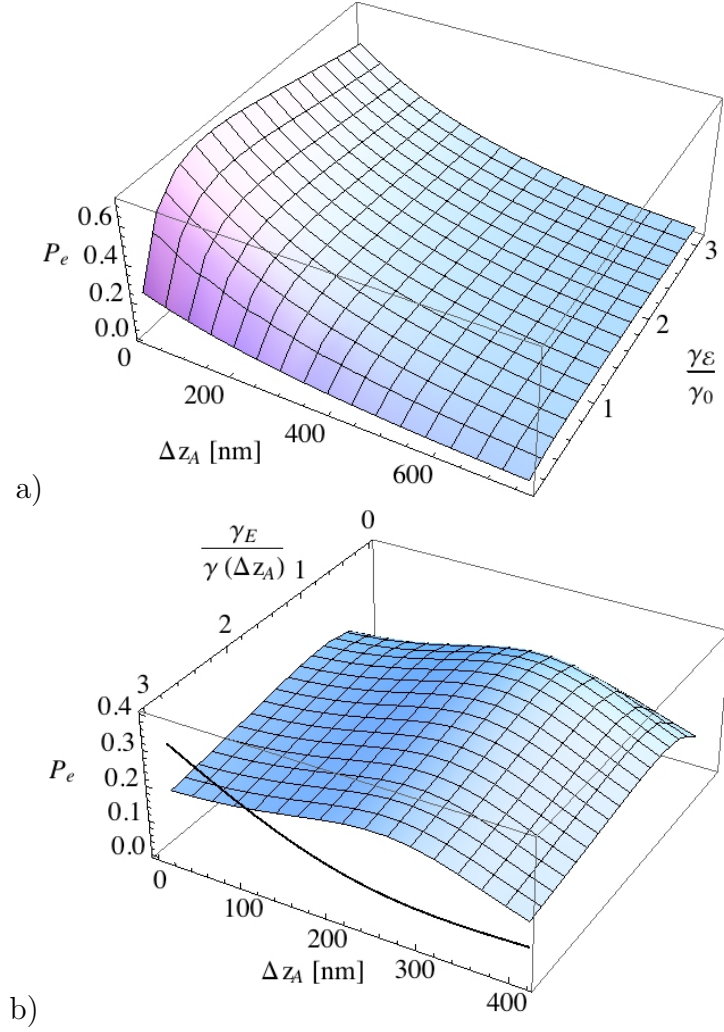


Figure 5.3: Excitation probability P_e of a harmonic oscillator as a function of its distance Δz_A from the metal film and of the frequency width γ_E of the incoming single-photon pulse. a) P_e for the case when the oscillator's decay rate is kept at the free-space decay rate γ_0 . b) The variation of the oscillator's decay rate $\gamma(\Delta z_A)$ with the distance is taken into account. The solid line on the front displays the value of $0.1\gamma(\Delta z_A)/\gamma_0$. The factor of 0.1 has been included for presentational purposes only.

The physical origin of the increasing decay rate is non-radiative decay into modes other than SPs. It has been shown in Ref. [109] that the decay rate of an atom near a (semi-infinite) absorbing dielectric is proportional to $\epsilon'' \Delta z_A^{-3}$, where ϵ'' is the imaginary part of the dielectric permittivity. This means that if an atom is close to a lossy dielectric, it couples very strongly to dissipative modes in the medium.

In our case, the metal film corresponds to such a lossy medium. Despite its small width, it can induce a non-radiative decay of the oscillator if the latter is too close to the film. The oscillator then decays more quickly than the single-photon pulse can excite it, which limits the achievable excitation probability. We remark that the lossy nature of the metal film implies that our findings are not in disagreement with time reversal. Quantum mechanics has a time-reversal symmetry only when the evolution is unitary. The noise currents, which accompany the absorption of photons in a metal, lead to decoherence of our system, so that the time evolution is irreversible.

5.5 Summary

In this chapter we have proposed an experiment to analyze the role of SPs in atomic excitation processes. An incoming single-photon pulse, which mimics the time inversion of spontaneously emitted light, is incident on an atom near a metal film. In absence of dielectric losses such a pulse should excite the atom with a high probability P_e .

However, non-radiative decay of the atom, due to coupling to the lossy metal film,

limits P_e to values around 35%. The reason is that, as the atom gets closer to the metal, the non-radiative decay will happen on a faster time scale than the excitation through the photon. The reduced excitation probability limits the effectiveness of single photon interactions in the Kretschmann configuration.

Chapter 6

Conclusion

In this thesis, two primary aspects of the physics involving surface plasmons have been studied: the effect of dipole images on the collective emission of radiation by a set of classical dipoles and the excitation of atoms by single-photon pulses. The common mathematical technique that was used is Green's functions for the electromagnetic field in the presence of layered and lossy dielectrics. This choice was made so that the theory of quantum electrodynamics in the presence of absorbing dielectrics could be employed, which is necessary to describe the interaction between photons and atoms.

The physical parameters that were necessary to generate surface plasmons in the Kretschmann configuration were determined in Chapter 2. To study the radiation that propagates through the medium and from emitting sources, the dyadic Green's functions are obtained for multi-layered dielectrics. The Green's functions would be applied to all our studies of radiation dynamics.

In Chapter 3, we first studied the influence of surface plasmons on cooperative emission from an ensemble of emitters. Superradiance provides a means to acquire information about the state of a series of emitters by observing the associated increase in radiation intensity and decrease of atomic lifetimes. We saw that when the emitted light generated surface plasmons, the emission rate was generally increased and a gain in intensity, related to the separation distance from the interface, was obtained. Because of the imaging effect of the dipoles in the metal, however, we saw that

normally superradiant configurations of dipoles would be dampened and become subradiant while still possessing the N^2 hallmark for superradiance. The additional subradiant states potentially offer additional opportunities for storing light in atomic dipoles.

The excitation of a single emitter by a photon was described in Chapter 5 using a QED formalism constructed in Chapter 4. This enabled us to include the losses and absorption intrinsic to the metal film in our description. We considered a photon that originated far away from the metal interface and established an upper bound on the excitation probability. A nearly optimal excitation probability was only obtained when non-radiative decay was ignored. When the losses were properly accounted for, the excitation probability was effectively halved. This finding implies that the use of a surface plasmon excitation device for quantum information may be limited, at least for the Kretschmann geometry that has been studied in this thesis.

In future work, it would be of interest to find ways to overcome the limitations of surface plasmons that we have found here. The Kretschmann configuration is experimentally relevant and theoretically convenient, but it has the disadvantage that a large fraction of the emitted radiation can escape into the vacuum above the metal film. This puts a loss-independent upper bound on the excitation probability of the single emitter and results in the superradiant emission not being emitted into a singular mode. To remedy the situation, an additional dielectric mirror could be used to sandwich the emitter between the metal film and mirror similarly to an optical cavity. Provided the separation distance is smaller than the wavelength, this would reduce emission into the vacuum to negligible levels.

Furthermore, the surface plasmon can freely propagate in two dimensions on

a flat metal film, allowing the surface plasmons to disperse over a larger surface introducing additional losses to heating. In the context of plasmonics, extensive amount of work is currently undertaken to explore more general geometries that control surface plasmon dispersion, for instance narrow grooves, which effectively channel the surface plasmon into one dimension [34, 37, 110]. Our methods could generally be adapted to these cases. However, finding the radiative Green's function for complicated systems would have to be done numerically.

Appendix A

Green's Functions of Layered Dielectrics

A.1 General relations for the Green's functions

The Green's function has a number of very useful properties. Some central relations are

$$G_{ik}^*(\mathbf{r}, \mathbf{r}', \omega) = G_{ik}(\mathbf{r}, \mathbf{r}', -\omega^*), \quad (\text{A.1})$$

$$G_{ki}(\mathbf{r}', \mathbf{r}, \omega) = G_{ik}(\mathbf{r}, \mathbf{r}', \omega), \quad (\text{A.2})$$

and the integral relation

$$\text{Im } G_{ij}(\mathbf{r}, \mathbf{r}', \omega) = \int d^3r'' \frac{\omega^2}{c^2} \epsilon''(\mathbf{r}'', \omega) G_{ik}(\mathbf{r}, \mathbf{r}'', \omega) G_{jk}^*(\mathbf{r}', \mathbf{r}'', \omega). \quad (\text{A.3})$$

The following integral appears in some calculations,

$$\begin{aligned} \int_0^\infty d\omega \frac{\omega}{c^2} \text{Im } G_{ik}(\mathbf{r}, \mathbf{r}', \omega) &= \frac{1}{2ic^2} \int_{-\infty}^\infty d\omega \omega G_{ik}(\mathbf{r}, \mathbf{r}', \omega) \\ &= \frac{\pi}{2\epsilon_\infty} \delta_{ik} \delta(\mathbf{r} - \mathbf{r}'), \end{aligned} \quad (\text{A.4})$$

where $\epsilon_\infty \equiv \lim_{|\omega| \rightarrow \infty} \epsilon(\mathbf{r}, \omega)$. It can be derived using the residue theorem by employing that the Green's function is holomorphic in the upper half plane and

$$\lim_{|\omega| \rightarrow \infty} q^2(\mathbf{r}, \omega) G_{ik}(\mathbf{r}, \mathbf{r}', \omega) = -\delta_{ik} \delta(\mathbf{r} - \mathbf{r}'), \quad (\text{A.5})$$

with $q(\mathbf{r}, \omega) = \sqrt{\epsilon(\mathbf{r}, \omega)}\omega/c$. It is worthwhile to note that Knöll, Scheel, and Welsch [96] also give a relation of the form

$$\lim_{|\omega| \rightarrow \infty} \frac{\omega^2}{c^2} G_{ik}(\mathbf{r}, \mathbf{r}', \omega) = -\delta_{ik} \delta(\mathbf{r} - \mathbf{r}'). \quad (\text{A.6})$$

These two relations are equivalent if one keeps in mind that $\lim_{\omega \rightarrow \infty} \epsilon(\mathbf{r}, \omega) = 1$ for real physical systems. However, sometimes one wishes to relax this condition and simply consider a medium with constant refractive index n . If $n \neq 1$, this is not in agreement with the Kramer-Kronig relations anymore, but one nevertheless may expect that many aspects of the physics will be correctly described.

A.2 Bulk dielectric dyadic Green's function

The Green function for a homogenous isotropic medium is determined by Eq. (2.17), and is given by

$$G_{\mu\nu}(\mathbf{r}, \mathbf{r}', \omega) = \left(\frac{\partial}{\partial r_\mu} \frac{\partial}{\partial r_\nu} + \delta_{\mu\nu} q^2(\omega) \right) q^{-2}(\omega) g(\mathbf{r}, \mathbf{r}', \omega), \quad (\text{A.7})$$

where $g(\mathbf{r}, \mathbf{r}', \omega)$ is the scalar Green function

$$g(\mathbf{r}, \mathbf{r}', \omega) = \frac{e^{iq(\omega)|\mathbf{r}-\mathbf{r}'|}}{4\pi|\mathbf{r}-\mathbf{r}'|}. \quad (\text{A.8})$$

The transverse part of the vacuum Green's function \mathbf{G}^V , has the useful property

$$\text{Im}G_{\mu\nu}(\mathbf{r}, \mathbf{r}, \omega) = \frac{\omega}{6\pi c} \delta_{\mu\nu}. \quad (\text{A.9})$$

In momentum (\mathbf{k}) space, the dyadic Green function $G_{\mu\nu}(\mathbf{k}, \omega)$ is obtained through the transform

$$G_{\mu\nu}(\mathbf{k}, \omega) = \left(\delta_{\mu\nu} - \frac{k_\mu k_\nu}{q^2(\omega)} \right) \frac{1}{k^2 - q^2(\omega)}. \quad (\text{A.10})$$

The imaginary part of q should be larger than zero to guarantee that the poles of \mathbf{G} as a function of ω lie in the lower half. In this way the Green's function $\mathbf{G}(t)$ will be zero for $t < 0$ when the Fourier transform is calculated using the residue theorem. A lossless medium can be described by taking the limit $\text{Im}q(\omega) \rightarrow 0$. It is worthwhile

to note that the second expression is the Fourier transform of Eq. (A.7). This also shows that Eq. (A.7) is the full Green's function and not the transverse part.

The imaginary part of the Green function appears frequently in both classical and quantum treatments of the electromagnetic field. In non-absorbing media, where $\varepsilon(\omega) \in \Re$, only the transverse components of the Green function are complex. The imaginary component is

$$\begin{aligned} \text{Im}G_{\mu\nu}(\mathbf{r}, \mathbf{r}', \omega) = & \frac{q}{4\pi} \left(\left[\left(\frac{1}{q\rho} - \frac{1}{(q\rho)^3} \right) \delta_{\mu\nu} - \left(\frac{1}{q\rho} - \frac{3}{(q\rho)^3} \right) \frac{\rho_\mu \rho_\nu}{\rho^2} \right] \sin q\rho \right. \\ & \left. + \left[\frac{1}{(q\rho)^2} \delta_{\mu\nu} - \frac{3}{(q\rho)^2} \frac{\rho_\mu \rho_\nu}{\rho^2} \right] \cos q\rho \right), \end{aligned} \quad (\text{A.11})$$

with $\boldsymbol{\rho} = \mathbf{r} - \mathbf{r}'$. In momentum space \mathbf{k} , the imaginary part of $\text{Im}G_{\mu\nu}(\mathbf{r}, \mathbf{r}', \omega)$ for a lossless medium can be expressed as follows

$$\text{FTIm}G_{\mu\nu}(\mathbf{r}, \mathbf{r}', \omega) = \frac{1}{16q(\omega)\pi^2} e^{i\mathbf{k}\cdot\mathbf{r}'} \left(\delta_{\mu\nu} - \frac{k_\mu k_\nu}{q^2(\omega)} \right) \delta(k - q(\omega)) \quad (\text{A.12})$$

A.2.1 Lossless homogeneous medium

Now k and q are always positive so that we can set $k + q = k + q^* = k + q$ because it makes no difference in the limit $\text{Im} q \rightarrow 0$. Consequently we get

$$\begin{aligned} \lim_{\text{Im} q \rightarrow 0} \text{Im} G_{ij}(\mathbf{r}, \omega) &= \frac{1}{2i} \frac{1}{(2\pi)^3} \int d^3k \frac{e^{i\mathbf{k}\cdot\mathbf{r}}}{k + q} \left\{ \left(\delta_{ij} - \frac{k_i k_j}{q^2} \right) \frac{1}{(k - q)} - \left(\delta_{ij} - \frac{k_i k_j}{q^2} \right) \frac{1}{(k - q^*)} \right\} \\ &= \frac{1}{16q(\omega)\pi^2} \int d^3k e^{i\mathbf{k}\cdot\mathbf{r}} \left(\delta_{ij} - \frac{k_i k_j}{k^2} \right) \delta(k - q(\omega)) \end{aligned} \quad (\text{A.13})$$

In particular, in the case $\mathbf{r} = 0$,

$$\text{Im} G_{ij}(\mathbf{r} = \mathbf{0}, \omega) = \frac{q(\omega)}{6\pi} \delta_{ij}. \quad (\text{A.14})$$

It is worth to note that the imaginary part is automatically transverse because it is on-shell. Another useful relation for the Fourier transformation with respect to \mathbf{r} is

$$\text{FT}(\text{Im } G_{ij}(\mathbf{r} - \mathbf{r}_A, \omega))(\mathbf{k}) = (2\pi)^{3/2} \frac{e^{-i\mathbf{k}\cdot\mathbf{r}_A}}{16q(\omega)\pi^2} \left(\delta_{ij} - \frac{k_i k_j}{k^2} \right) \delta(k - q(\omega)). \quad (\text{A.15})$$

For a comparison with the interface it is useful to consider the partial Fourier transform of the Green's function,

$$\begin{aligned} \tilde{G}_{ki}(\mathbf{k}_{\parallel}, \omega, z_A, z) &= \int_{-\infty}^{\infty} \frac{dk_z}{\sqrt{2\pi}} e^{ik_z(z_A - z)} G_{ij}(\mathbf{k}, \omega) \\ &= \int_{-\infty}^{\infty} \frac{dk_z}{(2\pi)^2} e^{ik_z(z_A - z)} \left(\delta_{ij} - \frac{k_i k_j}{q^2} \right) \frac{1}{k_{\parallel}^2 + k_z^2 - q^2}. \end{aligned} \quad (\text{A.16})$$

This can be evaluated using the Residue theorem. Keeping in mind that the imaginary part of the refractive index should be positive, we should replace q by $q + i\epsilon$. The poles for k_z then appear at $k_z = \pm(\beta_1 + \epsilon')$, with $\beta_1 = \sqrt{q^2 - k_{\parallel}^2}$. The contour has to be closed in the upper half plane for $z_A - z > 0$, and in the lower half plane for $z_A - z < 0$. In each of these two cases only one of the two poles is enclosed. The result of this calculation is

$$\tilde{G}_{ki}(\mathbf{k}_{\parallel}, \omega, z_A, z) = \frac{e^{i\beta_1|z_A - z|}}{4\pi q^2} \begin{pmatrix} \frac{i(q^2 - k_x^2)}{\beta_1} & -\frac{ik_x k_y}{\beta_1} & i \operatorname{sgn}(z - z_A) k_x \\ -\frac{ik_x k_y}{\beta_1} & \frac{i(q^2 - k_y^2)}{\beta_1} & i \operatorname{sgn}(z - z_A) k_y \\ i \operatorname{sgn}(z - z_A) k_x & i \operatorname{sgn}(z - z_A) k_y & \frac{ik_{\parallel}^2}{\beta_1} \end{pmatrix} \quad (\text{A.17})$$

A.3 Reflection and transmission Green's function

This section contains all the reflected and transmitted portions of the Green's function. As an example of their derivation, the $\tilde{G}_{xx}(\mathbf{k}_p, \omega; z, z')$ is derived.

Solving for $\tilde{G}_{xx}(\mathbf{k}_p, \omega; z, z')$

From Eq. (2.36), we see that $\tilde{G}_{xx}(\mathbf{k}_p, \omega; z, z')$ is continuous across the interface. From Eq. (2.33) we acquire

$$-ik_p \tilde{G}_{zx}(\mathbf{k}_p, \omega; z, z') = \frac{k_p^2}{\epsilon \frac{\omega^2}{c^2} - k_p^2} \partial_z \tilde{G}_{xx}(\mathbf{k}_p, \omega; z, z'). \quad (\text{A.18})$$

I can then express Eq. (2.36) as

$$\partial_z \tilde{G}_{xx}(\mathbf{k}_p, \omega; z, z') + \frac{k_p^2}{\epsilon \frac{\omega^2}{c^2} - k_p^2} \partial_z \tilde{G}_{xx}(\mathbf{k}_p, \omega; z, z'), \quad (\text{A.19})$$

and rearranging I acquire the continuous quantity

$$\frac{\epsilon \frac{\omega^2}{c^2}}{\epsilon \frac{\omega^2}{c^2} - k_p^2} \partial_z \tilde{G}_{xx}(\mathbf{k}_p, \omega; z, z'). \quad (\text{A.20})$$

Since $\frac{\omega^2}{c^2}$ is a conserved quantity, and $\epsilon \frac{\omega^2}{c^2} - k_p^2$ is the normal wave vector component k_z , this can be re-expressed as

$$\frac{\epsilon}{k_z^2} \partial_z \tilde{G}_{xx}(\mathbf{k}_p, \omega; z, z'). \quad (\text{A.21})$$

The differential equation for $\tilde{G}_{xx}(\mathbf{k}_p, \omega; z, z')$ is acquired by eliminating $\tilde{G}_{zx}(\mathbf{k}_p, \omega; z, z')$ from the Equations (2.27) and (2.33). Differentiating Eq. (2.33) with respect to z , multiplying by $\frac{-ik_p}{k_p^2 - \epsilon \frac{\omega^2}{c^2}}$ and adding to Eq. (2.27) we acquire

$$- \left(\epsilon \frac{\omega^2}{c^2} - \frac{\epsilon \frac{\omega^2}{c^2}}{k_p^2 - \epsilon \frac{\omega^2}{c^2}} \partial_z^2 \right) \tilde{G}_{xx}(\mathbf{k}_p, \omega; z, z') = \delta(\mathbf{r} - \mathbf{r}') \quad (\text{A.22})$$

$$- \left(\epsilon \frac{\omega^2}{c^2} + \frac{\epsilon \frac{\omega^2}{c^2}}{k_z^2} \partial_z^2 \right) \tilde{G}_{xx}(\mathbf{k}_p, \omega; z, z') = \delta(\mathbf{r} - \mathbf{r}') \quad (\text{A.23})$$

$$(k_z^2 + \partial_z^2) \tilde{G}_{xx}(\mathbf{k}_p, \omega; z, z') = -\frac{k_z^2}{\epsilon \frac{\omega^2}{c^2}} \delta(\mathbf{r} - \mathbf{r}'). \quad (\text{A.24})$$

The following equation can be used in determining the solution to the above differential equation

$$(\beta^2 + \partial_z^2) \frac{e^{i\beta|z-z'|}}{2i\beta} = \delta(\mathbf{r} - \mathbf{r}') \quad (\text{A.25})$$

I will use the notation of $q = \sqrt{\epsilon} \frac{\omega}{c}$ and $\beta = k_z = \sqrt{\epsilon \frac{\omega^2}{c^2} - k_p^2}$ from this point on. Our solution for the source term of $\tilde{G}_{xx}(\mathbf{k}_p, \omega; z, z')$ is then

$$\frac{i\beta}{2q^2} e^{i\beta|z-z'|}. \quad (\text{A.26})$$

Using this source term, we now can construct the Green's function term $\tilde{G}_{xx}(\mathbf{k}_p, \omega; z, z')$ for a planar interface.

Consider a planar interface at $z = 0$ in the x-y plane, separating two dielectric medium with $\epsilon = \epsilon_1$ for $z < 0$ and $\epsilon = \epsilon_2$ for $z > 0$. Now consider a source in the region $z < 0$ and $z' < 0$. The wave vector and the component normal to the surface will be notated by $q_i = \sqrt{\epsilon_i} \frac{\omega}{c}$ and $\beta_i = \sqrt{q_i^2 - k_p^2}$ respectively, with the subscript i indicating the half space of the medium. The reflected and transmitted components of the Green's function are solutions to the Helmholtz equation $(\beta_i^2 + \partial_z^2)$ and have solutions of the form $e^{\pm i\beta_i z}$ depending on propagation direction. $\tilde{G}_{xx}(\mathbf{k}_p, \omega; z, z')$ for the two half spaces is then

$$\tilde{G}_{xx}(\mathbf{k}_p, \omega; z, z') = \begin{cases} \frac{i\beta_1}{2q_1^2} e^{i\beta_1|z-z'|} + B e^{-i\beta_1 z} & z < 0 \\ C e^{i\beta_2 z} & z > 0. \end{cases} \quad (\text{A.27})$$

From Eq. (2.36) and continuity at $z = 0$ we acquire the expression

$$\frac{i\beta_1}{2q_1^2} e^{i\beta_1|z'|} + B = C. \quad (\text{A.28})$$

The second necessary equation comes from the continuous quantity Eq. (A.21). The

derivative of the source term is

$$\begin{aligned}
\partial_z e^{i\beta_i|z-z'|} &= \partial_z (e^{i\beta_i(z-z')} \Theta(z-z') + e^{-i\beta_i(z-z')} \Theta(z'-z)) \\
&= (e^{i\beta_i(z-z')} \delta(z-z') - e^{-i\beta_i(z-z')} \delta(z-z')) \\
&\quad + i\beta_i (e^{i\beta_i(z-z')} \Theta(z-z') - e^{-i\beta_i(z-z')} \Theta(z'-z)) \\
&= 2i \sin(\beta_i(z-z')) \delta(z-z') + i\beta_i e^{i\beta_i|z-z'|} \text{sgn}(z-z') \\
&= 0 + i\beta_i e^{i\beta_i|z-z'|} \text{sgn}(z-z'). \tag{A.29}
\end{aligned}$$

Applying the boundary condition Eq. (2.36) to Eq. (A.27) and using the above expression (and noting that $\text{sgn}(z-z')$ is positive because $z=0$ and $z'<0$) the acquired expression is

$$\begin{aligned}
i\beta_1 \frac{\epsilon_1}{\beta_1^2} \left(\frac{i\beta_1}{2q_1^2} e^{i\beta_1|z'|} - B \right) &= i\beta_2 \frac{\epsilon_2}{\beta_2^2} C \\
\frac{i\beta_1}{2q_1^2} e^{i\beta_1|z'|} - B &= \frac{\epsilon_2 \beta_1}{\epsilon_1 \beta_2} C \tag{A.30}
\end{aligned}$$

Using the method of Ref. [89] (See also Ref. [90]) the dyadic Green functions of a multiple layered planar dielectric are solved. Due to the translational invariance of the problem of a planar dielectric interface, it is useful to decompose the Green's function into transverse and normal components through the Fourier transform

$$G_{\mu\nu}(\mathbf{r}, \mathbf{r}', \omega) = \int \frac{d^2 \mathbf{k}_p}{(2\pi)^2} e^{i\mathbf{k}_p \cdot (\mathbf{r}_p - \mathbf{r}'_p)} \tilde{G}_{\mu\nu}(\mathbf{k}_p, \omega; z, z'), \tag{A.31}$$

where \mathbf{k}_p is the wave vector component tangential to the interface and \mathbf{r}_p is the corresponding position component.

For sources located in region 3 ($z' > d$) and $z > d$ the elements of $\tilde{G}_{\mu\nu}(\mathbf{k}_p, \omega; z, z')$

are

$$\begin{aligned} \tilde{G}_{xx} = & \frac{1}{\mathbf{k}_p^2} e^{-i\beta_3(z+d)} \left(k_x^2 \tilde{R}_{3,2}^{TM} Z_{xx}(\mathbf{k}_p, z') \right. \\ & \left. + k_y^2 \tilde{R}_{3,2}^{TE} Z_{yy}(\mathbf{k}_p, z') \right) \end{aligned} \quad (\text{A.32})$$

$$\begin{aligned} \tilde{G}_{xy} = & \frac{k_x k_y}{\mathbf{k}_p^2} e^{i\beta_3(z-d)} \left(\tilde{R}_{3,2}^{TM} Z_{xx}(\mathbf{k}_p, z') \right. \\ & \left. - \tilde{R}_{3,2}^{TE} Z_{yy}(\mathbf{k}_p, z') \right) \end{aligned} \quad (\text{A.33})$$

$$\tilde{G}_{xz} = \frac{k_x}{\mathbf{k}_p} \tilde{R}_{3,2}^{TM} Z_{xz}(\mathbf{k}_p, z') e^{i\beta_3(z-d)} \quad (\text{A.34})$$

$$\tilde{G}_{yx} = \tilde{G}_{xy} \quad (\text{A.35})$$

$$\begin{aligned} \tilde{G}_{yy} = & \frac{1}{\mathbf{k}_p^2} e^{i\beta_3(z-d)} \left(k_y^2 \tilde{R}_{3,2}^{TM} Z_{xx}(\mathbf{k}_p, z') \right. \\ & \left. + k_x^2 \tilde{R}_{3,2}^{TE} Z_{yy}(\mathbf{k}_p, z') \right) \end{aligned} \quad (\text{A.36})$$

$$\tilde{G}_{yz} = \tilde{G}_{xz}, \quad k_x \leftrightarrow k_y \quad (\text{A.37})$$

$$\tilde{G}_{zx} = -\frac{k_x}{\beta_3} \tilde{R}_{3,2}^{TM} Z_{xx}(\mathbf{k}_p, z') e^{i\beta_3(z-d)} \quad (\text{A.38})$$

$$\tilde{G}_{zy} = -\frac{k_y}{\beta_3} \tilde{R}_{3,2}^{TM} Z_{xx}(\mathbf{k}_p, z') e^{i\beta_3(z-d)} \quad (\text{A.39})$$

$$\tilde{G}_{zz} = -\frac{k_p}{\beta_3} \tilde{R}_{3,2}^{TM} Z_{xz}(\mathbf{k}_p, z') e^{i\beta_3(z-d)} \quad (\text{A.40})$$

and for $z < 0$ the terms are

$$\tilde{G}_{xx} = \frac{1}{\mathbf{k}_p^2} e^{-i\beta_1 z + i\beta_2 d} \left(k_x^2 \tilde{S}_{3,1}^{TM} Z_{xx}(\mathbf{k}_p, z') + k_y^2 \tilde{S}_{3,1}^{TE} Z_{yy}(\mathbf{k}_p, z') \right) \quad (\text{A.41})$$

$$\tilde{G}_{xy} = \frac{k_x k_y}{\mathbf{k}_p^2} e^{-i\beta_1 z + i\beta_2 d} \left(\tilde{S}_{3,1}^{TM} Z_{xx}(\mathbf{k}_p, z') - \tilde{S}_{3,1}^{TE} Z_{yy}(\mathbf{k}_p, z') \right) \quad (\text{A.42})$$

$$\tilde{G}_{xz} = \frac{k_x}{\mathbf{k}_p} \tilde{S}_{3,1}^{TM} Z_{xz}(\mathbf{k}_p, z') e^{-i\beta_1 z + i\beta_2 d} \quad (\text{A.43})$$

$$\tilde{G}_{yx} = \tilde{G}_{xy} \quad (\text{A.44})$$

$$\tilde{G}_{yy} = \frac{1}{\mathbf{k}_p^2} e^{-i\beta_1 z + i\beta_2 d} \left(k_y^2 \tilde{S}_{3,1}^{TM} Z_{xx}(\mathbf{k}_p, z') + k_x^2 \tilde{S}_{3,1}^{TE} Z_{yy}(\mathbf{k}_p, z') \right) \quad (\text{A.45})$$

$$\tilde{G}_{yz} = \tilde{G}_{xz}, \quad k_x \leftrightarrow k_y \quad (\text{A.46})$$

$$\tilde{G}_{zx} = -\frac{k_x}{\beta_3} \tilde{S}_{3,1}^{TM} Z_{xx}(\mathbf{k}_p, z') e^{-i\beta_1 z + i\beta_2 d} \quad (\text{A.47})$$

$$\tilde{G}_{zy} = -\frac{k_y}{\beta_3} \tilde{S}_{3,1}^{TM} Z_{xx}(\mathbf{k}_p, z') e^{-i\beta_1 z + i\beta_2 d} \quad (\text{A.48})$$

$$\tilde{G}_{zz} = -\frac{k_p}{\beta_3} \tilde{S}_{3,1}^{TM} Z_{xz}(\mathbf{k}_p, z') e^{-i\beta_1 z + i\beta_2 d} \quad (\text{A.49})$$

where

$$Z_{xx}(\mathbf{k}_p, z') = \frac{i\beta_3}{2k_3^2} e^{i\beta_3|d-z'|} \quad (\text{A.50})$$

$$Z_{yy}(\mathbf{k}_p, z') = \frac{i}{2\beta_3} e^{i\beta_3|d-z'|} \quad (\text{A.51})$$

$$Z_{xz}(\mathbf{k}_p, z') = \frac{ik_p}{2k_3^2} e^{i\beta_3|d-z'|}, \quad (\text{A.52})$$

with $\beta_i = \sqrt{k_i^2 - k_p^2}$ and $k_i = \sqrt{\varepsilon_i} \frac{\omega}{c}$.

The transmission and reflection of radiation at the interface is characterized by the generalized Fresnel reflection and transmission coefficients. Consider a series of

interfaces, where i increases for z increasing in $z > 0$. For reflection in region i , from an interface between regions i and $i - 1$, the generalized reflection coefficient is

$$\tilde{R}_{i,i-1}^{TM/TE} = \frac{R_{i,i-1}^{TM/TE} + \tilde{R}_{i-1,i-2}^{TM/TE} e^{i2\beta_{i-1}(d_{i-1}-d_{i-2})}}{1 + R_{i,i-1}^{TM/TE} \tilde{R}_{i-1,i-2}^{TM/TE} e^{i2\beta_{i-1}(d_{i-1}-d_{i-2})}}. \quad (\text{A.53})$$

The generalized transmission coefficients are

$$\tilde{T}_{i,i-1}^{TM/TE} = \frac{T_{i,i-1}^{TM/TE}}{1 + R_{i,i-1}^{TM/TE} \tilde{R}_{i-1,i-2}^{TM/TE} e^{i2\beta_{i-1}(d_{i-1}-d_{i-2})}}. \quad (\text{A.54})$$

These are expressed in the usual Fresnel coefficients

$$R_{i,i-1}^{TM} = \frac{\varepsilon_{i-1}\beta_i - \varepsilon_i\beta_{i-1}}{\varepsilon_{i-1}\beta_i + \varepsilon_i\beta_{i-1}} \quad (\text{A.55})$$

$$R_{i,i-1}^{TE} = \frac{\beta_i - \beta_{i-1}}{\beta_i + \beta_{i-1}} \quad (\text{A.56})$$

$$T_{i,i-1}^{TM} = \frac{2\varepsilon_i\beta_{i-1}}{\varepsilon_{i-1}\beta_i + \varepsilon_i\beta_{i-1}} \quad (\text{A.57})$$

$$R_{i,i-1}^{TE} = \frac{2\beta_i}{\beta_i + \beta_{i-1}}. \quad (\text{A.58})$$

Appendix B

Stationary Phase Method

To evaluate the two-dimensional integral in Eq. (2.22) we use the stationary phase method (see, e.g., Ref. [58]). The method of stationary phase for double integrals and its derivation is a lengthy discussion. The subject in its entirety is beyond the scope of these notes.

Consider a general double integral over the domain S

$$A(r) = \iint_S dp dq a(p, q) e^{ir\Phi(p, q)}. \quad (\text{B.1})$$

as $r \rightarrow \infty$. Again the function $a(p, q)$ can be thought of as an amplitude modulation of the oscillating term $e^{ir\phi(p, q)}$. Of interest are critical points of the first kind, whose points that are within the domain S . The function $\phi(p, q)$ is stationary for those points that satisfy the condition

$$\frac{\partial\phi(p, q)}{\partial p} = \frac{\partial\Phi(p, q)}{\partial p} = 0. \quad (\text{B.2})$$

The derivation of the contribution of the critical point is not important here. The derivation is solving an integral of a quadratic function of the two variables p and q with coefficients that are second order partial derivatives of $\phi(p, q)$. Two quantities of importance, which depend entirely upon the second order partial derivatives, are

$$\Sigma = \Phi_{xx} + \Phi_{yy}, \quad (\text{B.3})$$

$$\Delta = \Phi_{xx}\Phi_{yy} - \Phi_{xy}^2. \quad (\text{B.4})$$

The contribution to the integral from a critical point is

$$A^{(1)}(r) \sim \frac{2\pi i \sigma}{r \sqrt{|\Delta|}} a(p_1, q_1) e^{ir\Phi(p_1, q_1)}, \quad (\text{B.5})$$

where (The eqnarray environment fails me here. I need array and multiple columns),

$$\sigma = 1 \text{ when } \Delta > 0, \Sigma > 0 \quad (\text{B.6})$$

$$= -1 \text{ when } \Delta > 0, \Sigma < 0 \quad (\text{B.7})$$

$$= -i \text{ when } \Delta < 0. \quad (\text{B.8})$$

There are two contributions to the phase of the integrand: the Fourier transform term and the phase of the Greens function itself, which depends on the phase of the Fresnel coefficients and a phase factor that depends on the position z' of the source. Because the film thickness d is much smaller than λ the Fresnel coefficients vary slowly with \mathbf{k}_p . For this reason we need only to consider the position of the source. For brevity we here will only discuss the Green's function for the observation point \mathbf{r} in region 1 and the source position \mathbf{r}' in region 3. Because of the general form of the Green's function in this case (see Eqs. (A.41) - (A.49)) integral (2.22) can generally be written as

$$G_{\mu\nu}(\mathbf{r}, \mathbf{r}', \omega) = \int \frac{d^2 \mathbf{k}_p}{(2\pi)^2} e^{i\mathbf{k}_p \cdot (\mathbf{r} - \mathbf{r}')} e^{-i\beta_1 z} e^{i\beta_3 |d - z'|} \\ \times D_{\mu\nu}(k_x, k_y, \omega), \quad (\text{B.9})$$

where the coefficients $D_{\mu\nu}(k_x, k_y, \omega)$ are related to the Fresnel coefficients and can be formally defined as $D_{\mu\nu}(k_x, k_y, \omega) = \tilde{G}_{\mu\nu}(\mathbf{k}_p, \omega; z, z') e^{i\beta_1 z} e^{-i\beta_3 |d - z'|}$. The phase term of interest is then

$$\Phi = \mathbf{k}_p \cdot (\mathbf{r} - \mathbf{r}') - \beta_1 z + \beta_3 |d - z'|. \quad (\text{B.10})$$

Recognizing that $z' > d$, and that $\mathbf{k}_p = (k_x, k_y, 0)$ is the same in region 1 and 3 we get

$$\Phi = k_x(x - x') + k_y(y - y') - \beta_1 z + \beta_3(z' - d) \quad (\text{B.11})$$

The phase is then expanded in powers of $k_1 r$. To do so we introduce the quantities

$$s_x = \frac{x}{r}, \quad s_y = \frac{y}{r} \quad (\text{B.12})$$

$$s'_x = \frac{x'}{r}, \quad s'_y = \frac{y'}{r} \quad (\text{B.13})$$

$$p = \frac{k_x}{k_1}, \quad q = \frac{k_y}{k_1} \quad (\text{B.14})$$

$$s_z = \frac{z}{r} = (1 - s_x^2 - s_y^2)^{1/2} \quad (\text{B.15})$$

$$s'_z = \frac{z'}{r} = (1 - s'^2_x - s'^2_y)^{1/2} \quad (\text{B.16})$$

$$m = -\frac{\beta_1}{k_1} = -(1 - p^2 - q^2)^{1/2} \quad (\text{B.17})$$

$$m' = \frac{\beta_3}{k_1} = + \left(\left(\frac{k_3}{k_1} \right)^2 - p^2 - q^2 \right)^{1/2}, \quad (\text{B.18})$$

where (s_x, s_y, s_z) determine the direction of the observation point relative to the source, and p, q are re-scaled integration variables. We can then express the phase as

$$\Phi = k_1 r (p(s_x - s'_x) + q(s_y - s'_y) + m s_z + m' s'_z). \quad (\text{B.19})$$

The integral is evaluated in the limit of large $k_1 r$. The stationary points are determined by setting the derivatives $\partial\Phi/\partial p$ and $\partial\Phi/\partial q$ to zero which yields

$$\frac{s_x - s'_x}{s_z + s'_z \frac{m}{m'}} = \frac{p}{m} \quad \text{and} \quad \frac{s_y - s'_y}{s_z + s'_z \frac{m}{m'}} = \frac{q}{m}. \quad (\text{B.20})$$

Because $r \gg r'$ we generally have $s'_i \ll s_i$. This is not true if we observe the far field very close to the z -axis (so that $s_x \approx s'_x$) or very close to the plane of the

interface (so that $s_z \approx s'_z$). Ignoring these special cases we can simplify the stationary points to

$$\frac{s_x}{s_z} = \frac{p}{m} \quad \text{and} \quad \frac{s_y}{s_z} = \frac{q}{m}, \quad (\text{B.21})$$

which is the usual result of the far field approximation that \mathbf{k} and \mathbf{r} are parallel.

To determine the contribution of the critical points to the integral the second order partial derivatives at the stationary points must be evaluated. These evaluated derivatives are

$$\frac{\partial^2 \Phi}{\partial x^2} = - \left(1 + \left(\frac{s_x}{s_z} \right)^2 \right), \quad (\text{B.22})$$

$$\frac{\partial^2 \Phi}{\partial y^2} = - \left(1 + \left(\frac{s_y}{s_z} \right)^2 \right), \quad (\text{B.23})$$

$$\frac{\partial^2 \Phi}{\partial x \partial y} = - \frac{s_x s_y}{s_z^2}. \quad (\text{B.24})$$

If we parametrize the stationary point as $p = \frac{k_x}{k_1} = \sin \phi \cos \theta$, and $q = \frac{k_y}{k_1} = \sin \phi \sin \theta$, the Green's function in stationary phase approximation becomes

$$\begin{aligned} G_{\mu\nu}(\mathbf{r}, \mathbf{r}', \omega) &= \frac{i}{2\pi} \left(\frac{k_i}{r} \frac{z}{r} \right) e^{ik_1 r} e^{-ik_1 \sin \phi (\cos \theta x' + \sin \theta y')} e^{-i\beta_1 z} e^{i\beta_3 |d-z'|} \\ &\times D_{\mu\nu}(k_1 \sin \phi \cos \theta, k_1 \sin \phi \sin \theta, \omega). \end{aligned} \quad (\text{B.25})$$

The terms $\beta_j = k_{z,i}$ are evaluated at $k_p = k_1 \sin \phi$, such that $\beta_j = \sqrt{k_j^2 - k_1^2 \sin^2 \phi}$. The effect of the stationary phase method on the integral is a leading term that is proportional to z . This results in the vanishing of terms near the boundary with the exception of those tied to TE radiation. Expressing $D_{\mu\nu}$ in terms of $\tilde{G}_{\mu\nu}$ then yields Eq. (3.18).

Appendix C

Spontaneous Decay of the Harmonic Oscillator

We consider the dynamics of the coupled atom-radiation system when its initial state corresponds to an excited atom with no photons present,

$$|\psi_{\text{init}}\rangle = \hat{b}_0^\dagger|0\rangle \otimes |\text{vac}\rangle. \quad (\text{C.1})$$

Here, \hat{b}_0 corresponds to the harmonic oscillator's lowering operator in Schrödinger picture, $|0\rangle$ denotes its ground state, and $|\text{vac}\rangle$ describes the electromagnetic vacuum state. For the initial state (C.1), the spontaneously emitted single-photon field can be found, upon using Equations (4.41) and (4.42), through

$$\mathbf{E}_i^{(\text{se})}(\mathbf{r}, s) = \langle 0| \otimes \langle \text{vac}| \hat{\mathbf{E}}_i(\mathbf{r}, s) |\psi_{\text{init}}\rangle \quad (\text{C.2})$$

$$= \frac{i}{g} \mathbf{e}_k \frac{\Gamma_{ik}(\mathbf{r}, s) + i\Delta_{ik}(\mathbf{r}, s)}{s + i\omega'_0 + \gamma}. \quad (\text{C.3})$$

To find the emitted field after a long time $t \gg 1/\gamma$ we recall that the inverse Laplace transform is defined as $\mathbf{E}_i^{(\text{se})}(\mathbf{r}, t) = (2\pi i)^{-1} \int_{-i\infty+\epsilon}^{i\infty+\epsilon} e^{ts} \mathbf{E}_i^{(\text{se})}(\mathbf{r}, s) ds$, with $\epsilon > 0$. This can be evaluated using the residue theorem. The function $\mathbf{E}_i^{(\text{se})}(\mathbf{r}, s)$ has two contributions: one arriving from the pole $s = -i\omega'_0 - \gamma$, and a branch cut arising from the pole at $s = -i\omega$ in Eq. (4.40). The former generates an exponentially decaying term, which can be neglected for large times. We then find

$$\mathbf{E}_i^{(\text{se})}(\mathbf{r}, t) \approx i \frac{g\hbar}{\pi\epsilon_0} \mathbf{e}_k \int_0^\infty d\omega \frac{e^{-i\omega t}}{i(\omega'_0 - \omega) + \gamma} \frac{\omega^2}{c^2} \text{Im} G_{ik}(\mathbf{r}, \mathbf{r}_A, \omega). \quad (\text{C.4})$$

Writing $\text{Im} G_{ik} = (2i)^{-1}(\text{Im} G_{ik} - \text{Im} G_{ik}^*)$ and using the conjugation property Eq. (A.1), one can show that $G_{ik}^*(\mathbf{r}, \mathbf{r}_A, \omega)$ corresponds to an off-resonant contribution, which

can be neglected. We then obtain

$$\begin{aligned} \mathbf{E}_i^{(\text{se})}(\mathbf{r}, t) &\approx \frac{g\hbar}{2\pi\epsilon_0} \mathbf{e}_k \int_0^\infty d\omega \frac{e^{-i\omega t}}{i(\omega'_0 - \omega) + \gamma} \\ &\times \frac{\omega^2}{c^2} G_{ik}(\mathbf{r}, \mathbf{r}_A, \omega). \end{aligned} \quad (\text{C.5})$$

We are interested in the case when the atom is placed above the metal film and the emitted field is observed on the side of the prism. In the far-field limit $kr \gg 1$ (see App. C of Ref. [99]), the Green's function takes the approximate form in Eq. (3.18) with $\mathbf{k} = k_1 \frac{\mathbf{r}}{r}$ and \mathbf{k}_\parallel the projection of this vector on the (x - y -) plane of the interface, as well as $k_1 = \omega\sqrt{\epsilon_1}/c$.

The light pulse (C.5) contains an infinite range of frequencies. This is necessary because the oscillator corresponds to a point dipole at position \mathbf{r}_A , so that the emitted light is initially strongly localized. In a renormalized treatment, the oscillator has a finite size, so that, for an isotropic smearing function $\tilde{h}(\mathbf{r})$ the renormalization procedure outlined above simply results in a frequency cutoff in the integral over ω . The precise value of this cutoff only affects the value of the renormalized resonance frequency ω'_0 . To a very good approximation, the shape of the pulse is determined by a narrow frequency range of a width in the order of $\Delta\omega_{\text{max}} = 100\gamma$ around the oscillator's resonance frequency. Within this range, only the exponentials and the Lorentzian denominator vary significantly with ω . We can therefore approximate the emitted field by

$$\begin{aligned} \mathbf{E}_i^{(\text{se})}(\mathbf{r}, t) &\approx \frac{ig\hbar}{4\pi^2\epsilon_0} \mathbf{e}_k e^{-i\omega'_0(t-n_1\frac{r}{c})} \frac{k_1 z}{r^2} \frac{\omega_0'^2}{c^2} \tilde{G}_{ik}(\mathbf{k}_\parallel, \omega'_0; z') \\ &\times e^{-i\mathbf{k}_\parallel \cdot \mathbf{r}'} \int_{-\Delta\omega_{\text{max}}}^{\Delta\omega_{\text{max}}} d\Delta\omega \frac{e^{-i\Delta\omega(t-n_1\frac{r}{c})}}{-i\Delta\omega + \gamma}. \end{aligned} \quad (\text{C.6})$$

We will assume that the oscillator is placed above the origin of the coordinate system,

so that $e^{-i\mathbf{k}_{\parallel}\cdot\mathbf{r}'} = 1$. The integral over $\Delta\omega$ can easily be performed. In the limit $\Delta\omega_{\max} \rightarrow \infty$, which gives an excellent and convenient approximation we obtain

$$\mathbf{E}_i^{(\text{se})}(\mathbf{r}, t) \approx \frac{ig\hbar}{2\pi\epsilon_0} \mathbf{e}_k e^{-i\omega'_0(t-n_1\frac{r}{c})} \frac{k_1 z}{r^2} \tilde{G}_{ik}(\mathbf{k}_{\parallel}, \omega'_0; z') \frac{\omega'_0{}^2}{c^2} \Theta\left(t - n_1\frac{r}{c}\right) e^{-\gamma(t-n_1\frac{r}{c})}, \quad (\text{C.7})$$

with Θ the step function, $k_1 = \omega_0 n_1 / c$, and \mathbf{k}_{\parallel} the projection of $k_1 \mathbf{r} / r$ on the x - y -plane.

The pulse (C.7) has a clear physical interpretation. It corresponds to a light pulse that travels with the velocity of light c/n_1 through the prism. The step function ensures that the front of the pulse arrives at distance r not earlier than $t = n_1 r / c$. For larger times, the pulse at this point decreases exponentially because of the oscillator's decay. The expression $e^{-i\omega'_0(t-n_1\frac{r}{c})} k_1 z / r^2$ describes the far-field of an oscillating point dipole. The factor $\tilde{G}_{ik}(\mathbf{k}_{\parallel}, \omega_0; z')$ essentially contains Fresnel coefficients and describes the modulation of the light intensity with observation direction \mathbf{r} / r . In particular, this factor describes the narrow emission cone associated with the generation of SPs.

Appendix D

Excitation Probability for a Single-Photon Pulse

To find the excitation probability, we use the initial state $|\psi_0\rangle = \hat{a}^\dagger|\text{vac}\rangle \otimes |0\rangle$, which describes a single-photon pulse. The mode annihilation operator \hat{a} given by Eq. (5.2), with the field amplitude of Eq. (5.9).

$$\begin{aligned} P_e(t) &= \left| \langle 0 | \hat{b}(t) | \psi_0 \rangle \right|^2 \\ &= \left| [\hat{b}(t), \hat{a}^\dagger] \right|^2. \end{aligned} \quad (\text{D.1})$$

Using solution (4.41), the commutator can be evaluated as

$$\begin{aligned} [\hat{b}(t), \hat{a}^\dagger] &= \frac{1}{2\pi i} \int_{\epsilon-i\infty}^{\epsilon+i\infty} ds e^{ts} [\hat{b}(s), \hat{a}^\dagger] \\ &= \frac{g\epsilon_\infty}{\pi^2} \int_{\epsilon-i\infty}^{\epsilon+i\infty} ds e^{ts} \frac{\mathbf{e}_k}{s + i\omega'_0 + \gamma} \int_0^\infty \frac{d\omega}{s + i\omega} \\ &\quad \times \int d^3r \mathcal{E}_i(\mathbf{r}) \frac{\omega}{c^2} \text{Im} G_{ki}(\mathbf{r}_A, \mathbf{r}, \omega). \end{aligned} \quad (\text{D.2})$$

The integral over s can be solved using the residue theorem. There are two poles at $s = -i\omega$ and $s = -i\omega'_0 - \gamma$. Assuming that $t \gg \gamma^{-1}$, the exponential suppresses the contribution of the second pole. We therefore get

$$\begin{aligned} [\hat{b}(t), \hat{a}^\dagger] &\approx \frac{-2g\epsilon_\infty}{\pi} \int_0^\infty d\omega \frac{e^{-i\omega t}}{\omega - \omega'_0 + i\gamma} \frac{\omega}{c^2} \\ &\quad \times \int d^3x \mathbf{e}_k \text{Im} G_{ki}(\mathbf{r}_A, \mathbf{x}, \omega) \mathcal{E}_i(\mathbf{x}). \end{aligned} \quad (\text{D.3})$$

To further evaluate this commutator, we make use of the planar symmetry of the metal interface, which guarantees that the Green's function is homogeneous in

the x - y plane. As shown in appendix B of Ref. [99], one can perform a Fourier transformation in the x - y -plane so that

$$G_{ki}(\mathbf{r}_A, \mathbf{x}, \omega) = \int \frac{d^2 k_{\parallel}}{2\pi} e^{i\mathbf{k}_{\parallel} \cdot (\mathbf{r}_A - \mathbf{x})} \tilde{G}_{ki}(\mathbf{k}_{\parallel}, \omega, z_A, z), \quad (\text{D.4})$$

The commutator (D.3) can then be expressed as

$$\begin{aligned} [\hat{b}(t), \hat{a}^\dagger] &= \frac{ig\epsilon_\infty}{\pi} e_k \int_0^\infty d\omega \frac{e^{-i\omega t}}{\omega - \omega'_0 + i\gamma} \frac{\omega}{c^2} \int d^2 k_{\parallel} \int_{-\infty}^\infty dz \\ &\times \left(\mathcal{E}_i(\mathbf{k}_{\parallel}, z) e^{i\mathbf{k}_{\parallel} \cdot \mathbf{r}_A} \tilde{G}_{ki}(\mathbf{k}_{\parallel}, \omega, z_A, z) \right. \\ &\quad \left. - \mathcal{E}_i(-\mathbf{k}_{\parallel}, z) e^{-i\mathbf{k}_{\parallel} \cdot \mathbf{r}_A} \tilde{G}_{ki}^*(\mathbf{k}_{\parallel}, \omega, z_A, z) \right). \end{aligned} \quad (\text{D.5})$$

For a photon pulse that is incident from the prism ($z < 0$) and an atom placed above the metal film ($z_A > 0$), the Green's function $\tilde{G}_{ki}(\mathbf{k}_{\parallel}, \omega, z_A, z)$ is proportional to $e^{i\beta_1(z_A - z)}$. Defining

$$\tilde{G}_{ki}(\mathbf{k}_{\parallel}, \omega, z_A) \equiv e^{i\beta_1 z \operatorname{sgn}(z_A - z)} \tilde{G}_{ki}(\mathbf{k}_{\parallel}, \omega, z_A, z), \quad (\text{D.6})$$

we then find

$$\begin{aligned} [\hat{b}(t), \hat{a}^\dagger] &= \frac{ig\epsilon_\infty}{\pi} e_k \int_0^\infty d\omega \frac{e^{-i\omega t}}{\omega - \omega'_0 + i\gamma} \frac{\omega}{c^2} \int d^2 k_{\parallel} \int_{-\infty}^\infty dz \\ &\times \left(\mathcal{E}_i(\mathbf{k}_{\parallel}, z) e^{i\mathbf{k}_{\parallel} \cdot \mathbf{r}_A} e^{-i\beta_1 z} \tilde{G}_{ki}(\mathbf{k}_{\parallel}, \omega, z_A) \right. \\ &\quad \left. - \mathcal{E}_i(-\mathbf{k}_{\parallel}, z) e^{-i\mathbf{k}_{\parallel} \cdot \mathbf{r}_A} e^{i\beta_1 z} \tilde{G}_{ki}^*(\mathbf{k}_{\parallel}, \omega, z_A) \right). \end{aligned} \quad (\text{D.7})$$

If $\beta_1 = \sqrt{\epsilon_1 \omega^2 / c^2 - \vec{k}_{\parallel}^2} \geq 0$ for all Fourier components of the electric field, this can be evaluated to

$$\begin{aligned} [\hat{b}(t), \hat{a}^\dagger] &= i\sqrt{\frac{2}{\pi}} \int_0^\infty d\omega \frac{g\epsilon_\infty \mathbf{e}_k e^{-i\omega t}}{\omega - \omega'_0 + i\gamma} \frac{\omega}{c^2} \int d^2 k_{\parallel} e^{i\mathbf{k}_{\parallel} \cdot \mathbf{r}_A} \\ &\times \left\{ \tilde{G}_{ki}(\mathbf{k}_{\parallel}, \omega, z_A) \mathcal{E}_i(\mathbf{k}_{\parallel}, k_z = \beta_1) \right. \\ &\quad \left. - \tilde{G}_{ki}^*(-\mathbf{k}_{\parallel}, \omega, z_A) \mathcal{E}_i(\mathbf{k}_{\parallel}, k_z = -\beta_1) \right\}. \end{aligned} \quad (\text{D.8})$$

The field amplitude $\mathcal{E}_i(\mathbf{k})$ describes a pulse that starts on the prism side ($z < 0$) and is incident on the atom. Its general direction of propagation is therefore upwards, so that it only contains Fourier components with $k_z > 0$. We therefore arrive at the result

$$[\hat{b}(t), \hat{a}^\dagger] = i\sqrt{\frac{2}{\pi}} \int_0^\infty d\omega \frac{g\epsilon_\infty \mathbf{e}_k e^{-i\omega t}}{\omega - \omega'_0 + i\gamma} \frac{\omega}{c^2} \int d^2k_\parallel e^{i\mathbf{k}_\parallel \cdot \mathbf{r}_A} \times \tilde{G}_{ki}(\mathbf{k}_\parallel, \omega, z_A) \mathcal{E}_i(\mathbf{k}_\parallel, k_z = \beta_1). \quad (\text{D.9})$$

Because of the rotational symmetry of the interface we express the wavevector \mathbf{k} in spherical coordinates k, θ, ϕ , so that $\beta_1 = \sqrt{\omega^2 n_1^2 / c^2 - k'^2 \sin^2 \theta}$. For an incident photon close to the SP resonance angle, $\sin \theta$ is not close to unity. Consequently, $\beta_1 > 0$, so that it is justified to use Eq. (D.8).

For a dipole orientation \mathbf{e} along the z -axis, the field amplitude (5.9) depends on the azimuthal angle ϕ only through the factor in parentheses. Furthermore, the Green's function's dependence on ϕ can be written in terms of a rotation matrix,

$$\tilde{G}_{ki}(\vec{k}'_\parallel, \omega, z_A) = (R(\phi) \cdot \bar{G}(k'_\parallel, \omega, z_A) \cdot R^{-1}(\phi))_{ki} \quad (\text{D.10})$$

$$R(\phi) = \begin{pmatrix} \cos \phi & -\sin \phi & 0 \\ \sin \phi & \cos \phi & 0 \\ 0 & 0 & 1 \end{pmatrix}. \quad (\text{D.11})$$

The integration over ϕ is then easy to perform. Using the explicit form of the Green's function given in Ref. [99], we then arrive at

$$[\hat{b}(t), \hat{a}^\dagger] = \sqrt{\frac{2}{\pi}} \int_0^\infty dk_\parallel \int_0^\infty \frac{d\omega}{\omega} \frac{e^{-i\omega t}}{\omega - \omega'_0 + i\gamma} \times \frac{2g k_\parallel^3 \mathcal{A} \beta_2 \epsilon_1 \epsilon_2 e^{i(\beta_2 d - \beta_3 (d - z_A))}}{e^{2i\beta_2 d} (\beta_2 \epsilon_1 - \beta_1 \epsilon_2) (\beta_2 \epsilon_3 - \beta_3 \epsilon_2) - (\beta_2 \epsilon_1 + \beta_1 \epsilon_2) (\beta_3 \epsilon_2 + \beta_2 \epsilon_3)}. \quad (\text{D.12})$$

Because the incident pulse is confined in the inclination angle θ , a change of integration variables from $k_{\parallel} = n_1 \frac{\omega}{c} \sin \theta$ to θ is convenient. Doing so yields Eq. (5.13).

Bibliography

- [1] U. Schröder, *Surface Science* **102**, 118 (1981).
- [2] H. Raether, *Surface Plasmons on Smooth and Rough Surfaces and on Gratings* (Springer-Verlage, Berlin, 1988).
- [3] R. H. Ritchie, *Phys. Rev.* **106**, 874 (1957).
- [4] E. A. Stern and R. A. Ferrell, *Phys. Rev.* **120**, 130 (1960).
- [5] R. A. Ferrell, *Phys. Rev.* **111**, 1214 (1958).
- [6] C. J. Powell and J. B. Swan, *Phys. Rev.* **118**, 640 (1960).
- [7] J. Bladel, *Electromagnetic Fields* IEEE Press Series on Electromagnetic Wave Theory (John Wiley & Sons, 2007).
- [8] U. Fano, *Phys. Rev.* **51**, 288 (1937).
- [9] M. I. Stockman, *Physics Today* **64**, 39 (2011).
- [10] A. Otto, *Z. Physik* **216**, 398 (1968).
- [11] E. Kretschmann and H. Raether, *Z. Nature* **23**, 2135 (1968).
- [12] M. Fleischmann, P. Hendra, and A. McQuillan, *Chemical Physics Letters* **26**, 163 (1974).
- [13] D. L. Jeanmaire and R. P. V. Duyne, *Journal of Electroanalytical Chemistry and Interfacial Electrochemistry* **84**, 1 (1977).
- [14] M. Moskovits, *Rev. Mod. Phys.* **57**, 783 (1985).

- [15] E. Ru and P. Etchegoin, *Principles of Surface-Enhanced Raman Spectroscopy: And Related Plasmonic Effects* (Elsevier, 2008).
- [16] B. Liedberg, C. Nylander, and I. Lunström, *Sensors and Actuators* **4**, 299 (1983).
- [17] L. Zhang and D. Uttamchandani, *Electronics Letters* **24**, 1469 (1988).
- [18] I. Pockrand, J. Swalen, J. G. II, and M. Philpott, *Surface Science* **74**, 237 (1978).
- [19] S. Lofas and B. Johnsson, *J. Chem. Soc., Chem. Commun.* , 1526 (1990).
- [20] M. Bayindir *et al.*, *Phys. Rev. B* **63**, 081107 (2001).
- [21] T. Baba, *Nat. Photon* **2**, 465 (2008).
- [22] R. J. Schoelkopf, P. Wahlgren, A. A. Kozhevnikov, P. Delsing, and D. E. Prober, *Science* **280**, 1238 (1998).
- [23] W. Lu, Z. Ji, L. Pfeiffer, K. W. West, and A. J. Rimberg, *Nature* **423**, 422 (2003).
- [24] T. W. Ebbesen, C. Genet, and S. I. Bozhevolnyi, *Physics Today* **61**, 44 (2008).
- [25] J. J. Burke, G. I. Stegeman, and T. Tamir, *Phys. Rev. B* **33**, 5186 (1986).
- [26] D. Zhang *et al.*, *Plasmonics* , 1, 10.1007/s11468-011-9308-2.
- [27] R. B. Nielsen *et al.*, *Opt. Lett.* **33**, 2800 (2008).
- [28] R. M. Bakker *et al.*, *New Journal of Physics* **10**, 125022 (2008).
- [29] H. G. Craighead and G. A. Niklasson, *Applied Physics Letters* **44**, 1134 (1984).

- [30] J. R. Krenn *et al.*, Applied Physics Letters **77**, 3379 (2000).
- [31] R. Jin *et al.*, Science **294**, 1901 (2001),
<http://www.sciencemag.org/content/294/5548/1901.full.pdf>.
- [32] B. J. Wiley *et al.*, Nano Letters **7**, 1032 (2007),
<http://pubs.acs.org/doi/pdf/10.1021/nl070214f>.
- [33] D. A. Miller, IEEE **6**, 88 (2000).
- [34] S. A. Maier, M. D. Friedman, P. E. Barclay, and O. Painter, App. Phys. Lett. **86**, 071103 (2005).
- [35] M. I. Stockman, Phys. Rev. Lett. **93**, 137404 (2004).
- [36] J. A. Dionne, L. A. Sweatlock, H. A. Atwater, and A. Polman, Phys. Rev. B **73**, 035407 (2006).
- [37] S. I. Bozhevolnyi, V. S. Volkov, E. Devaux, J.-Y. Laluet, and T. W. Ebbesen, Nature **440**, 508 (2006).
- [38] A. Hosseini and Y. Massoud, Applied Physics Letters **90**, 181102 (2007).
- [39] D. E. Chang, A. S. Sorensen, E. A. Demler, and M. D. Lukin, Nat Phys **3**, 807 (2007).
- [40] D. J. Bergman and M. I. Stockman, Phys. Rev. Lett. **90**, 027402 (2003).
- [41] N. I. Zheludev, S. L. Prosvirnin, N. Papasimakis, and V. A. Fedotov, Nat. Photon **2**, 351 (2008).
- [42] C. H. Gan and G. Gbur, Opt. Express **14**, 2385 (2006).

- [43] J. Bosbach, C. Hendrich, F. Stietz, T. Vartanyan, and F. Träger, *Phys. Rev. Lett.* **89**, 257404 (2002).
- [44] J. R. Krenn *et al.*, *Applied Physics Letters* **77**, 3379 (2000).
- [45] T. Zentgraf, A. Christ, J. Kuhl, and H. Giessen, *Phys. Rev. Lett.* **93**, 243901 (2004).
- [46] A. Derode *et al.*, *Phys. Rev. Lett.* **90**, 014301 (2003).
- [47] G. Lerosey *et al.*, *Phys. Rev. Lett.* **92**, 193904 (2004).
- [48] M. I. Stockman, S. V. Faleev, and D. J. Bergman, *Phys. Rev. Lett.* **88**, 067402 (2002).
- [49] J. Seidel, S. Grafström, and L. Eng, *Phys. Rev. Lett.* **94**, 177401 (2005).
- [50] Z. I., P. L., N. Papasimakis, and F. A., *Nat Photon* **2**, 351 (2008).
- [51] G. A. Siviloglou, J. Broky, A. Dogariu, and D. N. Christodoulides, *Phys. Rev. Lett.* **99**, 213901 (2007).
- [52] M. V. Berry and N. L. Balazs, *American Journal of Physics* **47**, 264 (1979).
- [53] A. Salandrino and D. N. Christodoulides, *Opt. Lett.* **35**, 2082 (2010).
- [54] W. Liu, D. N. Neshev, I. V. Shadrivov, A. E. Miroshnichenko, and Y. S. Kivshar, *Opt. Lett.* **36**, 1164 (2011).
- [55] A. Minovich *et al.*, *Phys. Rev. Lett.* **107**, 116802 (2011).
- [56] W. L. Lama, R. Jodion, and L. Mandel, *Am. J. Phys.* **40**, 32 (1972).
- [57] J. D. Bekenstein and M. Schiffer, *Phys. Rev. D* **58**, 064014 (1998).

- [58] L. Mandel and E. Wolf, *Optical Coherence and Quantum Optics* (Cambridge University Press, New York, 1995).
- [59] R. H. Dicke, Phys. Rev. **93**, 99 (1954).
- [60] T. Brandes, Phys. Rep. **408**, 315 (2005).
- [61] A. Hilliard *et al.*, Phys. Rev. A **78**, 051403 (2008).
- [62] N. Lambert, C. Emary, and T. Brandes, Phys. Rev. Lett. **92**, 073602 (2004).
- [63] G. Nienhuis and C. Alkemade, Physica B+C **81**, 181 (1976).
- [64] E. M. Purcell, H. C. Torrey, and R. V. Pound, Phys. Rev. **69**, 37 (1946).
- [65] G. S. Agarwal, Phys. Rev. A **12**, 1475 (1975).
- [66] R. J. Glauber and M. Lewenstein, Phys. Rev. A **43**, 467 (1991).
- [67] T. Suzuki and P. K. L. Yu, J. Opt. Soc. Am. B **12**, 570 (1995).
- [68] E. Snoeks, A. Lagendijk, and A. Polman, Phys. Rev. Lett. **74**, 2459 (1995).
- [69] R. Bonifacio and H. Morawitz, Phys. Rev. Lett. **28**, 1559 (1976).
- [70] P. G. Brooke, K.-P. Marzlin, J. D. Cresser, and B. C. Sanders, Phys. Rev. A **77**, 033844 (2008).
- [71] E. Chang, A. S. Sørensen, and M. D. Lukin, Phys. Rev. B **76**, 035402 (2007).
- [72] E. Chang, A. S. Sørensen, and M. D. Lukin, Phys. Rev. Lett. **97**, 053002 (2006).
- [73] C. Santori, M. Pelton, G. Solomon, Y. Dale, and Y. Yamamoto, Phys. Rev. Lett. **86**, 1502 (2001).

- [74] J. I. Cirac, P. Zoller, H. J. Kimble, and H. Mabuchi, *Phys. Rev. Lett.* **78**, 3221 (1997).
- [75] X. Maître *et al.*, *Phys. Rev. Lett.* **79**, 769 (1997).
- [76] I.-C. Hoi *et al.*, *Phys. Rev. Lett.* **107**, 073601 (2011).
- [77] D. Loss and D. P. DiVincenzo, *Phys. Rev. A* **57**, 120 (1998).
- [78] J. I. Cirac and P. Zoller, *Phys. Rev. Lett.* **74**, 4091 (1995).
- [79] H.-J. Briegel, T. Calarco, D. Jaksch, J. Cirac, and P. Zoller, *Journal of Modern Optics* **47**, 415 (2000).
- [80] M. K. Tey *et al.*, *Nat Phys* **4**, 924 (2008).
- [81] M. Brune *et al.*, *Phys. Rev. Lett.* **72**, 3339 (1994).
- [82] A. D. Boozer, A. Boca, R. Miller, T. E. Northup, and H. J. Kimble, *Phys. Rev. Lett.* **98**, 193601 (2007).
- [83] M. Stobiska, G. Alber, and G. Leuchs, *EPL (Europhysics Letters)* **86**, 14007 (2009).
- [84] G. Lerosey *et al.*, *Phys. Rev. Lett.* **92**, 193904 (2004).
- [85] G. Lerosey, J. de Rosny, A. Tourin, A. Derode, and M. Fink, *Appl. Rev. Lett.* **88**, 154101 (2006).
- [86] R. Carminati, J. J. Sáenz, J.-J. Greffet, and M. Nieto-Vesperinas, *Phys. Rev. A* **62**, 012712 (2000).
- [87] L. Novotny, B. Hecht, and D. W. Pohl, *J. Appl. Phys.* **81**, 1798 (1997).
- [88] H. T. Dung, L. Knöll, and D.-G. Welsch, *Phys. Rev. A* **66**, 063810 (2004).

- [89] A. A. Maradudin and D. L. Mills, Phys. Rev. B **11**, 1392 (1975).
- [90] H. T. Dung, L. Knöll, and D.-G. Welsch, Phys. Rev. A **57**, 3931 (1998).
- [91] N. Ashcroft and N. Mermin, *Solid state physics* Holt-Saunders International Editions: Science : Physics (Holt, Rinehart and Winston, 1976).
- [92] S. Irvine and A. Elezzabi, Generation of 2 keV, 30 fs electron pulses via surface plasmon waves, in *Lasers and Electro-Optics, 2005. (CLEO)* Vol. 3, pp. 2331–2333, 2005.
- [93] A. Hoffmann, Z. Lenkefi, and Z. Szentirmay, Journal of Physics: Condensed Matter **10**, 5503 (1998).
- [94] G. Torosyan, C. Rau, B. Pradarutti, and R. Beigang, Applied Physics Letters **85**, 3372 (2004).
- [95] J. A. Dionne, L. A. Sweatlock, H. A. Atwater, and A. Polman, Phys. Rev. B **72**, 075405 (2005).
- [96] L. Knöll, S. Scheel, and D.-G. Welsch, *Coherence and Statistics of Photons and Atoms* (John Wiley and Sons, New York, 2001).
- [97] S. John and T. Quang, Phys. Rev. A **50**, 1764 (1994).
- [98] P. Jackson, *Classical Electrodynamics (3rd ed.)* (Wiley, New York, 1998).
- [99] J. J. Choquette, K.-P. Marzlin, and B. C. Sanders, Phys. Rev. A **82**, 023827 (2010).
- [100] C. Cohen-Tannoudji, J. Dupont-Roc, and G. Grynberg, *Photons and atoms: introduction to quantum electrodynamics* Wiley-Interscience publication (Wiley, 1989).

- [101] V. Bonch-Bruевич and S. Tiablikov, *The Green function method in statistical mechanics* (North-Holland Pub. Co., 1962).
- [102] Y. Wang and I. Khoo, *Optics Communications* **11**, 323 (1974).
- [103] A. Archambault, F. Marquier, J.-J. Greffet, and C. Arnold, *Phys. Rev. B* **82**, 035411 (2010).
- [104] G. S. Agarwal, *Phys. Rev. A* **11**, 230 (1975).
- [105] H. T. Dung, L. Knöll, and D.-G. Welsch, *Phys. Rev. A* **62**, 053804 (2000).
- [106] B. Huttner and S. M. Barnett, *Phys. Rev. A* **46**, 4306 (1992).
- [107] S. M. Barnett, B. Huttner, R. Loudon, and R. Matloob, *Journal of Physics B: Atomic, Molecular and Optical Physics* **29**, 3763 (1996).
- [108] S. M. Barnett, B. Huttner, and R. Loudon, *Phys. Rev. Lett.* **68**, 3698 (1992).
- [109] M. S. Yeung and T. K. Gustafson, *Phys. Rev. A* **54**, 5227 (1996).
- [110] G. A. Wurtz *et al.*, *Opt. Express* **16**, 7460 (2008).